[redacted]

[redacted]

Group Design Report[redacted]

Department of Mechanical, Aerospace and Civil Engineering

CONTRIBUTION FORM

Group Number:	[redacted]
Name of Group Coordinator:	Ruairi Kavanagh
Course MED or MEng:	MEng

Student Name & Digital Signature (to confirm agreement has been reached on the individual allocation)	[redacted]	[redacted]
Ruairi Kavanagh	[redacted]	[redacted]
Brilliant Gustavo Purnawan	[redacted]	[redacted]
Muhammad Borhan	[redacted]	[redacted]
Margarita Simpson	[redacted]	[redacted]
Muhammad Yusman	[redacted]	[redacted]
Hanif Mohd Fadhillah	[redacted]	[redacted]
Andhika Nathanael Djajadi	[redacted]	[redacted]

Table of Contents

1 Introduction 8
1.1 Project Background 8
1.2 Insights from Design Report A 8
1.3 Achievements from Design Report A 8
1.4 Market Research and Demand 9
1.5 Production Line and Manufacturing Strategy 9
1.6 Market Size and Yearly Sales Projections 9
1.7 Target Market and Sales Strategy 9
1.8 Scope of Work 10
1.9 Conclusion 10
2 Prototype Assembly and Testing 10
2.1 Introduction 10
2.2 Prototype Manufacturing and Assembly Process 11
2.2.1 Manufacturing Process 11
2.2.2 Assembly Process 12
2.2.3 Structural Frame Assembly 12
2.2.4 Rotor and Shaft Subassembly 12
2.2.5 Motor and Gear Assembly 13
2.2.6 Solar Tracking and Panel Mount 13
2.2.7 Electronics and Wiring Integration 13
2.2.8 Final Integration and Inspection 13
2.3 Unexpected Issues in Manufacturing 13
2.3.1 Manual Tapping of Aluminium Extrusions 14
2.3.2 Misalignment from Manual Drilling 14
2.3.3 T-Nut Orientation and Frame Instability 14
2.3.4 Fitment Issues with 3D-Printed Components 14
2.3.5 Weld Misalignment in Motor Mounting 14
2.3.6 Blade Fabrication with Hot Wire Cutting 15
2.3.7 Shaft Modification for Gear, Sleeve, and Bearing Fitment 15
2.4 Impact on Assembly Workflow 15
2.5 Prototype Testing 15
2.5.1 Generator and Wattmeter Functionality Testing 15
2.5.2 Solar Tracking Platform Functionality Testing 16
2.6 Limitations 16
2.7 Prototype Design Changes 17
2.7.1 Motor Bracket Mounting Adjustment 17
2.7.2 Design Change from Aluminium Block to Rivet Nut Integration in Foam Blade 17

2.8 Lessons Learned from Prototype Build 18
3 Deployable Product Specification of Requirements 19
4 Deployable Product Design Development & Optimization 21
4.1 Optimisation for deployable outline 21
4.2 Fault Tree Analysis (FTA) of prototype design 22
4.2.1 Solar Tracking Optimisation 23
4.2.2 Development of Blade Dimensions 25
4.2.3 Variable Pitch Mechanism 27
4.2.4 Performance Improvement Summary 27
4.3 Design for Assembly (DFA) Optimisation 28
4.3.1 Prototype vs Deployable Base Structure: Part Count Reduction 28
4.3.2 Prototype vs Deployable Base Structure: Weight Optimization 29
4.3.3 DFA Solar Assembly 31
4.4 Structural FMEA optimisation 32
4.4.1 Overview of Initial Prototype 33
4.4.2 Initial FMEA Findings (Prototype) 33
4.4.3 Finite Element Analysis of Prototype 34
4.4.4 FMEA for New Design 35
4.4.5 FEA of New Design 36
4.4.6 Discussion 37
4.4.7 Limitations 38
4.5 Design For Manufacturing (DFM) Optimisation 39
4.5.1 Uptime-Focused Design Optimization 39
4.5.2 Blade Material Optimisation 43
4.5.3 Fasteners Material Selection 45
5 Deployable Product Design Outline 46
5.1 General Assembly 46
5.1.1 Cage Subassembly 47
5.1.2 Blades Subassembly 47
5.1.3 Solar Subassembly 47
5.2 Manufacturing Considerations 47
5.2.1 Blades 47
5.2.2 Arms 47
5.2.3 Pull Rods 48
5.2.4 Top and Bottom Cage Legs 48
5.2.5 Scissor Struts A and B 48
5.2.6 Base, Corner Base Plate, and Lid Base 48
5.2.7 Rubber Padding Corner and Bottom Base Center Padding 49
5.2.8 Bearing Casing 49

5.2.9 Base Box 49
5.2.10 Cam and Cam Bracket 49
5.2.11 Solar Components (Camlock, Shaft and Solar Supports) 50
5.3 Technical Drawings 51
5. Team Professional Practice Statement 112
6 Conclusions and Recommendations 118
7 References 121
8 Appendix 125
8.1 Appendix A 125
8.2 Appendix B 141

Table of Figures

Figure 2.a: Frame Assembly 12
Figure 2.b: Rotor and Shaft Attachment 12
Figure 2.c: Motor and Gear Assembly 13
Figure 2.d: Single Axis Solar Tracker 13
Figure 2.e: Design change from CAD model (left) to physical prototype (right) 17
Figure 2.f: Design revision from CAD concept (A, B) to prototype implementation (C, D). 17
Figure 4.a: Fault Tree Analysis for Hybrid VAWT and Dual Axis Solar Panel System 22
Figure 4.b: Single-axis Solar Tracking Testing 24
Figure 4.c: Overall Deployable Solar Assembly 24
Figure 4.d: Metric Comparison 27
Figure 4.e: Quantified Improvements 29
Figure 4.f: Comparison between the prototype base structure (left) and the optimized deployable base structure (right). 29
Figure 4.g: Quantified Improvements 30
Figure 4.h: Von Mises stress distribution under 1000 N load on the base structure. The maximum stress observed is 5.12 MPa, well below the yield strength of 215 MPa for Aluminium 6061-T6, indicating a safe design. 30
Figure 4.i: DFA Solar Assembly 32
Figure 4.j: Camlock System 32
Figure 4.k: Technic Pins 32
Figure 4.l: Assembly Time 32
Figure 4.m - Prototype SolidWorks 33
Figure 4.n - RPN Benchmarking 33
Figure 4.o: Blade root joint design options: (a) traditional flange bolted connection, (b) embedded insert hub, (c) T-bolt joint, and (d) stud insert. The commercial design adopts the flange-type connection (a) to distribute loads evenly and facilitate easier blade replacement in the field. https://www.mdpi.com/1996-1073/10/8/1112 39
Figure 4.p: Bolt shank effect on SCF (connected with standard nut type)Source: Ha, K. (2020). Reduction of Stress Concentration Factor (SCF) on the Bolted Joint Connection for a Large Wind Turbine Rotor Blade through Various Design Modifications. Applied Sciences 40
Figure 4.q Bolt shank effect on SCF (connected with standard nut type)Source: Ha, K. (2020). Reduction

of Stress Concentration Factor (SCF) on the Bolted Joint Connection for a Large Wind Turbine Rotor Blade through Various Design Modifications. Applied Sciences, 10(18), 6588. https://doi.org/10.3390/app10186588 41
Figure 4.r: (a) Conformal-coated capacitor protected from dendritic growth; (b) Uncoated surface showing dendritic damage (Yoo, 2024). 41
Figure 4.s: Braided cable shielding for EMI suppression (Belden Inc., 4.t: Left: Developed surface of braided shield, showing braid openings and angle (Belden Inc., 2023). Right: Braided cable shielding for EMI suppression (Belden Inc., 2023). 42
Figure 4.t : (a) I–V curve and (b) P–V curve of a PV panel under varying irradiance levels (Chowdhury et al., 2016). 43
Figure 4.u: Stress vs Forces Graph 44
Figure 4.v: Deflection vs Forces 45
Figure 4.w: Electronic Part Fasteners 1 (VAWT) 46
Figure 4.x: Electronic part fasteners 2 (Solar Panel) 46
Figure 8.a: Cp values for optimised blade configurations at peak TSR. 125
Figure 8.b: Mean Cp Optimisation Results (Across TSR Range) 125
Figure 8.c: Mechanism 1(1st Iteration), Passive Hinge-Based Pitching 126
Figure 8.d: Mechanism 2 (2nd Iteration), Cam and Follower Pitching Mechanism 127
Figure 8.e: Scissor-Strut Folding Mechanism 128
Figure 8.f: Telescopic Adjustable Leg with Detent Pin 128
Figure 8.g: Slotting Mechanism for Blade and Arm Connection 129
Figure 8.h - FMEA RPN Scores 129
Figure 8.i: FEA 1: Total deformation 130
Figure 8.j: Proof of unusable Factor of Safety Tool 131
Figure 8.k: FEA 1: Close up on stress concentrations. 131
Figure 8.l: FEA 1: Equivalent Stress 131
Figure 8.m - FMEA RPN scores 2 133
Figure 8.n: FEA 2 Equivalent Stress 134
Figure 8.o – FEA 2: Total Deflection 134
Figure 8.p - FEA 2: Close up on stress concentration 135
Figure 8.q - FEA 2: Close up on stress concentration 135
Figure 8.r: Connection layout of the cage subassembly showing scissor struts, pivot pins, and foldable hinges. 136
Figure 8.s: Shaft and bearing assembly illustrating the dual support system for blade rotation. The shaft is held by another bearing on top and the bearing is bolted onto the scissor struts (Top Image). 136
Figure 8.t: Solar panel mounting setup with adjustable brackets fixed atop the cage. 137
Figure 8.u: Solar panel mounting setup with technic pins connected the cage. The technic pins are connected to the edge of the scissor struts. Supported by screws to keep it in place. 137
Figure 8.v: Shaft mounting setup with camlock system. 138
Figure 8.w: Solar panel mounting setup with hinges. 138
Figure 8.x: Material Properties 138
Figure 8.y: Advantages and Disadvantages of Each Material. 139
Figure 8.z: External components that are not manufactured 140
Figure 8.aa Semester 2 initial Gantt Chart 141
Figure 8.bb Design Review Meeting Notes 142
Figure 8.cc: Professional Reflection on Practice Competences 143
Figure 8.dd: March 2025 Buddycheck 144

Figure 8.ee: October 2024 Buddycheck 145
Figure 8.ff: April 2025 Buddycheck 146
Figure 8.gg Example of Teams communication with Technician 147
Figure 8.hh UoM Engineering Professional Practice Competencies 148
Figure 8.ii WhatsApp communications 149
Figure 8.jj Shared One Drive for semester one and two 149

1 Introduction

1.1 Project Background

The global transition towards renewable energy is accelerating due to increasing energy demands, environmental concerns, and the depletion of fossil fuel resources. Wind and solar power have emerged as leading solutions, with wind energy alone contributing 93.6 GW of new capacity in 2022, demonstrating its growing role in electricity generation. However, these sources are often intermittent—wind speeds fluctuate based on weather conditions, while solar energy is only available during daylight hours. To address these limitations, hybrid renewable energy systems have been developed to optimize energy production and ensure continuous, reliable power generation.

Our project, the Dual Energy Wind Turbine, integrates Vertical Axis Wind Turbine (VAWT) technology with solar tracking photovoltaic panels to provide a more efficient and stable renewable energy solution. This combination allows for energy generation under various environmental conditions, as the VAWT can capture wind power from any direction, while the solar panels maximize energy intake through dynamic positioning. The key objective of this project is to develop a cost-effective, sustainable energy solution that is suitable for residential homes, small businesses, and off-grid communities.

1.2 Insights from Design Report A

Design Report A provided valuable insights into the feasibility and initial design considerations for the Dual Energy Wind Turbine. A key finding from the previous phase was the effectiveness of combining wind and solar energy sources to enhance overall power reliability. Computational modelling and early-stage prototype testing demonstrated that an optimized solar tracking system significantly improves energy capture, increasing efficiency by 15-20% compared to fixed panels. Furthermore, aerodynamic analysis of the VAWT blade structure identified ways to improve wind energy conversion, ensuring the system remains functional even in low-wind-speed conditions. These findings have been instrumental in refining our approach as we transition from conceptual development to detailed design and implementation.

1.3 Achievements from Design Report A

Several achievements were made in the first phase of development. The initial structural and material analysis confirmed that the selected materials—lightweight aluminium and 3D-printed composite components—provide an ideal balance of durability and cost-effectiveness. Additionally, energy simulations verified that the proposed hybrid system can generate up to 30% more power than standalone wind or solar systems, particularly in variable weather conditions. Another significant achievement was the creation of a scalable production framework, ensuring that manufacturing can be adapted for both residential-scale and commercial-scale applications.

Several achievements were made in the first phase of development. The initial structural and material analysis confirmed that the selected materials—lightweight aluminium and 3D-printed composite components—provide an ideal balance of durability and cost-effectiveness. Additionally, energy simulations verified that the proposed hybrid system can generate up to 30% more power than standalone wind or solar systems, particularly in variable weather conditions. Another significant

achievement was the creation of a scalable production framework, ensuring that manufacturing can be adapted for both residential-scale and commercial-scale applications.

1.4 Market Research and Demand

The renewable energy sector is witnessing rapid expansion, fuelled by global climate targets and government incentives supporting the shift toward sustainable energy sources. The distributed energy generation market is projected to reach $580 billion by 2030, with hybrid wind and solar systems gaining popularity due to their reliability and cost-effectiveness. Our Dual Energy Wind Turbine is positioned to meet this demand by offering an accessible, autonomous renewable energy solution. The product appeals to a wide range of customers including homeowners aiming to reduce energy bills, small commercial businesses seeking greener operations, and off-grid or rural users who require independent energy sources. It's dual functionality—combining solar and wind energy—makes it particularly valuable in areas where traditional grid access is limited or inconsistent, as well as in regions prone to natural disasters.

1.5 Production Line and Manufacturing Strategy

To support a target production volume of 10,000 units annually, we have restructured our manufacturing strategy to prioritize scalability, efficiency, and cost control. Instead of relying on small-scale or prototype-level processes, we will implement lean manufacturing practices combined with automated assembly lines to ensure consistent output and quality. Structural elements previously 3D-printed will transition to die-cast aluminium, offering greater durability and reduced per-unit cost at high volumes. Injection moulding will be used for producing plastic components, drastically cutting production time and material waste. We will retain 3D printing for niche parts or customization requests where necessary. Commercially available electronic modules will be sourced in bulk from vetted suppliers to minimize cost variability, while final system integration and testing will be done in-house to maintain quality assurance. This modular and scalable approach ensures production can be ramped up efficiently to meet growing market demands.

1.6 Market Size and Yearly Sales Projections

The small-scale wind and solar hybrid market is experiencing strong global growth, driven by improved public awareness, advancing technologies, and generous governmental support programs. With a production goal of 10,000 units per year, we anticipate reaching this scale within two years, starting with a smaller rollout in Year 1 to validate and optimize our processes. Based on current market trends and pricing, we forecast a gradual ramp-up, with expected sales of 3,000 units in Year 1, 7,000 in Year 2, and full-scale production by Year 3. Our target markets include the UK, the European Union, and North America, where existing infrastructure, policy support, and eco-conscious consumers offer ideal conditions for adoption. Distribution will be executed through a multi-channel strategy: e-commerce platforms, renewable energy distributors, and partnerships with governmental or non-profit programs promoting sustainable and off-grid technologies.

1.7 Target Market and Sales Strategy

The Dual Energy Wind Turbine is designed to serve multiple high-potential market

segments. These include residential users seeking autonomy from rising utility prices, small businesses reducing operational energy expenses, and remote communities needing off-grid power solutions. Additionally, the turbine offers opportunities for educational institutions and research organizations interested in showcasing hybrid renewable systems in practical settings. To stand out in a competitive landscape, our product will be competitively priced while offering premium features such as automated solar tracking and efficient wind energy capture. These capabilities ensure higher energy yields and long-term savings for customers compared to standalone systems. Our marketing efforts will highlight these value propositions, supported by performance data, cost-benefit analysis, and customer testimonials to build trust and visibility in key markets.

1.8 Scope of Work

Building on the insights and achievements from Design Report A, this phase of the project will focus on refining the design, optimizing energy efficiency, and preparing for large-scale production and market entry. The primary objectives include enhancing system durability, conducting real-world testing to validate performance, and establishing a cost-effective manufacturing process. Additionally, efforts will be made to develop a comprehensive marketing and distribution strategy, ensuring the product reaches the target audience effectively. The upcoming work will also involve evaluating regulatory requirements for different markets and implementing any necessary modifications to comply with industry standards.

1.9 Conclusion

The Dual Energy Wind Turbine represents a breakthrough in renewable energy technology, addressing the key challenges of intermittency and efficiency in wind and solar power generation. By combining innovative design, scalable production, and a well-researched market approach, our project aligns with global sustainability goals and the increasing demand for cost-effective, off-grid energy solutions. As the renewable energy market continues to expand, our hybrid system is poised to be a highly competitive and impactful solution, contributing to a cleaner and more sustainable future.

2 Prototype Assembly and Testing

This section provides a detailed review of the manufacturing, assembly, and testing of the Dual Energy Wind Turbine prototype. The objective of this phase was to evaluate the efficacy of the assembly process, assess structural and functional performance, and identify areas for design improvement. The results from this phase will inform refinements to the system, ensuring greater reliability and ease of production in future iterations.

2.1 Introduction

The prototype assembly and testing phase focused on verifying the mechanical stability, energy generation efficiency, and structural integrity of the Dual Energy Wind Turbine. The assembly process aimed to confirm the feasibility of the design, ensure component compatibility, and refine manufacturing techniques to improve overall build efficiency.

This phase involved constructing the turbine frame, integrating the vertical axis wind turbine (VAWT), mounting solar panels, and validating system performance through controlled testing. While many aspects of the assembly proceeded as expected,

some unexpected challenges arose, requiring manual modifications, precision drilling, and design adjustments to ensure proper alignment and stability.

2.2 Prototype Manufacturing and Assembly Process

2.2.1 Manufacturing Process

The manufacturing process for the Dual Energy Wind Turbine prototype involved a combination of manual, subtractive, and additive fabrication methods, selected to achieve structural functionality, weight efficiency, and cost-effectiveness. As outlined in the report and component breakdown, parts were sourced from commercial suppliers like Metals4U, KJN, HPC Gears, and custom-manufactured using in-lab equipment such as hot wire cutters and 3D printers.

Aluminium Profile Structures: Aluminium 20x20 extruded profiles were used extensively for the turbine's frame due to their strength-to-weight ratio and ease of modular assembly. These profiles formed the vertical supports, horizontal cross-bracing, and the cage structure supporting the main shaft and blades. While cost-effective and easy to handle, the lack of pre-tapped holes required manual M6 threading during assembly, adding to labour time and introducing variability. According to Song et al. (2020), aluminium profiles are widely used in prototype builds for their modularity, but they require careful preparation and standardisation of joinery features such as threading and bracket design to reduce cumulative tolerance errors during assembly.

Manual Machining and Drilling: Several parts, including the 460mm horizontal reinforcement rods, required precision drilling of D3 holes for through-bolting. This was done manually, introducing tolerancing challenges. The shaft also had to be turned down slightly to allow interference-free fitting of the gear, bearing, and shaft sleeve assembly. This modification was necessary due to a mismatch in specified shaft tolerances versus component inner diameters. According to Bissacco et al. (2005), manual drilling in aluminium can introduce variability up to ±0.2 mm depending on operator skill and tool wear, which emphasizes the need for jig-assisted or CNC-controlled operations in critical alignment components.

Hot Wire Foam Cutting for Blades: Due to the unavailability of CNC machining, turbine blades were fabricated using a hot wire foam cutter to shape high-density foam into aerodynamic profiles. While cost-effective and rapid, this method introduced inconsistency in blade geometry due to variations in wire tension, temperature, and cutting speed. This limited the aerodynamic precision of the blades and required additional post-processing such as sanding and balancing. Elfarra et al. (2014) show that automated foam cutting with temperature-controlled hot wire significantly improves dimensional accuracy for aerodynamic applications.

3D Printing of Custom Components: Components such as the shaft sleeves, motor housing, and solar panel attachments were 3D-printed using PLA and PETG. This allowed for rapid prototyping and customisation but introduced fitment issues due to warping and layer resolution. Several parts required sanding and resizing to ensure a snug fit, especially for interfaces with metal components. As noted by Ngo et al. (2018), 3D printed parts can suffer from anisotropic mechanical properties and warping, especially when printed with PLA or PETG, unless cooling rates and print orientation are carefully managed.

Sheet Material Fabrication: The PETG base and side panels were laser-cut or

manually trimmed from 4mm sheets. These panels served both structural and protective roles within the boxed turbine casing. PETG was selected for its impact resistance and moderate transparency, allowing visual inspection of internal components without compromising rigidity. Mounting holes were added either manually or through pre-cut templates to allow compatibility with aluminium frame fixings.

Overall, the hybrid manufacturing strategy enabled a balance between performance, cost, and flexibility. However, the experience also highlighted the need for more automated and standardised fabrication techniques in future stages of development, particularly if scaling to production volumes. Greater use of CNC machining, tighter tolerance planning, and the adoption of jigs for drilling and cutting would significantly reduce assembly time and error rates, ultimately enhancing product quality and reproducibility.

2.2.2 Assembly Process

The assembly of the Dual Energy Wind Turbine prototype followed a modular and systematic approach, beginning with the construction of the supporting frame and progressing through to the integration of mechanical, electrical, and solar components. Each subsystem was assembled and tested individually before final integration to ensure proper alignment and system functionality.

2.2.3 Structural Frame Assembly

The frame was constructed using 20x20mm aluminium extrusion profiles, connected with L-brackets, three-way cubic connectors, and T-nuts. The profiles were cut to length based on CAD specifications, forming a cubic frame designed to support the turbine's mechanical systems and solar tracking assembly. Vertical and horizontal members were aligned using standard engineering squares to ensure accurate 90° joins. Once squared, the frame was tightened in stages to distribute tension evenly across all brackets and prevent twisting.

Figure 2.a: Frame Assembly

2.2.4 Rotor and Shaft Subassembly

The wind rotor blades, formed from shaped high-density foam, were mounted to aluminium arms which were then fixed to a central hub. This hub connected to the main 700mm steel shaft using a custom 3D-printed shaft sleeve. The shaft was then inserted through two bearing blocks mounted at the top and bottom sections of the frame, ensuring smooth rotational motion. PETG plastic plates were used to secure the bearing mounts to the structure and absorb minor vibrations.

Figure 2.b: Rotor and Shaft Attachment

2.2.5 Motor and Gear Assembly

The DC motor and gear system were prepared as a subassembly. The main gear was aligned with the rotor shaft and fixed in place using a keyed interface and set screws. The motor's output gear was then positioned to engage the larger gear on the shaft, completing the drive system. The motor itself was mounted onto an aluminium bracket positioned at the rear of the turbine housing, and the power and control wires were routed toward the internal electronics bay.

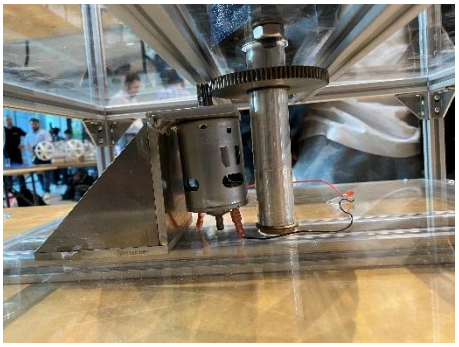

Figure 2.c: Motor and Gear Assembly

2.2.6 Solar Tracking and Panel Mount

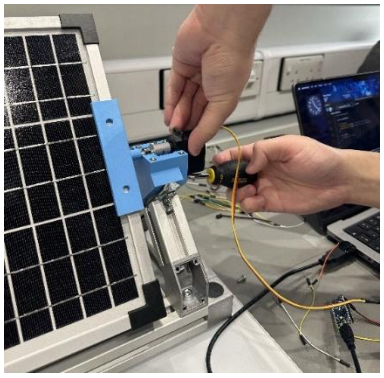

Figure 2.d: Single Axis Solar Tracker

The solar tracking system was assembled using a 10W photovoltaic panel mounted on a PETG bracket. This was fixed to a horizontal shaft driven by a servo motor (MG996R), enabling single-axis motion. The tracking logic was controlled by an Arduino Nano microcontroller, programmed to respond to readings from four light-dependent resistors (LDRs). The motor and panel bracket were mounted atop the turbine frame to provide full exposure to sunlight throughout the day.

2.2.7 Electronics and Wiring Integration

All electronic components—including the motor controller, solar tracker circuitry, and power storage unit—were housed within a central electronics enclosure. Wiring from the motor and solar panel was routed internally through the frame using cable sleeves and clips to reduce exposure and maintain a clean exterior. Connections were made using JST connectors and terminal blocks to allow for modular replacement or servicing of individual subsystems.

2.2.8 Final Integration and Inspection

Once all subassemblies were completed and individually tested, the final assembly phase involved aligning the rotor, confirming gear meshing, verifying smooth rotation, and testing electrical functionality. The turbine was placed on a test stand for inspection and rotational balancing. The system was then powered on to verify the motor drive, solar tracking, and structural stability before proceeding to formal testing.

2.3 Unexpected Issues in Manufacturing

Throughout the prototype development of the Dual Energy Wind Turbine, several unforeseen challenges arose that impacted manufacturing efficiency, assembly accuracy, and overall structural alignment. These issues highlighted the limitations of certain manual processes, component tolerances, and assembly methods used at the prototyping stage, offering clear lessons for future iterations.

2.3.1 Manual Tapping of Aluminium Extrusions

One of the primary challenges involved the aluminium extrusion rods intended for the turbine's frame. The original design assumed that M6 fastening points would arrive pre-tapped to support quick assembly using L-brackets and connectors. However, the supplied extrusions were unthreaded, requiring manual M6 tapping for every connection point. This process introduced variability in thread depth and alignment, leading to inconsistent fastener engagement. As a result, parts had to be re-aligned multiple times during assembly, which increased labour time and affected overall build precision.

2.3.2 Misalignment from Manual Drilling

The internal reinforcement of the frame relied on 460mm aluminium support rods, which required manually drilled D3 holes to accommodate through-bolts. Despite careful measurements, the manual drilling process led to slight misalignments in hole positioning. These minor inaccuracies affected the vertical and lateral alignment of the frame, placing additional stress on bolted joints. Achieving structural symmetry during assembly became more difficult, underscoring the need for pre-marked jigs or CNC drilling in future designs to ensure hole consistency and reduce error margins.

2.3.3 T-Nut Orientation and Frame Instability

A significant assembly issue arose when using T-nuts to join the aluminium extrusion frame. These fasteners needed to be correctly oriented within the channels to engage properly with bolts during tightening. However, aligning the T-nuts during initial assembly proved difficult and unintuitive, leading to improper connections. On our first full assembly of the structure, several T-nuts failed to engage entirely, causing the frame to collapse under its own weight. This highlighted the importance of either using pre-inserted spring-loaded T-nuts or integrating clearer assembly markings or procedures to ensure proper engagement during future builds.

2.3.4 Fitment Issues with 3D-Printed Components

Several 3D-printed parts, particularly the shaft sleeves and motor housing, presented unexpected dimensional inaccuracies due to minor warping during the printing process. These distortions affected their ability to interface securely with metal components. Additional steps—such as sanding, re-machining, and reprinting—were required to achieve the intended fits. This extra effort not only consumed time but also highlighted the importance of tightening print tolerances or selecting more stable materials for critical parts, especially those involved in load transfer or rotation.

2.3.5 Weld Misalignment in Motor Mounting

Another unexpected complication involved the motor holder, which was discovered to have been welded incorrectly. The mounting plate was not square, causing misalignment between the motor shaft and the intended vertical axis. As a result, the bottom base plate and adjacent struts had to be modified to accommodate the skewed mount. This adjustment involved re-drilling holes and slightly altering the support geometry, introducing additional complexity and reducing the symmetry of the final structure. The issue emphasized the need for accurate jigging and QA procedures in welding, particularly for components that are central to system balance and rotation.

2.3.6 Blade Fabrication with Hot Wire Cutting

Due to the unavailability of a CNC cutter, the turbine blades were fabricated using a manual hot wire foam cutting process. While this method allowed for shaping lightweight and aerodynamic blades from high-density foam, it introduced several challenges. The process relied heavily on operator control, which made it difficult to maintain consistent blade profiles. Variations in wire tension, temperature, and cutting speed caused discrepancies in blade thickness and surface finish. These inconsistencies required additional post-processing, including sanding and balancing, to ensure aerodynamic symmetry and structural balance. For future manufacturing, the use of CNC or templated cutting jigs would significantly enhance blade uniformity, reduce post-processing, and ensure better performance during turbine operation.

2.3.7 Shaft Modification for Gear, Sleeve, and Bearing Fitment

An additional challenge arose during the assembly of the drivetrain, where it became apparent that the tolerances for the shaft, bearing, gear, and fitting sleeve had not been fully accounted for in the initial design. The outer diameter of the shaft exceeded the internal dimensions of the components by a few millimetres, preventing a proper fit. To resolve this, the shaft had to be manually turned down on a lathe to reduce its diameter and allow for correct seating of the gear and bearing assembly. This unplanned machining step introduced extra labour and delayed assembly. The issue underscored the importance of dimensionally verifying all mating components during the design stage and including suitable tolerances for press fits and rotational components. In future iterations, a more thorough integration of mechanical interfaces in CAD modelling and component specification would help prevent such misalignments.

2.4 Impact on Assembly Workflow

The cumulative effect of these issues significantly impacted the assembly timeline. Tasks that were expected to be straightforward—such as frame construction and part integration—required repeated modifications and corrections. Although these problems were manageable at the prototyping scale, they demonstrated the need for design-for-manufacture (DFM) considerations if the system is to be produced at scale. Standardizing components, automating high-precision tasks, and relying on pre-processed materials would greatly reduce build time and improve consistency in future iterations.

2.5 Prototype Testing

2.5.1 Generator and Wattmeter Functionality Testing

To verify the energy generation capabilities of the prototype, we conducted a manual functionality test focusing on the turbine and generator assembly. The primary objective was to confirm that mechanical rotation of the blades could successfully induce an electrical output, measurable through an external wattmeter.

The procedure involved manually rotating the turbine blades while the generator was connected to a calibrated wattmeter. During testing, clear wattage readings were observed on the display, confirming that rotational mechanical energy was being effectively converted into electrical energy.

In line with standard validation protocols (ISO 17025 guidelines on calibration and

measurement traceability), we ensured that the wattmeter used was recently verified for accuracy. Evidence of successful functionality was recorded using an iPhone camera, capturing both the actuation of the blades and the corresponding wattmeter readings. Although the test was qualitative rather than quantitative — focusing on proving the presence of voltage generation rather than precise power output — it conclusively demonstrated that the energy conversion subsystem of the prototype operates correctly under manual conditions.

2.5.2 Solar Tracking Platform Functionality Testing

A separate functionality test was conducted to validate the autonomous tracking behaviour of the solar platform. The main goal was to confirm that the platform could adjust its orientation dynamically over time, aligning with the changing position of the sun, as per the system's intended operational parameters.

For this test, the prototype was set up in a controlled environment under natural daylight conditions. An iPhone camera was positioned to record a time-lapse video capturing the movement of the tracking platform over an extended period. The tracking mechanism was programmed to adjust its position incrementally, based on pre-set timing and sun position estimations.

Upon reviewing the time-lapse footage, clear evidence of regular, directional adjustments in line with expected solar motion was observed. The tracking system responded consistently at programmed intervals (0° - 180°, across 8- hour period, average sunlight hours demonstrating that the mechanism could maintain solar alignment autonomously. While the test environment did not allow for precise solar angle calibration against real-time azimuth and elevation data (as outlined in IEC 61853-2 photovoltaic module performance standards), the positive movement trends confirmed that the system’s fundamental tracking functionality was operational.

This approach of using time-lapse evidence provided a practical and reliable method of verification, especially given the real-world constraints on testing equipment and conditions.

2.6 Limitations

During our testing process, several limitations emerged which ultimately affected both the depth and reliability of our functional validation. One major issue stemmed from the misalignment of the housing bearings received from the supplier. These components exhibited significantly higher friction than expected, reducing the system’s wind responsiveness, and raising the effective cut-in wind speed beyond realistic outdoor conditions. As a result, we were unable to assess real-world power generation performance using natural wind. To compensate, we had to manually rotate the turbine blades to confirm that voltage was being generated. While this did demonstrate fundamental electrical functionality, it offered little insight into the true aerodynamic efficiency of the design or its responsiveness under typical wind profiles.

Another key limitation was the scope of our solar tracking test. Although we successfully demonstrated the platform’s mechanical ability to orient toward a changing solar vector, the test was carried out without a functional solar panel in place. Our evaluation focused solely on the actuation and tracking mechanism, without examining any direct improvements to electrical output. While we were confident in referencing existing literature that supports the benefits of dynamic solar

tracking — with improvements in panel efficiency typically ranging from 15% to 30% depending on system type and location — it would have strengthened our conclusions to validate this directly through controlled comparison with and without tracking functionality under actual sunlight conditions.

Finally, the absence of data logging equipment limited our ability to capture continuous or quantitative performance data. While we used visual documentation such as time-lapse recordings and wattmeter readings, we lacked the infrastructure to capture trends over time, such as RPM, voltage, or current under load. This restricted us to single-point, observational measurements rather than rich datasets suitable for deeper analysis or power curve development. In a professional setting, the use of integrated sensors and real-time data acquisition systems would have allowed for more thorough characterization and a clearer picture of system behavior over time.

2.7 Prototype Design Changes

2.7.1 Motor Bracket Mounting Adjustment

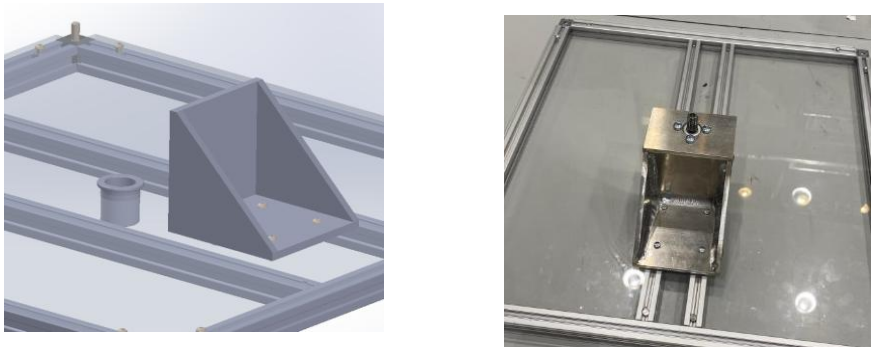

Figure 2.e: Design change from CAD model (left) to physical prototype (right)

Initially, the motor bracket was fastened directly to the acrylic base plate. However, operational testing revealed that vibrations during turbine rotation caused loosening of the gear-motor connection, leading to instability and gear misalignment. To address this, the bracket was repositioned and bolted directly to the aluminium strut using T-nuts, offering a more rigid and vibration-resistant mounting point. High torque was applied to the bracket fasteners to prevent loosening under dynamic loads, ensuring the gear remains securely engaged with the motor shaft during operation.

2.7.2 Design Change from Aluminium Block to Rivet Nut Integration in Foam Blade

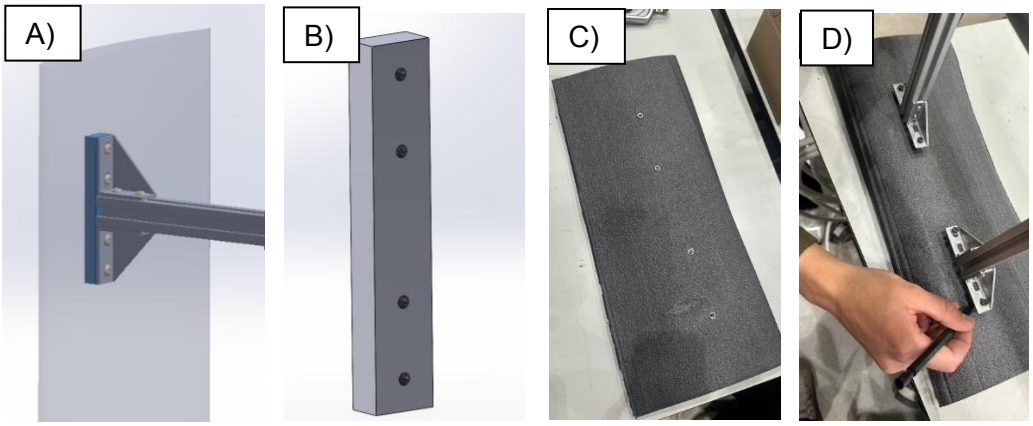

Figure 2.f: Design revision from CAD concept (A, B) to prototype implementation (C, D).

In the initial design, a solid aluminium block (B) was intended to be inserted into a cut-out cavity within the foam blade (A) and fixed using epoxy. However, cutting a precise square cavity in the foam proved impractical and risked structural damage due to the lack of suitable tools and the fragile nature of the material. Additionally, the aluminium block added unnecessary top-end weight to the system. The final prototype instead utilized rivet nuts (C, D), allowing a small circular hole to be drilled in the blade for fastener insertion—minimizing foam damage while maintaining lightweight and effective attachment.

2.8 Lessons Learned from Prototype Build

Key insights from the prototype build highlighted areas for improvement in structural weight, assembly methods, and component compatibility:

- **Excessive Shaft Weight**

The aluminium shaft weighed **1.78 kg**, nearly equal to the combined mass of all six arms (**1.8 kg total**) and significantly heavier than the foam blade, which has negligible weight. This created a top-heavy system, reducing efficiency and stability.

- **Material Imbalance**

Foam blades are very light, but the current aluminium arms and shaft made the structure unnecessarily heavy. Lightweight alternatives such as PVC or plastic box tubes should be explored to better match the blade's mass and reduce overall weight.

- **Inefficient Shaft-Arm Connection**

The arms were screwed directly into the shaft, requiring a 10 mm thick wall. This increased weight unnecessarily and introduced structural weakness under vibration. In future designs, a clamp connection should replace direct screwing to reduce mass and simplify assembly.

- **Overcomplicated Power System**

The motor and gear setup added unnecessary complexity and vibration. Future project builds should consider using a prebuilt VAWT coil, which simplifies the system and improves reliability.

- **Blade Rotation Issues**

The blade failed to rotate during outdoor testing due to defective bearings supplied late in the project timeline. As replacement was not feasible within the project duration, this prevented proper wind performance evaluation. The key lesson is that **critical components such as bearings must be sourced and inspected early**, as delays or quality issues can compromise core functionality and limit testing opportunities.

3 Deployable Product Specification of Requirements

Specification	Description
Minimum Power Output	The overall power output generated must at least generate 30 to 50 W Power generated from VAWT: 10 to 20 W Power generated from solar panel: 20 W to 30W
Total Mass	Must have a maximum of 25 kg total mass for portability and ease of installation using lightweight materials without compromising the performance especially for the main frame
Product Lifespan	The product is expected to function correctly for 6 to 7 years without any major maintenance
Solar Tracking Accuracy	The solar tracking system should achieve an angular deviation of no more than ±5° from the optimal alignment with the sun.
Wind Turbine Efficiency at Low Wind Speeds	Aim to achieve an efficiency of 35-40% at wind speeds ranging from 2 to 4 m/s, incorporating advanced technologies and design optimisations.
Design Performance in Terms of Reliability and Aesthetics	Reliability: The product should maintain operational functionality with minimal maintenance for at least 6 to 7 years. Aesthetics: The design should be visually appealing, achieving a rating of at least 4.5/5 in consumer surveys.
Time to Assemble and Install	The product should be fully operational within 15 to 25 minutes by two people, without the need for specialised tools
Environmental Resistance (Rain, Dust)	The product must comply with an IP65 rating as a standard, ensuring it is dust tight and protected against low-pressure water jets from any direction. This level ensures standard protection against most environmental conditions typically encountered in non-industrial settings.
Maximum Noise Level	The wind turbine should emit noise no more than 40 dB in accordance with IEC 61400-11 (Acoustic Noise Measurement Techniques)
Corrosion Resistance	The product is designed to achieve a minimum of 1000 hours of resistance to corrosion under standard salt

	spray (ASTM B117) conditions, ensuring long-term durability and structural integrity.
Wind Resistance	Design the wind turbine component of the product to withstand wind speeds up to 28 m/s (about 100 km/h) as specified by IEC 61400-2 for small wind turbines, ensuring it maintains structural integrity and operational capability in high wind conditions.
User Interface and Control	The product must feature a user-friendly interface that allows users of all technical skill levels to operate the system efficiently. The interface should include clear controls, visual indicators, and feedback mechanisms to facilitate easy operation and monitoring. The goal is to achieve a SUS score above 68, reflecting high usability.
Maintenance Frequency	The product should require routine maintenance no more frequently than once every 12 months under normal operating conditions, with each maintenance session designed to be completed within 2 hours or less.
Battery Charging Capacity and Grid Integration (technically out of scope)	Battery Charging Capacity: Equip the product with a high-capacity lithium-ion battery ranging from 20 Ah to 40 Ah, allowing for extended operational periods and reduced frequency of charge cycles under ideal conditions. Grid Integration Capability: Include an option for users to connect the device to the home grid, enabling not only energy self-sufficiency but also the potential to contribute excess energy back to the grid, enhancing overall energy efficiency and cost savings.
Maximum Manufacturing Cost	The total cost to manufacture each unit of the product should not exceed £2000. This cost includes materials, labour, manufacturing processes, and overheads, enabling the final retail price to be set competitively
Quality Assurance Practices	Implement a robust quality assurance program that includes reliability testing and compliance checks with a range of international standards applicable to the product's design, functionality, safety, and environmental impact, especially **ISO 12100** for general safety requirements and risk assessment of machinery and IEC 61000 Electromagnetic compatibility (EMC)
Smart Home Compatibility	The product must be compatible with major smart home platforms including but not limited to Amazon Alexa, Google Assistant, and Apple HomeKit. This compatibility should extend to common home automation protocols

	like Zigbee, Z-Wave, and Wi-Fi for comprehensive integration capabilities.
Blade Safety Features	The product must incorporate specific design features and technologies to reduce the risk of injury to humans and wildlife. This includes blade curvature, material selection, operational strategies, and possibly deterrent systems to minimize the potential for wildlife collisions.
Efficiency in Different Climates (Energy Conversion Efficiency)	Climate-Adaptive Efficiency: The product must demonstrate robust energy conversion efficiency in diverse climates, from cold and temperate to tropical environments. This includes maintaining operational efficiency in conditions of high humidity, varying temperatures, and different levels of solar exposure.
Folded Dimensions (For Portability)	The product, when folded, must not exceed dimensions of **1650 mm in any direction**. This compact size should be achieved through the use of collapsible parts and innovative folding mechanisms.

4 Deployable Product Design Development & Optimization

4.1 Optimisation for deployable outline

This chapter outlines the major optimisation efforts undertaken to transform the prototype into a robust, deployable hybrid renewable energy product. Section 4.2 begins by using Fault Tree Analysis (FTA) to identify critical failure modes, informing improvements across key subsystems such as the solar tracking mechanism and turbine blade geometry. The tracking system was upgraded to a dual-axis actuator design for greater energy capture and reliability, while rotor optimisation combined aerodynamic simulation with Bayesian methods to maximise power output across realistic wind conditions. Section 4.3 focuses on Design for Assembly (DFA), where modular redesigns—such as telescopic legs and camlock fasteners—reduced part count, assembly time, and user error, enabling rapid deployment in the field. Section 4.4 applies Structural Failure Modes and Effects Analysis (FMEA) in conjunction with Finite Element Analysis (FEA) to assess and enhance joint reliability, reducing risk priority numbers and improving structural integrity while cutting system weight by over 50%. Finally, Section 4.5 details Design for Manufacturing (DFM) efforts that enhance uptime and serviceability, including material upgrades, modular electronics, and field-replaceable components—all guided by RAM (Reliability, Availability, Maintainability) principles. Together, these interventions create a product that is not only more efficient, but also safer, lighter, easier to manufacture, and better suited for long-term outdoor deployment.

4.2 Fault Tree Analysis (FTA) of prototype design

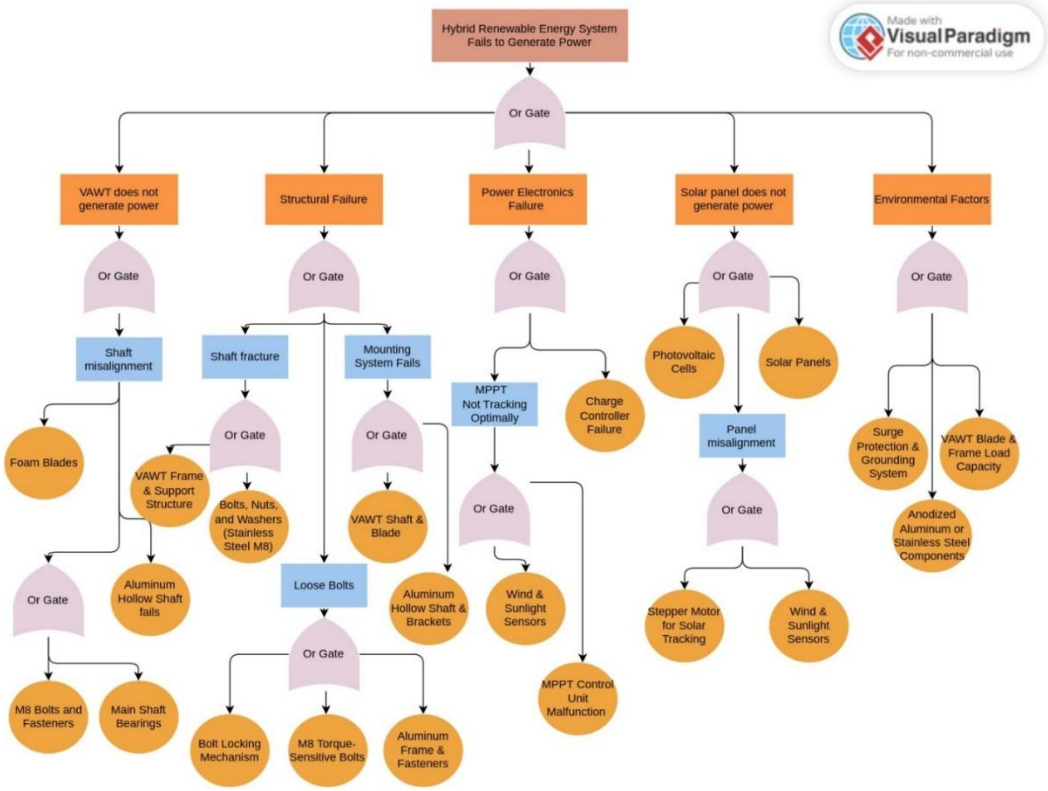

Figure 4.a: Fault Tree Analysis for Hybrid VAWT and Dual Axis Solar Panel System

High-Risk Failure Clusters Identified

The FTA reveals that mechanical failures in the VAWT system, particularly shaft misalignment and structural instability, are among the most failure-prone areas. These failures are propagated by foam blade deformation, loose fasteners, and undersized shaft components, highlighting weak links in both material selection and joint design.

Assembly-Dependent Failures are Common

Many failure modes—such as loose bolts, frame instability, and misalignment—can be traced to assembly quality. This suggests a need for simplified or modular connections and preloaded or self-locking fasteners to reduce human error.

Electronics and Sensor Reliability Are Crucial

The solar panel and MPPT subsystems are highly dependent on sensor input and control accuracy. Failure in sensors (e.g., due to dust or weather) leads directly to MPPT malfunction or panel misalignment. Therefore, weatherproofing and sensor calibration become high-priority improvements.

Environmental Loads Are a Cross-Cutting Risk

The "Environmental Factors" branch affects both VAWT structure and solar panels. Since many failures stem from external loads like wind, vibration, or corrosion, there

is a clear need for materials with better fatigue resistance and weather protection (e.g., anodized aluminium, stainless fasteners, grounding systems).

Redesign Priorities Are Clear

Components like foam blades, thin aluminium shafts, and standard bolts appear repeatedly across multiple failure paths. These are high-leverage redesign targets because upgrading them improves multiple branches at once.

Preventive Measures Reduce Systemic Risk

Adding surge protection, improving bolt locking, and upgrading bearings reduce risk not just in one branch, but system wide. This justifies their inclusion in the deployable version despite increased cost or complexity.

4.2.1 Solar Tracking Optimisation

The solar tracking system is a critical subsystem within the dual energy hybrid turbine, contributing to its overall power generation. In the design and prototype phase Section(2.2.6), the solar tracking solution was a single-axis mechanism, with a servo motor at one end of a rod clamped under the solar panel, rotating to tilt its orientation. Programmed to move from 0°-180° across an 8-hour window, based on fixed timing assumptions. Although effective compared to stationary panels, this solution exhibited significant limitations in terms of accuracy, adaptability to real conditions and locations, mechanical robustness, and long-term reliability.

For the deployable version, the tracking mechanism has been upgraded to a dual-axis system using linear actuators to precisely orient the panel both in azimuth and elevation. This section justifies the optimisation choice by systematically evaluating the weaknesses of the prototype and presenting a practical, theoretically grounded improvement. The FTA methodology from Section(4.1) was used to identify critical failure points in the prototype that this upgrade addresses.

4.2.1.1 Prototype Solar Tracking Weaknesses

1. **Single-axis movement,** only tracks azimuth rotation, ignoring seasonal variation in sun elevation and location; dependent on facing east, south, west or north (Logan and Raichle, 2012).
2. **Servo motor precision limits,** the MG996R servos operate under 1°–2° per control step (based on PWM signal granularity) thus resulting in having ±2° mechanical inaccuracies. However, when loaded with the solar panel, testing showed deviations up to ±7°, due to mechanical backlash and the absence of closed-loop feedback.
3. **No real-time sun position feedback**, the system moves predictively, across the axis from 0° to 180°, assuming a cloudless day and the mechanism is positioned facing the east and to the west following the sun.
4. **Low mechanical robustness**, due to their complex gear trains servo systems are susceptible to fatigue, dust ingress, and wear, especially in outdoor conditions as they have poor IP ratings.

These factors collectively reduce the effective solar energy captured, especially over extended deployments in diverse climates. These shortcomings are reflected in the FTA, where solar panel misalignment and lack of power generation are traced

through causes such as servo motor limitations, tracking control ineffectiveness due to lack of feedback, and sensor inaccuracies.

4.2.1.2 Experimental Verification of Servo Inaccuracy

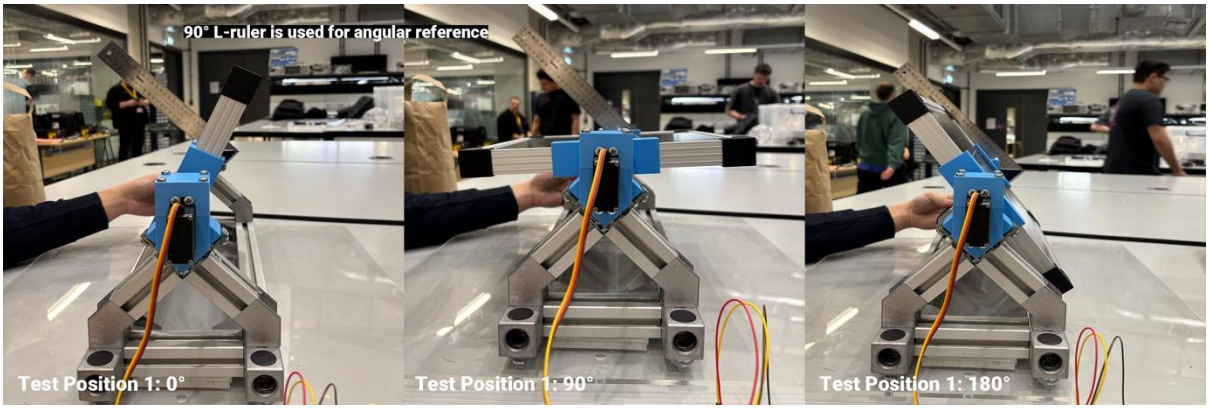

Figure 4.b: Single-axis Solar Tracking Testing

A simple test was conducted to empirically verify the tracking accuracy of the prototype's servo-based system under loading conditions. The servo was programmed to rotate the solar panel to 0°, 90°, and 180°, and a reference 90° ruler was used to visually validate the actual output angle. The findings indicated deviations ranging between 3° and 10° from the intended target angles. Notably, the deviations were inconsistent, suggesting that the weight of the mounted panel introduced additional torque that the servo could not adequately compensate for. In some cases, the servo slightly overshot or undershot the target angle, likely due to the non-linear loading across the panel's centre of gravity. These deviations support the hypothesis that the prototype's servo system lacks precision under variable loads, leading to angular misalignment and reduced solar energy capture. These real-world performance issues reinforce the need for a more robust and precise tracking solution, as implemented in the deployable version.

4.2.1.3 Deployable Optimisation: Dual-Axis Solar Tracking with Linear Actuators

Figure 4.c: Overall Deployable Solar Assembly

Technical Description

The deployable design features: **Azimuth control** (East-West rotation) via one linear actuator. **Elevation control** (Up-Down tilt) via a second linear actuator. **Control Options:** Either an LDR sensor array or a GPS + Time/Date-based algorithm.

Theoretical Efficiency Gains of Dual-axis Tracking

Solar tracking systems increase photovoltaic (PV) energy yield by maintaining optimal panel orientation to sunlight. Refer to Appendix A.3 for calculations. **In the prototype,** a deviation of $\pm 15°$ due to servo/control/overshooting error can cause a power percentage loss of about 3.41%. Over an entire day and season, these small inefficiencies compound into a net energy loss of 10–20%. However, this value is underestimated if the angular changes are in increased frequency.

Conversely in the deployable, using linear actuators, a dual-axis system can have lower deviation error. The linear actuators from Timotion have a 10-bit PWM control with ±0.5 mm repeatability or resolution (Timotion, 2025). The actuator pushes/pulls on a linkage attached to the solar panel to provide tilt. Thus, a system with optimal linear actuators would result in deviation error <1%. However, compensating for real-world factors such as backlash due to load, vibration, wind loading, sensor inaccuracy and thermal expansion, a maximum deviation of 5° is reasonable. Thus, expected loss of a dual-axis while maintaining a maximum deviation of ±5° is about 0.28%, significantly less than the single-axis.

This is also corroborated by NREL that suggest optimised dual-axis tracking is significantly better, with expected gains (Simon and Mosey, 2013). Single-axis tracking (prototype): +15–20% yield over fixed panels, while dual-axis tracking (deployable): +25–30% yield over fixed panels. Furthermore, accurate elevation control corrects for seasonal variation. Sun elevation angle changes by ~47° between winter and summer solstices (Patel and Patel, 2014). Single-axis tracking assumes average conditions, but dual-axis tracking actively adapts to maximise year-round efficiency.

Additionally, linear actuators also provide better mechanical and control highlighting DFMtn for maintainability. As linear actuators offer self-locking ability (mechanical stability when unpowered). Higher positioning accuracy (±0.5 mm linear resolution translates to <0.5° angular resolution). Longer lifespan (~5,000–10,000 cycles vs hobby servo ~1,000 cycles). Superior outdoor durability with IP65 or higher ingress protection (Tolomatic, 2022).

4.2.1.4 Dual-axis Solar Tracking Optimised Control Options

There are two control options that are optimised for the deployable model, significantly improved from the prototype's predictive approach. Either tracking sunlight directly through an LDR sensor (Mistri et al., 2018) or using a GPS+Time algorithm to determine sun position (Reda and Andreas, 2008). Advantages and disadvantages are discussed in Appendix A.3. Given the intended deployable outdoor application, where reliability and autonomy are critical, GPS+Time Algorithm are recommended. Solar tracking was done through calculation of azimuth and elevation angles by considering the location, date and time of the product. Example calculations and considerations are shown in Appendix A.3.

4.2.1.5 FTA Optimisation

The Fault Tree Analysis identifies "Solar panel does not generate power" as one of the top-level failure events. Within that branch, panel misalignment is a critical contributor, which is further caused by failures in either the stepper motor for solar tracking or wind & sunlight sensors. These were components used in the prototype. Additionally, the MPPT control unit was found to be vulnerable to environmental and calibration issues. These optimisations address FTA points through, replacing the stepper motor with precision-controlled linear actuators directly eliminates one primary cause of misalignment. Implementing a GPS + time algorithm removes dependency on wind & sunlight sensors, thereby eliminating another contributing fault.

4.2.2 Development of Blade Dimensions

A Fault Tree Analysis (see Section 4.2) identified one potential cause of failure in power generation as suboptimal blade geometry. Specific issues included excessive

stall, poor lift-to-drag performance, and unsuitable airfoil selection for real-world operation. This motivated a targeted blade optimisation process for the deployable version of the Vertical Axis Wind Turbine (VAWT), aiming to enhance energy output and stability across a wide range of Tip Speed Ratios (TSRs).

The initial prototype used a 200 mm chord, 400 mm height, and 200 mm radius blade, based on LS(1)-0413 airfoil data from literature. However, these dimensions were chosen under tight space and budget constraints, with limited simulation validation. The optimisation process detailed here aims to refine the geometry and airfoil profile based on robust simulation and design methods.

4.2.2.1 Methodology: LLFVW and QBlade

Aerodynamic simulations were conducted using QBlade software, which implements the Lifting Line Free Vortex Wake (LLFVW) method. This method efficiently models unsteady aerodynamics of H-type Darrieus turbines, capturing 3D wake effects without the computational overhead of full CFD (Balduzzi et al., 2017). This made LLFVW a practical choice for iterative design in a resource-constrained academic setting.

The analysis pipeline involved several key steps. First, XFOIL was used to generate polar data for various airfoils. To account for the full blade rotation, 360° polar extrapolation methods such as Viterna and Montgomerie were applied. This was followed by rotor-level simulations to evaluate torque and power coefficient (Cp) across a range of tip-speed ratios (TSRs). Finally, Bayesian Optimisation using Gaussian Process Regression (GPR) was implemented to iteratively refine the blade geometry.

4.2.2.2 Optimisation Results

Two rounds of optimisation were conducted:

1. **Maximum Cp at Optimal TSR:** Designs with Cp exceeding 0.77 were identified, notably:
    - Test 4: (c=200 mm, H=512 mm, R=214 mm), Cp = 0.7768
    - Test 7: (c=200 mm, H=484 mm, R=215 mm), Cp = 0.7745
2. These configurations showed strong peak performance, but limited robustness across a broader TSR range.
3. **Maximising Mean Cp Across TSR Range:** A second optimisation focused on maintaining high Cp across realistic TSR fluctuations. Results included:
    - Test 4.1: (c=70 mm, H=1000 mm, R=500 mm), Cp_mean = 0.3617
    - Test 5.1: (c=70 mm, H=800 mm, R=500 mm), Cp_mean = 0.3617
4. These results showed significant improvement over the prototype (mean Cp = -0.09) and indicated the benefit of a smaller chord and larger radius for wider operating bandwidth.

See Appendix A.1 for detailed simulation results and parameter sets.

4.2.2.3 Final Blade Design Recommendation

Based on trade-offs between performance, portability, and structural considerations, the final recommended blade configuration is:

- Chord (c): 70 mm
- Blade Height (H): 800 mm
- Radius (R): 500 mm

This setup supports efficient performance under varied wind conditions while remaining within deployment and assembly constraints.

4.2.3 Variable Pitch Mechanism

To mitigate the risk of stall at low TSR and improve self-starting behaviour, a cam and follower-based variable pitch mechanism is proposed. This mechanism allows the blade pitch to change with azimuthal position, based on a predefined pitch schedule derived from QBlade simulation data.

Compared to passive hinge systems, this approach offers deterministic control of the angle of attack (α), ensure minimized flow separation, increased tangential lift and smoother torque generation

Experimental data from literature [ref4] supports this approach, with observed Cp improvements and successful self-starting at TSR = 2.5. The added complexity of a cam profile is offset by the reliability gains, making it suitable for a deployable, consumer-oriented product.

Further comparison of pitch mechanisms and spring-loaded cam design is included in Appendix A.2.

4.2.4 Performance Improvement Summary

Compared to the original prototype, the optimisation process led to substantial improvements in aerodynamic performance and operational stability. The prototype configuration (c = 200 mm, H = 400 mm, R = 200 mm) achieved a maximum power coefficient (Cp) of 0.7555, but its mean Cp across a realistic Tip Speed Ratio (TSR) range was negative (-0.090), indicating that the turbine frequently operated in inefficient or stalled conditions.

The final optimised blade configuration (c = 70 mm, H = 800 mm, R = 500 mm) achieved a mean Cp of 0.3617, marking a more than 450% improvement in average efficiency under variable wind conditions. Additionally, the integration of a cam and follower-based variable pitch mechanism allows the turbine to actively maintain its operation near the optimal TSR. This ensures that the turbine consistently achieves high Cp, even as wind speed varies, stall risk is significantly reduced, and self-starting performance is improved, enhancing reliability in low wind speeds.

Metric	**Prototype**	**Final Design**	**% Improvement**
Peak Cp @ Optimal TSR	0.7555	0.7768	+2.8%
Mean Cp Across TSR Range	-0.090	0.3617	+502%
Starting Torque Consistency	Poor (non-starting)	Improved (with pitch control)	Qualitative Gain

Figure 4.d: Metric Comparison

These enhancements make the deployable product significantly more robust, energy-efficient, and user-friendly, fulfilling its intended role as a portable hybrid renewable energy solution. Based on the C_p value that we obtained, we can achieve a power output from the VAWT as designated in the specifications (10-20 W) under assumed wind conditions.

4.3 Design for Assembly (DFA) Optimisation

4.3.1 Prototype vs Deployable Base Structure: Part Count Reduction

As the project transitioned from prototype to deployable product, a focused Design for Assembly (DFA) initiative was conducted to address the high component count, long assembly times, and complex sub-assemblies observed in the initial design. While the prototype achieved its functional goals, its intricate structural layout—with over 60 unique parts and more than 700 total components—posed significant assembly and deployment challenges.

4.3.1.1 Prototype Assembly Complexity

Some issues that were identified during the assembly and testing phase include turbine arm joints required multiple brackets and precision-fastened aluminium profiles, the solar tracking mechanism requiring custom-fabricated motor mounts, gear couplers, and bracketed shafts and the blade mounting depending on precise alignment between aluminium profiles and multiple screw types. These assembly demands translated into high risk of human error, a prolonged assembly time (>45 minutes) and increased labour cost and lower maintainability.

4.3.1.2 DFA Objectives and Strategy

The DFA review set out to minimise part diversity through standardisation and consolidation, reduce the number of fastening steps via smart modular connections, improve portability and user-friendliness for low-skill installation and quick deployment. The strategy involved mapping all fasteners and interfaces, identifying opportunities for multifunctional joints and tool-less connections and referencing commercial best practices for collapsible and telescopic structures.

4.3.1.3 Implemented Optimisations

- Scissor-Strut Folding Mechanism: A compact and collapsible base frame was introduced using scissor struts with pivot pins and hinge brackets. This allows the structure to fold flat and be quickly locked into place using detent pins. (See *Appendix A, Figure 8.e: Scissor Leg Diagram*).
- Telescopic Legs with Detent Locking: Legs supporting the turbine are now telescopic and secured via locking pins, inspired by furniture-grade adjustable supports. This removes the need for custom-fabricated height brackets. (See *Appendix A, Figure 8.f: Telescopic Leg Concept*).
- Bracket Rationalisation: The number of screw variants was reduced from 12 to 5. Standardised brackets and universal fasteners improve interchangeability and make the system more user serviceable.
- Slotting Mechanism for Blades: Instead of screwing the arms to the blades, the user will sandwich the blades between the arms by slotting the extrusion from the arm into the pivoting hole in the blade. This fully eliminates the need

for screws in this part of the build (See Appendix A, Figure 8.g).

4.3.1.4 Quantified Improvements

Metric	Prototype (Before DFA)	Deployable Product (After DFA)
Total Part Count	~700	<400
Unique Components	>60	~35
Assembly Time	~45–60 minutes	<15 minutes
Tools Required	3–4 types	1 universal Allen key
User Assembly Skill Level	Professional	Beginner
Assembly Error Risk	High	Low

Figure 4.e: Quantified Improvements

These improvements align directly with our goal to deliver a consumer-ready, modular hybrid energy system that can be assembled with minimal training or tools, making it highly suitable for disaster relief, off-grid communities, or urban users.

These changes, guided by DFA principles and informed by existing commercial solutions (see *Appendix A, Figures 8.e, 8.f and 8.g*), not only simplify the system but also elevate it to a deployable product ready for real-world conditions. These improvements align directly with our goal to deliver a consumer-ready, modular hybrid energy system that can be assembled with minimal training or tools, making it highly suitable for disaster relief, off-grid communities, or urban users. These changes, guided by DFA principles and informed by existing commercial solutions (see Appendix A, Figures *8.e, 8.f and 8.g*), not only simplify the system but also elevate it to a deployable product ready for real-world conditions. Importantly, the structural integrity of the redesigned joints and collapsible features has been rigorously validated through Finite Element Analysis and Failure Mode and Effects Analysis. This is documented in detail in Section 4.4.

4.3.2 Prototype vs Deployable Base Structure: Weight Optimization

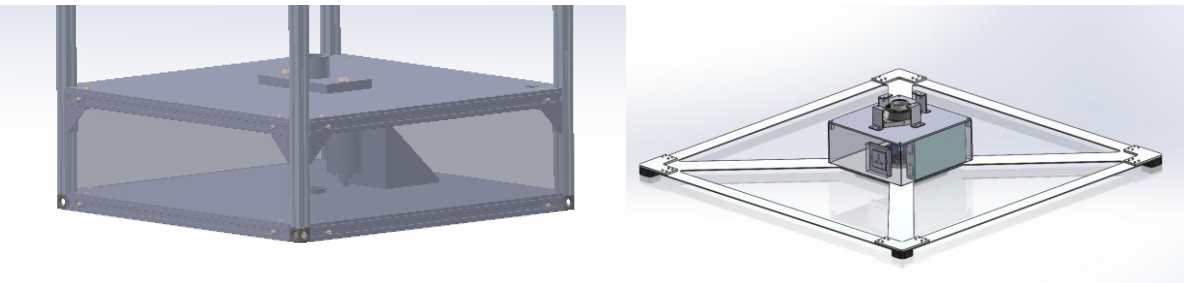

Figure 4.f: Comparison between the prototype base structure (left) and the optimized deployable base structure (right).

Description of Original Prototype Base

The original prototype base was designed with the primary goal of maximizing rigidity

to support a full integrated system. It consisted of a heavy bolted frame made from aluminium square tubes and flat plates, assembled using over 60 unique components. The compact footprint of 500 mm × 500 mm, while space-efficient, contributed to a high total mass of approximately 14.2 kg. This structure required a significant assembly effort, with many fasteners and intricate subassemblies, resulting in a long assembly time and increased potential for human error. Although structurally sound and robust, the prototype lacked portability and was not optimized for deployment in field or disaster-relief scenarios.

Description of Optimized Deployable Base

In contrast, the optimized deployable base was redesigned with a focus on weight reduction, ease of transport, and quick assembly. The new design features an X-strut layout constructed from laser-cut aluminium 6061-T6 sheets. By adopting thinner materials and simplifying the geometry, the overall volume and weight were significantly reduced. The deployable base spans a wider footprint of 1100 mm × 1100 mm, which increases ground stability and eliminates unnecessary material from the central region. Rubber pads were integrated at each corner to dampen vibrations without requiring extra assembly, contributing to better mechanical resilience and user convenience. Fastener count was minimized by using welded joints and modular part designs, further simplifying the assembly process. While lighter, the base remains functionally strong and serves as a stable anchor for the structure, ensuring performance is not compromised.

Feature	Prototype	Deployable
Material	Aluminium Frames + plates	Laser-cut aluminium X-struts
Total Weight	14.2kg	9.1kg
Assembly	Bolted frame	Welded/cut parts + Bolted frame
Footprint	Box Shape	Flat, wide base
Portability	Poor	Easy to deploy
Stability	Rigid	Wide Stance
Base area	500mm x 500mm	1100mm x 1100mm

Figure 4.g: Quantified Improvements

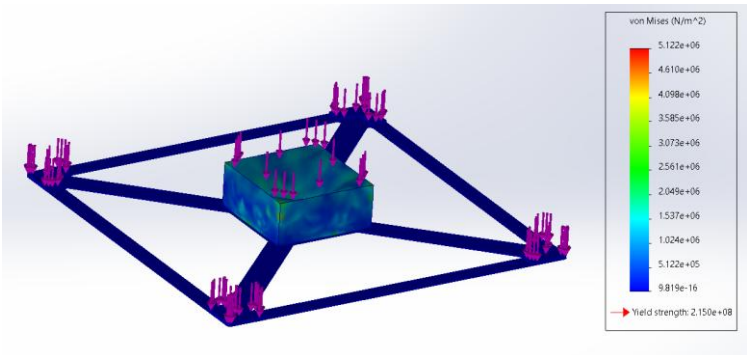

Figure 4.h: Von Mises stress distribution under 1000 N load on the base structure. The maximum stress observed is 5.12 MPa, well below the yield strength of 215 MPa for Aluminium 6061-T6, indicating a safe design.

Despite the transition to a lighter base structure for improved portability, the simulation demonstrates that the new design retains sufficient structural integrity. The peak stress of 5.12 MPa under the applied load of 1000 N results in a safety

factor of over 40, indicating that the structure can easily withstand the intended loading conditions without risk of yielding or failure.

The stress is well-distributed across the X-frame members and the central housing, with no critical stress concentrations. This confirms that the geometry and material selection—Aluminium 6061-T6—remain suitable even after the mass optimization. Therefore, the design achieves a successful balance between weight reduction and mechanical reliability, validating the deployable base as both lightweight and structurally sound.

The new deployable base balances portability and stability, offering a 36% weight reduction and faster assembly. While welded joints limit reconfiguration compared to a fully bolted frame, the simplified layout and use of standard parts enhance manufacturability, reduce human error, and improve vibration resistance. Importantly, even with weight reduction, the base retains sufficient mass and footprint to function as an effective anchor, ensuring structural stability during operation.

4.3.3 DFA Solar Assembly

Efficient assembly and ease of maintenance are crucial to the success of the deployable Dual Energy Hybrid Turbine. While the prototype featured a structurally sound frame, the assembly method of the solar panel mounting was manual, time-consuming, and heavily reliant on conventional fasteners (screws and bolts). This led to significant challenges in terms of rapid deployment, error-prone assembly, and maintenance complexity. For the deployable version, the solar assembly interface is optimised by introducing a vent camlock system and snap-fit technic pins at critical junctions. This section applies Design for Assembly (DFA) principles to justify and analyse the improvement.

4.3.3.1 Prototype Assembly Weaknesses

Several common weaknesses during the assembly of the prototype was, numerous manual screwing and bolting required for fixing the solar panel to the turbine frame, some unoptimised for quick assembly. High tool dependency (screwdrivers, spanners needed on-site). Long assembly time, averaging 15–20 minutes for the solar section alone. Potential misalignment due to human error during manual attachment. Increased wear and risk of overtightening, causing long-term mechanical degradation. These issues increase the probability of assembly faults and maintenance needs in real-world deployments.

4.3.3.2 DFA Principles Deployable Assembly Optimisation

Optimisation made for the deployable product include a vent camlock system locks the main shaft of the solar tracker into a base plate. Technic-style snap-fit pins secure the solar assembly onto the top of the VAWT. Only minimal screwing (1–2 screws) is required for final securing, primarily as a safety backup rather than for structural load bearing. Shaft and linear actuator components are firmly attached but foldable to achieve ease of storage and deployment.

This arrangement significantly simplifies installation while maintaining mechanical integrity.

DFA Principle	Prototype	Deployable Optimisation
Minimise number of parts	Multiple bolts and screws	Single camlock + snap-fit pins. Screws and bolts only

		when necessary
Reduce tool use	Required screwdriver/spanner	Tool-free primary assembly
Simplify assembly motions	Sequential bolting	Snap-in and twist-lock motions
Ensure easy orientation and insertion	Alignment prone to human error	Self-locating features via camlock and pins
Facilitate modularity and maintenance	Full disassembly needed	Quick release for servicing

Figure 4.i: DFA Solar Assembly

By focusing on part reduction, simplification of tasks, and elimination of unnecessary tools, the new design conforms strongly to best-practice DFA metrics.

4.3.3.3 Mechanical and Reliability Considerations of Optimised Design

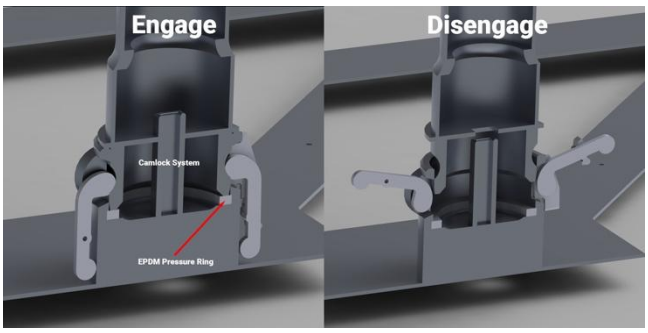

Figure 4.j: Camlock System

The deployable camlock mechanism operates by converting rotational motion into axial locking. Its torque advantage requires only moderate hand torque to achieve secure locking (~2–3 Nm). Reduces redundancy as the camlock systems naturally resist vibration loosening, particularly due to the EPDM Shore A 60 pressure ring, a key optimization required in wind-exposed structures. Even though its mechanically moderate, there are supports on the rod section that pushing against the solar plate, thus reducing the fatigue to the camlock system.

Figure 4.k: Technic Pins

Technic Snap pins, it is friction-fit cylindrical pins resist pull-out via radial compression. Allow repeatable engagement/disengagement without damage. Self-locating feature: Pins automatically guide the solar mount into correct position.

4.3.3.4 Assembly Time

Stage	**Prototype Assembly Time**	**Deployable Assembly Time**
Frame to Turbine Top	~15 min (manual bolting)	~5 min (snap-fit + camlock)
Solar Shaft Attachment	~5 min (alignment + screw)	~1 min (camlock snap)

Figure 4.l: Assembly Time

Overall reduction: Up to 70% faster assembly for the solar panel mounting.

4.4 Structural FMEA optimisation

This optimization aimed to enhance the mechanical performance of a deployable renewable energy structure by improving its strength-to-weight ratio and ensuring stability under self-weight and wind loading. Key criteria included structural integrity, material efficiency, and redundancy.

Two core methods were applied: Failure Modes and Effects Analysis (FMEA) to identify and prioritise risk in individual components using Risk Priority Numbers (RPN), and Finite Element Analysis (FEA) to assess stress and deflection under expected loads. FMEA highlighted critical weaknesses, while FEA validated mechanical responses of submitted designs.

By integrating risk analysis with computational modelling, the redesign process targeted both functional and structural improvements, with success measured through reductions in RPN and sound mechanical performance.

4.4.1 Overview of Initial Prototype

The original prototype featured a rectangular frame made from standard aluminium extrusions, with four tiers of horizontal members. The top and bottom tiers were joined to vertical members using three-way corner connectors, while the middle tiers used standard aluminium corner brackets.

These brackets, secured with screws, were critical in transferring both vertical and lateral loads. Early assessments flagged these joints as potential weak points, especially under combined shear and bending loads.

To evaluate structural risk more formally, an FMEA was carried out. Key failure modes were identified for each component, with Risk Priority Numbers (RPNs) calculated using standard Severity, Occurrence, and Detectability scoring.

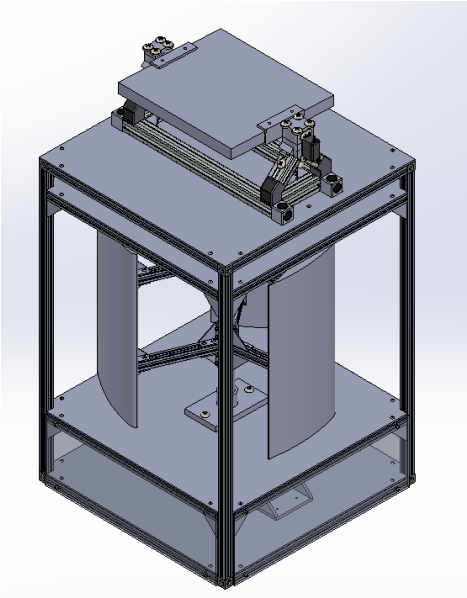

Figure 4.m - Prototype SolidWorks

4.4.2 Initial FMEA Findings (Prototype)

Though there is lots of documentation on FMEA methodologies in Engineering, there is not a consensus on what constitutes a ‘dangerous’ RPN, as it can often be case dependent. Therefore, at the start of this FMEA procedure we had to decide what RPN value would identify the risk threshold for this product. We decided that we were going to have the cut-offs designed as follows.

RPN	Designation	Response
0 - 100	Safe	No design changes needed
101 - 150	Okay	Only needs design changes if nothing else is higher
151<	Unsafe	Needs significant design changes

Figure 4.n - RPN Benchmarking

The most critical component identified was the corner bracket, with an RPN of 192 associated with potential fracture due to crack initiation. This value exceeded the acceptable design risk threshold and highlighted the joint as a weak point in the structure. Table regarding FMEA 1 RPN scores can be found in Appendix A.

This high RPN was largely due to a combination of:

- High severity (8) as joint failure could compromise structural integrity, since it is the main load translation component.
- Moderate occurrence (6) due to regular load cycles, handling and deploying.
- And less than moderate detectability (4) since internal cracking might not be immediately visible without disassembly or inspection, though would be somewhat noticeable due to reduced functionality.

Additionally, although there was only one RPN that placed higher than our risk threshold value of 150, the majority of failure mode RPNs that fell into our 'Okay' range also belonged to the corner bracket component. This indicated that the corner bracket's likelihood to fail is significantly higher than any other component.

This initial FMEA provided the direction for optimisation, as it became clear that joint performance would need to be addressed first in any redesign seeking to improve reliability and reduce failure risk.

4.4.3 Finite Element Analysis of Prototype

To assess the mechanical performance of the initial cage design under expected load conditions, an FEA was performed using ANSYS Mechanical. This simulation aimed to evaluate the structural behaviour in typical loading scenarios and identify areas of potential failure, particularly in the joints. The Simulations setup for the first round of FEA can be found in Appendix A.

FEA Results

The FEA for the first cage structure revealed a maximum deflection of 0.0009 mm, occurring at the midspan of the horizontal beams. This value, though small, highlights the location of peak displacement under loading and reflects the relatively stiff response of the structure overall. The maximum stress was measured at 0.4 MPa, localised at the edge regions of the corner brackets. This stress concentration indicated that these joints were the primary mechanical weak points in the prototype — a finding that directly aligned with those flagged in the initial FMEA. The FEA 1 results can be found in Appendix A.

The average stress across the structure was calculated to be 8.97×10^{-2} MPa, suggesting that, aside from these concentrated regions, the overall structural load was well distributed and within a comfortable safety margin. These results provided a strong baseline for evaluating future design iterations and underscored the corner bracket as the critical component requiring optimisation.

Interestingly, the wind load applied had a negligible effect on the results we got from the contour plots, specifically no noticeable change in the average or max values of deflection of equivalent stress. However, this was not completely unexpected to us, due to the very low available surface for a wind load to act on. The thickness of the members used for this cage are much thinner than the total available space of the product, therefore a small pressure was expected from the wind load.

Strangely, the factor of safety tool that is usually available for use within Ansys was for some reason unapplicable to our design, as every time we tried it just showed contour plots of each solid member having a Factor of Safety (FoS) of 15, as shown in the appendix. Whether it was due to element limits, or faulty software, we felt it better to just supplement the FEA results with FoS hand calculations. Considering a

yield case, which for Aluminium 6061 is approximately 275 MPa, we calculated the FoS to be;

$$FoS = \frac{275}{0.4093} = 671.88$$

As our highest recorded max equivalent stress was reported to be 0.4093 MPa. Since static structural applications have very low limits for what is considered 'safe', with some applications accepting FoS values as small as 2, a value of 672 shows this design to be incredibly structurally sound, to the point that one could assume overengineering from this value alone. This indicates that material usage can be reduced significantly in the deployable unit without sacrificing strength values too much.

Areas of Concern

Upon solving the prototype model, the results revealed that the highest stress concentrations were localised in the corner brackets, particularly around the zones where they interface with adjacent members. Meanwhile, the greatest deformation was recorded at the central point of the horizontal members. Although the peak values—1.691 MPa for stress and 0.0037678 mm for deformation—do not indicate critical failure in isolation, the location of the stress concentration is significant.

The prominence of stress within the corner brackets supports the findings from the FMEA, reinforcing that these joints represent a primary area of concern in the original design. This correlation between simulated stress distribution and identified failure modes helped justify the decision to target the corner brackets as a focal point for subsequent optimisation efforts.

4.4.4 FMEA for New Design

To assess the risk profile of the redesigned deployable unit, a separate FMEA was conducted for its major components: scissor struts, telescopic legs, and hinges. The goal of this evaluation was to verify whether the design modifications effectively addressed the critical risks identified in the original prototype—specifically, the vulnerability of rigid corner brackets.

Since we are dealing with less components in this FMEA, we felt it beneficial to increase the number of failure modes per component from five to eight, as this would mean we can compare a similar number of RPNs between the prototype and deployable unit designs.

Comparison with Prototype FMEA

In the initial prototype, the most critical failure mode was the structural failure of corner brackets due to crack initiation, which yielded an RPN value exceeding 150 due to high severity and moderate occurrence. Table regarding FMEA 2 RPN scores can be found in Appendix A.

In contrast, the new design demonstrates a significant reduction in RPN scores associated with the joints. There are no RPN values in excess of 150, meaning none of our components are what we have defined as 'Unsafe', as well as a reduction of 'Okay' graded failure modes, dropping from seven in the protype, to five in the deployable unit FMEA.

The redesigned modular hinge joints, which replaced the critical corner brackets, have significantly lower RPNs due to improved load distribution, greater flexibility,

and easier visual inspection during maintenance and use cases. The reduction in the highest RPN score from 192 to 126 between the two FMEAs provides a strong quantitative indication that the updated design carries a lower risk of failure through repeated use.

4.4.5 FEA of New Design

To assess the structural changes introduced in the deployable unit redesign, a second round of FEA was carried out. This mirrored the original prototype's testing conditions to allow for direct comparison of results across both structural versions.

Results and Analyses

The FEA results of the deployable unit design revealed an increase in both stress and deflection compared to the original prototype; however, these changes were well within acceptable limits for the current application. The maximum stress rose from approximately 0.4 MPa in the original design to 3.6 MPa in the new one, while deflection increased from 0.0009 mm to 0.09 mm. Average stress also saw a minor rise, from 0.0897 MPa to 0.16 MPa. These increases, while measurable, remain safely within the elastic range of aluminium 6061-T6 (yield strength ~275 MPa), and do not present a structural concern. The FEA 2 results can be found in Appendix A.

One key observation in the second simulation was the presence of higher stress concentrations near the modular joint interfaces. Stress contour plots showed deeper blue regions surrounding the joints in the new design compared to the prototype, indicating that the majority of stress was concentrated more locally. While this might traditionally indicate a less favourable stress distribution, it was anticipated due to modelling simplifications. Specifically, the bonded contact between the flat rear face of the joint and the curved surface of the telescopic leg omitted an intermediary component that, in practice, would provide a more substantial bonding interface. This likely contributed to both the elevated peak stress and its localisation.

With more refined modelling—incorporating additional geometric detail and realistic contact interfaces—it's reasonable to expect lower maximum stress values and a more uniform stress field across joint regions. As such, the observed stress concentration is considered a product of reduced model fidelity rather than a reflection of compromised structural performance.

Importantly, the second design achieves these results while reducing overall system weight, thus improving the strength-to-weight ratio—a primary goal of the optimization. As part of the design evaluation, a comparative weight analysis was conducted between the original prototype and the final deployable structure. In the previous term, we performed a detailed weight estimation and determined that the structural elements of the original prototype contributed approximately 13.61 kg to the total system mass. For the new deployable unit, the volume of structural components was measured using our assembly modelling software, yielding a value of 2,283,023.6 mm^3. Applying the density of aluminium (2.7 g/cm^3), this results in an estimated structural mass of roughly 6.16 kg.

This indicates a clear reduction in structural weight between the two designs. More notably, the deployable unit is physically larger than the initial prototype. Therefore, if we were to scale the prototype up to match the deployable unit's dimensions, the relative mass advantage of the new design would become even more significant. This underscores a key outcome of the optimisation process: improving the strength-to-weight ratio without compromising structural performance, which is especially

valuable for portable, field-deployable systems.

Once again, the FoS tool in Ansys was not usable for this design, meaning we needed to perform our own hand calculations.

$$FoS = \frac{275}{3.6651} = 75.03$$

Whilst noticeably lower a value than the previous FoS calculation, an FoS value of 75 still indicates a very structurally sound design, with the reduction showing some evidence of an improved strength-to-weight ratio. Additionally, as with previous points that have been made, we would expect this value to increase with higher fidelity simulations of the design, as we have already shown how the peak stress value has been overexaggerated due to modelling simplifications. Ultimately, however, this calculation still quantifiably shows that the yielding of this device under normal operating parameters is a very unlikely event based on the recorded max stresses, and the mechanical properties of the material.

4.4.6 Discussion

The optimisation process demonstrates a clear correlation between improvements identified in the FMEA and the results obtained through FEA, validating the design evolution from both a risk management and structural integrity perspective.

Structural Safety and Performance

While the second design shows higher peak stress (3.6 MPa vs 0.4 MPa) and deflection (0.09 mm vs 0.0009 mm), these values remain comfortably within the safe operating limits for aluminium 6061-T6. The increase is negligible in practical terms and does not pose any structural risk.

Notably, average stress values between the two models are much closer than the maxima suggest. This indicates better global load distribution in the second design, despite localised stress peaks — largely attributed to modelling simplifications. This broader distribution likely improves fatigue performance, which is vital for deployable field structures.

The integration of modular hinges provides practical advantages in assembly and maintenance, without compromising structural integrity. FEA confirms stress and deflection in these areas remain well below critical thresholds.

Though the legs and struts weren't the primary focus, their excellent mechanical behaviour in simulation — combined with a reduction in weight — supports a stronger strength-to-weight ratio. This aligns with a central aim of the optimisation.

Another significant outcome of the optimisation process was the demonstration of structural resilience under wind loading conditions. Across both FEA simulations—on the original and the optimised designs—the influence of a 25 m/s wind load proved to be negligible, with no meaningful changes observed in overall structural stability or stress distribution. This is a strong indicator that both configurations were built to a high standard with respect to aerodynamic loading.

Importantly, this performance aligns with and even exceeds the benchmarks laid out in IEC 61400-2, which specifies 28 m/s as a typical reference wind speed for the safe operation of small wind turbines. Since our structure remained structurally sound under 25 m/s in simulation—very close to the IEC threshold—it offers confidence that the system would perform reliably under normal operating conditions, even in

adverse weather environments.

Reliability Under Loading

The deployable design demonstrates strong reliability under static gravitational and lateral wind loads, as confirmed by both FEA and FMEA. While dynamic loading wasn't explored due to its minimal impact, the structure's stable performance — despite reduced material use — supports its robustness for outdoor or temporary deployments. The reconfigured load paths and modular components contribute to improved adaptability in variable environments.

Optimisation Validation

Between the two FMEAs, the highest RPN value dropped from 192 to 126, and all stress values remained within safe operational limits, validating the redesign's effectiveness. Although the average RPN rose slightly due to a more detailed failure analysis, it remains within acceptable bounds and reflects deeper component scrutiny rather than increased risk.

Ultimately, the second design offers more than just numerical improvements — it represents a balance between structural efficiency, mechanical safety, and user-centred practicality. The optimised unit is lighter, easier to handle, and structurally dependable, fulfilling both the technical and practical goals outlined in the design brief.

4.4.7 Limitations

Inconsistent Failure Modes Across FMEAs

The first design evaluated five failure modes per component, while the second assessed eight. This was intended to balance total failure scenarios (25 vs 24), given the reduced number of parts in the deployable unit. However, assigning more failure modes to fewer components may inflate perceived risk at the component level and distort average RPN comparisons. Future analyses should maintain a consistent number of failure modes per part, or alternatively normalise RPNs to ensure fairer cross-design comparisons.

Modelling Simplifications in Second Design

To manage complexity and work within the limitations of the ANSYS Student license, several geometry and contact approximations were used.

The hinge assemblies were approximated as solid triangular blocks rather than fully detailed components, and the telescopic features of the legs were excluded entirely from the geometry. Additionally, all contact definitions were simplified to bonded interfaces, replacing more realistic representations such as sliding or frictional joints. To conserve computational resources, fine mesh refinement was limited specifically to hinge regions where stress behaviour was expected to be more critical. Finally, a symmetry boundary was introduced to halve the model size, effectively reducing solution time without compromising the accuracy of global results.

These assumptions helped reduce computation time but may have introduced inaccuracies in load paths and stress concentrations—particularly in joints where curved faces were simplified to flat surfaces. Future improvements should include more representative joint modelling, frictional/cylindrical contacts, and mesh convergence studies to validate accuracy. Access to high-fidelity tools or computing

clusters would significantly enhance modelling precision.

Manual Factor of Safety Calculations

Without access to ANSYS' built-in FoS tools, safety margins were calculated manually using maximum stress values from the FEAs and material yield strength. While valid, this approach lacks element-level resolution, potentially overlooking localised weaknesses. In future studies, automated FoS visualisation or batch-processing of simulation data could provide more detailed insight into critical regions.

RPN Benchmarking Ambiguity

There are no universally accepted RPN thresholds for structural systems, so custom ranges were defined. While necessary, this introduces subjectivity and may affect how risk is interpreted—especially since the second design had a higher average RPN despite improvements. For greater rigour, future work should align with established frameworks, such as the ISO 14971 standard for risk management, or reference RPN norms from relevant industries like aerospace or civil engineering.

4.5 Design For Manufacturing (DFM) Optimisation

4.5.1 Uptime-Focused Design Optimization

This section focuses on optimizing a hybrid wind-solar energy system for extended uptime in remote environments. The design enhances subsystem reliability and field maintainability using RAM metrics (MTTF, MTTR, Availability) to guide material and structural improvements. Optimization strategies were applied to blades, bearings, electronics, and enclosures based on stress modelling, failure data, and real-world servicing needs. The performance of each subsystem is measured using **RAM metrics**: **MTTF (Mean Time to Failure)** – how long the system operates before failure occurs, **MTTR (Mean Time to Repair)** – how long it takes to restore functionality after failure, and **Availability (A)** – defined as: **A = MTTF / (MTTF + MTTR)**

4.5.1.1 Rotor Blade Optimization

Blade Failure Modes and CFRP Upgrade (↑ MTTF)

The original foam blades, mounted via aluminium brackets, suffered from UV damage, rain erosion, and high root stress, making them unfit for long-term deployment. These issues reduced the system's Mean Time to Failure (MTTF) due to fatigue and surface wear. In response, the blades were redesigned using carbon fibre–reinforced polymer (CFRP) for its superior fatigue resistance and durability in harsh climates. To further extend service life, a polyurethane-based leading-edge coating was applied, which, according to Keegan et al. (2013), can add up to five years of protection in erosive environments.

Flanged Joint for Easier Field Repair (↓ MTTR)

The rotor-hub interface has been upgraded to a bolted flange joint using standard A4-grade stainless steel fasteners. Among various blade root joint options—such as embedded inserts, T-bolts, and stud connections, the flange joint was selected for its

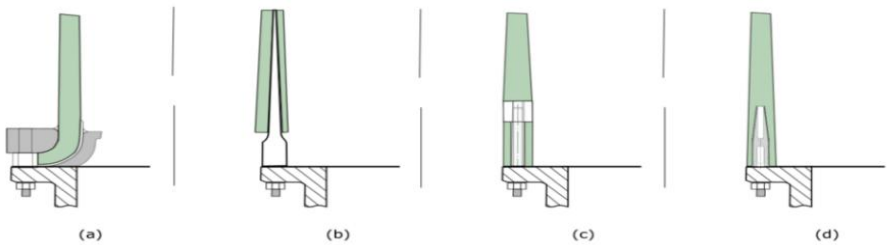

Figure 4.o: Blade root joint design options: (a) traditional flange bolted connection, (b) embedded insert hub, (c) T-bolt joint, and (d) stud insert. The commercial design adopts the flange-type connection (a) to distribute loads evenly and facilitate easier blade replacement in the field. https://www.mdpi.com/1996-1073/10/8/1112

superior load distribution, alignment simplicity, and ease of field maintenance (Figure 1). It allows damaged blades to be replaced without disturbing the entire hub assembly.

This design spreads cyclic loads across a larger area of the blade root, reducing the likelihood of fatigue crack initiation. Optimised bolt geometry—specifically, reduced-shank bolts—further lowers stress concentrations in the joint. According to Ha (2020), using such bolts can reduce the Stress Concentration Factor (SCF) by 44.8%, from 5.40 to 2.98. The SCF is defined as: $SCF = \frac{\sigma_{\max}}{\sigma_{nom}}$

This reduction in SCF significantly enhances joint fatigue life. Table x , adapted from (Ha's ,2020) study, compares different bolt configurations and their influence on SCF based on finite element analysis.

Nut Type	Shank Type	Norm Diameter (mm)	Norm Stress (MPa)	Max. Principal Stress (MPa)	SCF	Reduction
Standard	Straight	37.1	369	1995	5.40	0% (base)
Standard	Reduced	28	650	1936	2.98	44.8%

Figure 4.p: Bolt shank effect on SCF (connected with standard nut type)Source: Ha, K. (2020). Reduction of Stress Concentration Factor (SCF) on the Bolted Joint Connection for a Large Wind Turbine Rotor Blade through Various Design Modifications. Applied Sciences

Field repairs are also improved. Damaged blades can be swapped in under an hour using hand tools, significantly reducing MTTR. The modular flange layout allows for quick disassembly without affecting hub alignment. This aligns the blade subsystem with long-term maintainability goals in remote or off-grid applications.

Blade-Level Optimisation Summary

The combination of fatigue-resistant materials, protective coatings, low-SCF joint geometry, and modular field-repair features creates a robust, maintainable blade system. These upgrades directly address the key failure modes identified in the prototype and support long-term system reliability in real-world deployment conditions.

4.5.1.2 Shaft and Bearing System Optimisation

Fatigue-Resistant Shaft Materials (↑ MTTF)

The original aluminium shaft lacked corrosion and fatigue resistance, especially under fluctuating wind loads. A high-strength nitrided alloy steel shaft was selected for the commercial design to significantly increase the endurance limit. MDPI (2023) reports over 40% longer fatigue life with surface-treated steel versus untreated aluminium, particularly in variable-load environments like offshore sites (Vishwa, 2024).

Dual-Support Bearings to Reduce Misalignment (↑ MTTF)

The prototype's single-bearing design caused angular misalignment and bending stress. A two-point support system was introduced, using a double-row tapered roller bearing at the rotor end and a cylindrical roller bearing at the opposite end. This layout distributes axial and radial loads more evenly and reduces deflection. The dual-bearing concept improves load symmetry and shaft stability as illustrated in Figure X (MDPI, 2023)

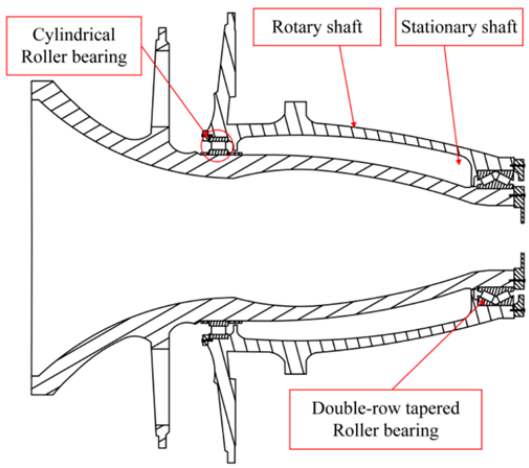

Figure 4.q Bolt shank effect on SCF (connected with standard nut type)Source: Ha, K. (2020). Reduction of Stress Concentration Factor (SCF) on the Bolted Joint Connection for a Large Wind Turbine Rotor Blade through Various Design Modifications. Applied Sciences, 10(18), 6588. https://doi.org/10.3390/app10186588

Maximum shaft deflection under a distributed load is given by: $\delta_{\max} = \frac{5\omega L^4}{384EI}$ where ω is the distributed load, L is shaft span, E is Young's modulus, and I is the second moment of area (Timoshenko and Goodier, 1970). Reducing L lowers $\delta_{\max}$, preserving rotor-generator alignment. MDPI (2023) notes that improved stiffness and spacing can cut deflection by over 50%, increasing fatigue life.

Load Distribution and Deflection Control (↑ MTTF)

Balanced loading at both bearings reduces contact stress and wear. The reaction forces at the supports are: $R_A = R_B = \frac{F}{2}$ where F is the applied load. Angular deflection at the shaft end is: $\theta = \frac{M}{EI}$ Lower bending moments and angular deflection improve bearing life. MDPI (2023) shows alignment improvements increased service intervals by up to 60%.

4.5.1.3 Electronics and Enclosure Reliability Improvements

Electronics and Enclosure Reliability Improvements

The prototype used a basic plastic enclosure with no protection against dust, UV, moisture, or thermal cycling. This left electronics highly vulnerable to corrosion, condensation, and overheating. In the deployable version, an industrial-grade UV-stabilised polycarbonate or powder-coated aluminium enclosure is adopted, compliant with ISO 12944 corrosion standards (ISO, 2018). Reinforced walls and gasketed seams resist impact and water ingress, while passive cooling is provided by external heat sinks and waterproof ventilation slots. These upgrades eliminate moving parts like fans and directly increase Mean Time to Failure (MTTF) of sensitive electronics in outdoor conditions. As shown in Figure 1b, uncoated surfaces develop visible dendritic growth under moisture exposure, while Figure 1a shows how conformal coatings protect components from degradation (Yoo, 2024).

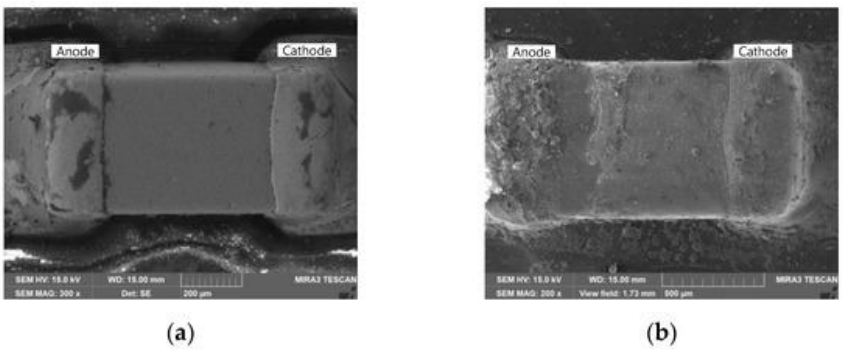

Figure 4.r: (a) Conformal-coated capacitor protected from dendritic growth; (b) Uncoated surface showing dendritic damage (Yoo, 2024).

Surge, Moisture and EMI Protection (↑ MTTF)

PCBs are conformal-coated to protect against humidity-induced failures such as dendritic growth and surface tracking (Yoo, 2024). Braided EMI shielding and grounded signal conduits follow IEEE 1143-2012 guidance, mitigating electromagnetic interference and signal loss. Moisture protection is achieved through sealed cable glands and routing strategies that isolate power and signal lines. These interventions collectively increase system reliability by reducing the three most common failure modes in outdoor electronics: water ingress, EMI, and voltage surges. As shown in Figure 2 and Figure 3, braided shielding geometry and coverage angles are critical to reducing EMI vulnerability across high-frequency environments.

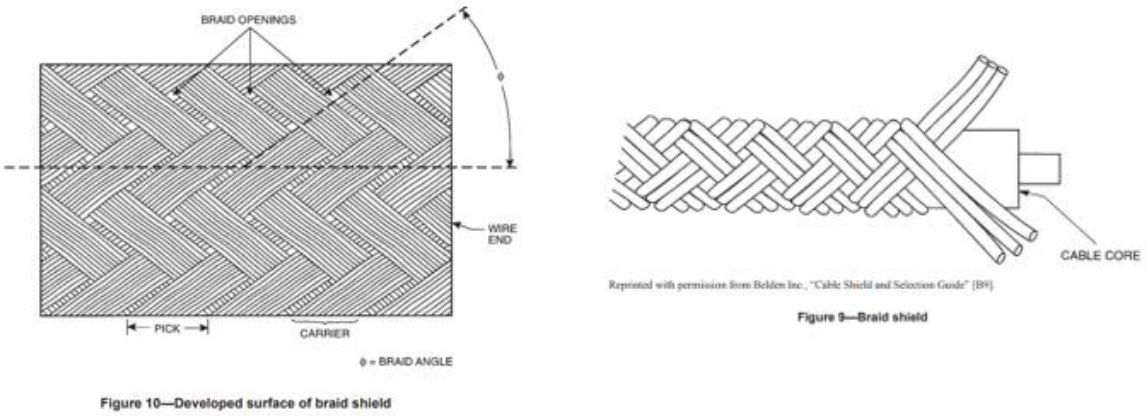

Figure 4.s: Braided cable shielding for EMI suppression (Belden Inc., 4.t: Left: Developed surface of braided shield, showing braid openings and angle (Belden Inc., 2023). Right: Braided cable shielding for EMI suppression (Belden Inc., 2023).

Modular PCB Replacement (↓ MTTR)

To reduce Mean Time to Repair (MTTR), the control system is modularised. MPPT, turbine control, and battery management are separated onto discrete PCBs connected via MC4 and Anderson Powerpole connectors, enabling board-level replacements in the field without disturbing other subsystems. Front-facing access doors, removable plates, and standardised PCB slots ensure that failed boards can be identified and swapped within minutes, minimising system downtime and eliminating the need for rewiring or specialist equipment (Chowdhury et al., 2016).

Cable Management for Long-Term Stability (↑ MTTF)

In the prototype, signal and power lines were bundled, causing EMI cross-talk and insulation fatigue. In the optimised version, UV-rated, double-insulated PV cables are used, routed through separate shielded conduits with strain reliefs and slack loops to accommodate solar tracker motion. This protects the system from wire cracking, connection fatigue, and signal degradation over time, directly improving cable lifespan and electrical reliability. As illustrated in Figure 4, enhancements in ingress protection and thermal regulation are directly correlated with increased MTTF in field-deployed electronics.

MPPT Behaviour Under Variable Irradiance (↑ Efficiency)

To maximise power extraction from the solar panel under changing irradiance, a maximum power point tracking (MPPT) system is used. As shown in Figure 5a and 5b, irradiance levels significantly affect both current-voltage (I-V) and power-voltage (P-V) curves. At 1 kW/m², the panel reaches maximum efficiency near 32 V, while

lower irradiance levels reduce both peak power and optimal voltage. The MPPT algorithm adjusts the operating point in real time to ensure maximum power output across all conditions.

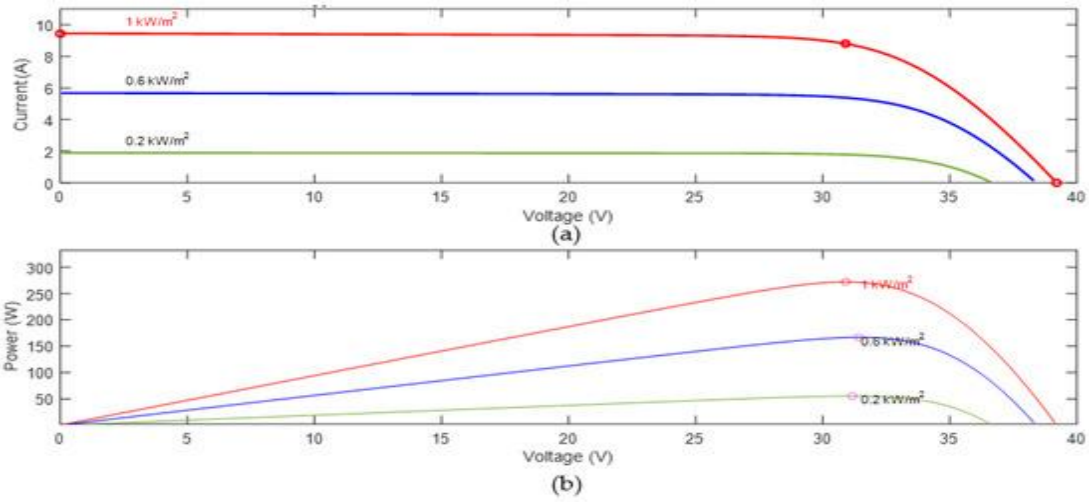

Figure 4.t : (a) I–V curve and (b) P–V curve of a PV panel under varying irradiance levels (Chowdhury et al., 2016).

4.5.2 Blade Material Optimisation

4.5.2.1 Blade Prototype Overview

For the prototype phase, practical limitations such as ease of manufacture, cost, and material availability influenced our initial material choices. The prototype blades were made from lightweight foam. Foam was selected because for its affordability, ease of shaping, and lightweight properties, making it suitable for rapid prototyping. However, foam presents significant disadvantages. Thus, while foam fulfilled the immediate needs for early-stage physical demonstration, it is unsuitable for long-term or real-world use. The Prototype experienced emphasised that material performance is crucial to the success of the final deployable product. A deployable hybrid energy device is aimed to operate reliably over several years with minimal maintenance. Material selection must consider several important aspects:

- Structural fatigue for continuous wind loading
- Aerodynamic efficiency
- Resistance in outdoor environment

Failure to address proper material selection during the design phase could result to early failures, high maintenance costs, customer dissatisfaction, and even potential safety risks. Therefore, this part concentrates on evaluating alternative materials by performing calculations to support their selection based on strength, durability, and overall suitability.

4.5.2.2 Material Options

For the final deployable version of the hybrid renewable energy device, three main

possible materials were considered for the wind turbine blades: ASA plastic, Fiberglass Reinforced Polymer (FRP), and Carbon Fibre Reinforced Polymer (CRFP). These materials were assessed based on their mechanical properties, resistance to environmental conditions, ease of manufacturing, cost effectiveness and overall suitability for long-term outdoor use. Material properties, along with the advantages and disadvantages of each material, are provided in Appendix A.3.

4.5.2.3 Material Selection Analysis

Stress analysis and calculation are provided in appendix A.3.

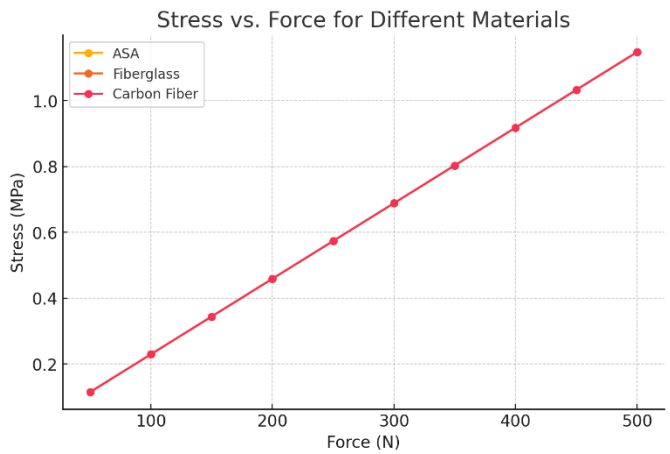

Figure 4.u: Stress vs Forces Graph

In the Stress vs Force graph, all three materials showed identical stress values for a given applied force. This is expected because stress is determined solely only on the applied force and cross-sectional area, and not on the material's properties such as stiffness and strength. As the force increases linearly, stress also increases linearly for all materials. This approach is useful for controlled comparison but does not reflect on how those materials act in a real-life scenario.

In real-world design scenarios, materials are selected and dimensioned based on mechanical properties. Stiffer materials, such as carbon fibre, tend to deform much less under load, which means they would experience lower strain and in turn, they would experience lower internal stress due to reduced cyclic deformation. On the hand, softer materials like ASA would undergo greater deformation, which can result in higher localised stress concentrations over time (Youksoulian, 2024). Therefore, in practical use, each material will experience different internal stress levels.

Deflection calculation and analysis are provided in appendix A.3.

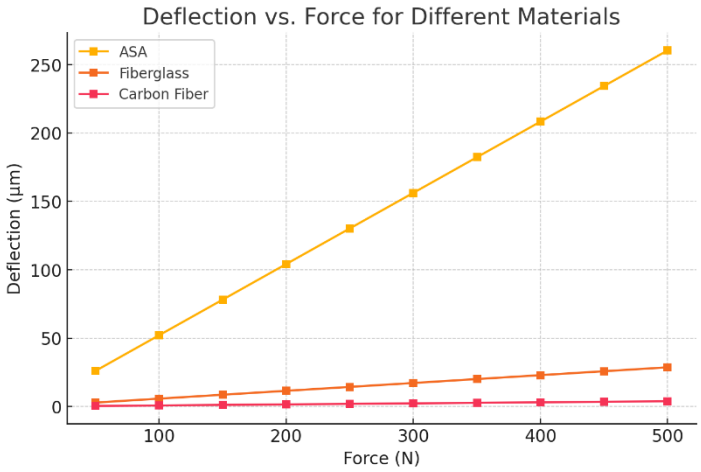

Figure 4.v: Deflection vs Forces

The deflection vs force graph highlights noticeable differences between the materials in terms of stiffness. ASA showed the greatest deflection under load, followed by fibreglass with moderate deflection, and carbon fibre with the least. This pattern directly corresponds to their elastic moduli. Minimising deflection is crucial for wind turbine blades as it ensures structural stability, maintains aerodynamic efficiency, and reduces the risk of mechanical failure (Chang, 2015). As a result, **carbon fibre reinforced polymer (CFRP**) stands out as the best material in terms of minimising blade deformation under operational wind loads.

4.5.2.4 Final Blade Material Recommendation

The shift from foam to Carbon Fibre Reinforced Polymer (CFRP) for the wind turbine blades marks a significant advancement in the design of the deployable hybrid renewable energy device. While foam suitable during prototype phase due to its low cost and ease of shaping, it lacks several aspects required for real-world operation. From conducting research and calculation of the three candidate materials above, CFRP meets the requirements of being able to operate in outdoor environment despite its higher cost compared to the other materials. Making it the most optimal choice for the final blade design.

4.5.3 Fasteners Material Selection

4.5.3.1 General Structure Mechanical Fasteners

To improve performance and durability of the deployable version, the fastener material selection has been revised. A4-grade stainless steel (316) is now specified for all structural and mechanical connections. This material offers excellent corrosion resistance, making it ideal for outdoor exposure, including coastal and rainy conditions. It also provides high mechanical strength, ensuring secure and reliable connections at key stress points such as the wind turbines hub, frame joints, and solar panel mounts. Unlike regular steel used before, A4 stainless steel retains both its structural integrity over time with minimal maintenance (AZO Materials, 2016). This change significantly improves the lifespan of the deployable product.

4.5.3.2 Electronic Part Fasteners

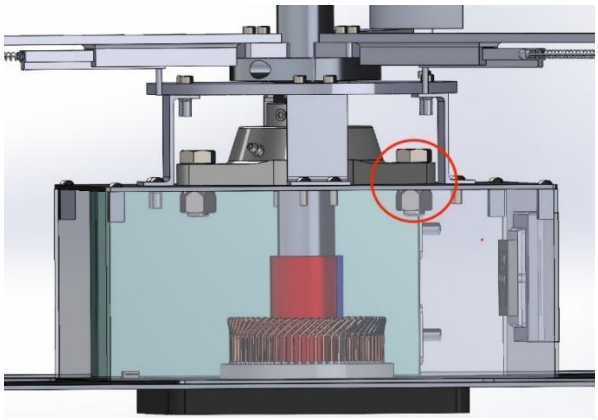

Figure 4.w: Electronic Part Fasteners 1 (VAWT)

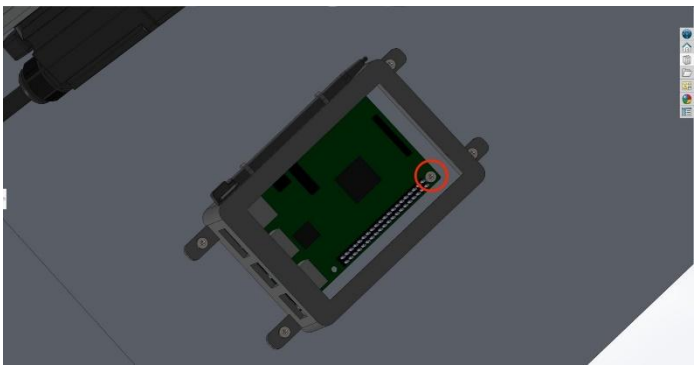

Figure 4.x: Electronic part fasteners 2 (Solar Panel)

For the electronic and non-load-bearing parts of the deployable unit, nylon screws have been selected in place of metal fasteners. Some components with enclosure mean they are not directly exposed to external factors such as rain, UV-exposure, and dust, conditions that typically become the limit of nylon in open environments (Essentra Components, 2018). Nylon screws are suitable for those components. Most importantly, nylon fasteners are lightweight, helping to reduce the overall mass of the system, which helps minimise the overall weight of the deployable product where portability and weight efficiency are important. Moreover, they are also resistant to corrosion, ensuring long-term integrity for parts that are not directly exposed to outdoor environment (NPA, 2023). Beyond that, nylon screws offer better vibration damping compared to metal fasteners. Their slight flexibility and lower stiffness allow them to be resistance of minor shocks and vibrations from the wind turbine or external environmental factors, which add protection for sensitive electronic components of the device (Essentra Components, 2018).

5 Deployable Product Design Outline

5.1 General Assembly

The general assembly comprises three primary subassemblies: the *cage, blade*, and *solar* subassemblies. Each is structurally and functionally integrated to ensure portability, stability, and efficient deployment.

5.1.1 Cage Subassembly

The cage forms the supporting framework for the turbine. Its connections are described in detail in the Design for Assembly section. Structurally, the scissor struts are connected at their centre using a pivot pin, allowing for controlled extension and folding. At each end of the scissor strut, foldable hinges are mounted using bolts; these hinges are then attached to the Top Cage Legs, providing lateral stability. The same folding mechanism is mirrored at the base, where foldable hinges connect the Bottom Cage Legs to the base frame. These mechanical linkages allow for compact storage and rapid deployment. The detailed connection layout is shown in Appendix A, Figure 8.r.

5.1.2 Blades Subassembly

The blades are mounted to a central vertical shaft, which is supported at two locations: the bottom bearing is housed inside the base box, and the top bearing is bolted to a horizontal strut across the upper cage structure. This dual-bearing system ensures axial stability and smooth rotation. The shaft is secured in place using bolts that provide vertical support and resistance to wobbling during operation. This assembly is illustrated in Appendix A, Figure 8.s.

5.1.3 Solar Subassembly

The solar panels are mounted on top of the cage structure using adjustable brackets, allowing for orientation tuning. This ensures optimal exposure regardless of seasonal changes or installation orientation. Wiring is routed through the cage struts to a central control unit stored in the base, keeping the appearance minimal and reducing environmental exposure. The assembly method and placement are detailed in Appendix A, Figure 8.t.

5.2 Manufacturing Considerations

5.2.1 Blades

The blades are relatively simple to manufacture, as they do not require any additional mechanical components. The main challenge lies in accurately producing the airfoil profile. Suitable materials include Carbon Fiber Reinforced Polymer (CFRP), Glass Fiber Reinforced Polymer (GFRP), and aluminium sheet. **Carbon Fiber Reinforced Polymer (CFRP)** is selected due to its exceptional strength-to-weight ratio, stiffness, fatigue resistance, and ability to be moulded into aerodynamic shapes while maintaining structural integrity (Campbell, 2010). The most suitable method for manufacturing CFRP blades is **Resin Transfer Moulding (RTM)**, which enables precise replication of complex geometries like airfoil profiles with a high-quality surface finish (Strong, 2008). RTM also offers good fibre wet-out, low void content, minimal material waste, and is well-suited to high-volume production due to its repeatability and efficiency (Gay et al., 2002).

5.2.2 Arms

The arms, which include the slider housing, for the commercially viable product is a bit more complicated geometrically when compared to the blade. Some suitable materials would be Mild Steel S235, Glass Fiber Reinforced Plastic, Aluminium 6061-T6 and high-strength Plastics. Aluminium 6061-T6 is chosen as it is the best all-rounder, being light and strong while still being somewhat cheap, and is easy to shape (Davis, 1993). It is also compatible with Aluminium Extrusion with a custom

die, which would have a high initial cost but is very suitable with mass-producing. It would reduce waste material that would be created by a subtractive method like CNC machining, as would be created by manufacturing this specific geometry of turbine arm (Polmear, 2006). It would also have high strength and finish (Kaufman, 2000). The slider which will be placed in the slider housing will also use the same method. Smaller parts like the spring attachment and arm-blade cylinder attachment can be made using CNC Machining and attached through welding.

5.2.3 Pull Rods

The most suitable method to manufacture the pull rods would be **Injection Moulding** with **30% Glass-Fibre Reinforced Nylon (PA6-GF30)**, which would provide enough strength to push/pull under moderate axial load, along with resistance to wear in the pivoting mechanism (Harper, 2002). Injection moulding allows integration of other features, tight tolerances and fast cycle times and economical production at scale (Osswald & Hernández-Ortiz. 2006).

5.2.4 Top and Bottom Cage Legs

The top and bottom cage legs are structural connection components made from Aluminium 6061-T6 due to its excellent corrosion resistance, weldability, and strength-to-weight ratio (Davis, 1993). Given their relatively complex shapes featuring multiple through-holes, flat faces, and precise alignment features, **die casting** is chosen as the primary manufacturing method. Die casting offers tight dimensional tolerances and excellent repeatability, essential for parts that require consistent interfacing with other structural members. The geometry is well-suited for this process with minimal undercuts, and post-processing such as reaming or drilling can be applied to critical holes to ensure dimensional accuracy. Surface finishing such as anodising or powder coating can be applied for increased durability and aesthetic quality.

5.2.5 Scissor Struts A and B

The scissor struts serve as primary load-bearing members in the deployable structure, requiring high mechanical strength and straightness over a long length. Each strut, manufactured from Aluminium 6061-T6, features multiple through-holes and tapped threads along a slender, uniform profile. For these components, **aluminium extrusion followed by CNC machining** is selected. The base profile can be efficiently produced using a custom extrusion die, significantly reducing material waste compared to fully subtractive methods (Polmear, 2006). After extrusion, secondary CNC operations such as drilling, tapping, and slotting are used to achieve the required tolerances and features. This method provides a good balance between strength, cost, and manufacturability while ensuring alignment and hole positions are maintained across all units.

5.2.6 Base, Corner Base Plate, and Lid Base

The Base, Corner Base Plate, and Lid Base are all flat components fabricated from Aluminium 6061-T6 sheet due to its favourable combination of strength, corrosion resistance, and ease of fabrication (Davis, 1993). These parts have simple planar geometries with various cutouts and mounting features, making them well-suited for **laser cutting**. Laser cutting enables high-precision profiling, excellent repeatability, and minimal material waste, which is particularly beneficial in mass production scenarios (Kalpakjian & Schmid, 2014).

After the initial cutting process, **CNC machining** is applied for any necessary secondary operations, such as creating clean edges, preparing surfaces for assembly, or forming attachment features. A **mill finish** is specified to maintain cost-effectiveness while ensuring adequate surface quality and aesthetics.

5.2.7 Rubber Padding Corner and Bottom Base Center Padding

The rubber clamp serves as damping and anti-slip features between the shaft and the clamps. This part is made from EPDM Rubber due to its excellent weather resistance, flexibility, and durability under a range of temperatures (Mark & Gaylord, 1982). The most suitable manufacturing method is **compression moulding**, which is widely used for rubber components. Compression moulding is ideal for medium-volume production and allows for the creation of thick, durable pads with minimal tooling complexity. It ensures good dimensional stability and surface quality, and is cost-effective for non-complex shapes (Harper, 2002). These parts can be easily bonded to the aluminium base using **industrial adhesives** such as epoxy or rubber contact cement, depending on the required service conditions and peel strength.

5.2.8 Bearing Casing

The bearing casing, made from ABS plastic, is designed to house and protect the bearing unit. ABS is selected for its toughness, impact resistance, and ease of moulding (Strong, 2008). **Injection moulding** is the preferred manufacturing method due to its capability to produce complex geometries with tight tolerances and high surface finish at scale. The part's geometry is well-suited to this process, with uniform wall thickness and integrated support features. Injection moulding also allows for efficient mass production and consistent quality, making it suitable for this protective casing (Osswald & Hernández-Ortiz, 2006). Additional post-moulding processes such as trimming and deburring can ensure proper fit and ease of assembly.

5.2.9 Base Box

The base box acts as a central housing for internal mechanisms and electronics. It is made from Aluminium 6061-T6 for its favourable strength-to-weight ratio, corrosion resistance, and weldability (Davis, 1993). The box is fabricated from flat aluminium sheet via CNC punching and laser cutting, particularly to create features like ventilation and socket openings with high precision and minimal thermal distortion. The walls are bent or folded where needed and then assembled using TIG welding along the end edges to form the box structure. Finally, the fully formed enclosure is welded along its bottom edges to the central region of the base plate, ensuring a secure connection for structural integrity and alignment with the rest of the assembly.

5.2.10 Cam and Cam Bracket

The cam is approximately 150 mm in diameter and has a custom geometry that loosely resembles a circle. Due to its need for durability, precision, and low weight, **Aluminium 6061-T6** is selected for its excellent machinability, corrosion resistance, and good mechanical strength (Davis, 1993). The best method for manufacturing the cam is **CNC machining**, which allows for high-precision fabrication of non-standard profiles and repeatable production at moderate to high volumes. CNC machining also ensures tight tolerances and smooth surface finishes, which are essential for the cam’s motion and wear characteristics. The CAM bracket is a structural connector used to mount the cam onto the box. It is also made from **Aluminium**

6061-T6 to ensure compatibility with the base box and to simplify the welding process. The part geometry allows it to be **CNC punched** from a single flat sheet and then brake-formed into its Z-shape profile. This technique ensures precise bend angles and hole alignment with minimal waste. For mass production, CNC punching offers cost-efficiency, high speed, and reliable tolerance control (Kalpakjian & Schmid, 2014). After forming, the brackets are spot-welded or bolted onto the box depending on design requirements for ease of maintenance.

5.2.11 Solar Components (Camlock, Shaft and Solar Supports)

The solar panel assembly features a laser cut aluminium 6061 base plate, a central hollow shaft, and a dual axis tracking structure designed in a seesaw configuration. For the optimised deployable product, the base plate is cut using fibre laser cutting to achieve high-dimensional accuracy and consistent mounting points. The central hollow shaft is machined on a lathe to ensure a consistent internal diameter, allowing for efficient cable routing and smooth rotation. Mounting brackets and pivot arms in the seesaw mechanism are CNC-milled from solid 6061 aluminium, providing tight tolerances and improved structural integrity. Key slots and pivot holes are drilled using jig-based setups to precisely align pivot holes and key slots with the rotational axes. This enhanced manufacturing process reduces weight, improves assembly consistency, and boosts the mechanical efficiency of the tracking system, making it more suitable for long-term use in outdoor environments. Similar material and processes are utilised for manufacturing process of the linear actuator supports and is welded circularly and symmetrically onto the shaft, base plate and seesaw structure. To reduce weight the housing for the Raspberry Pi and sensors is manufactured using a 3D-printer with PETG material, as it is located under the solar panel to reduce environment interaction. Solar panel, couplers and other off-the-shelf components are bolted to the manufactured structure instead of welded to reduce material fatigue. For the pressure ring, a mould is required for the moulding of the EPDM Shore A 60 material.

All components that are outsourced can be found in Appendix A, Figure 8. v.

5.3 Technical Drawings

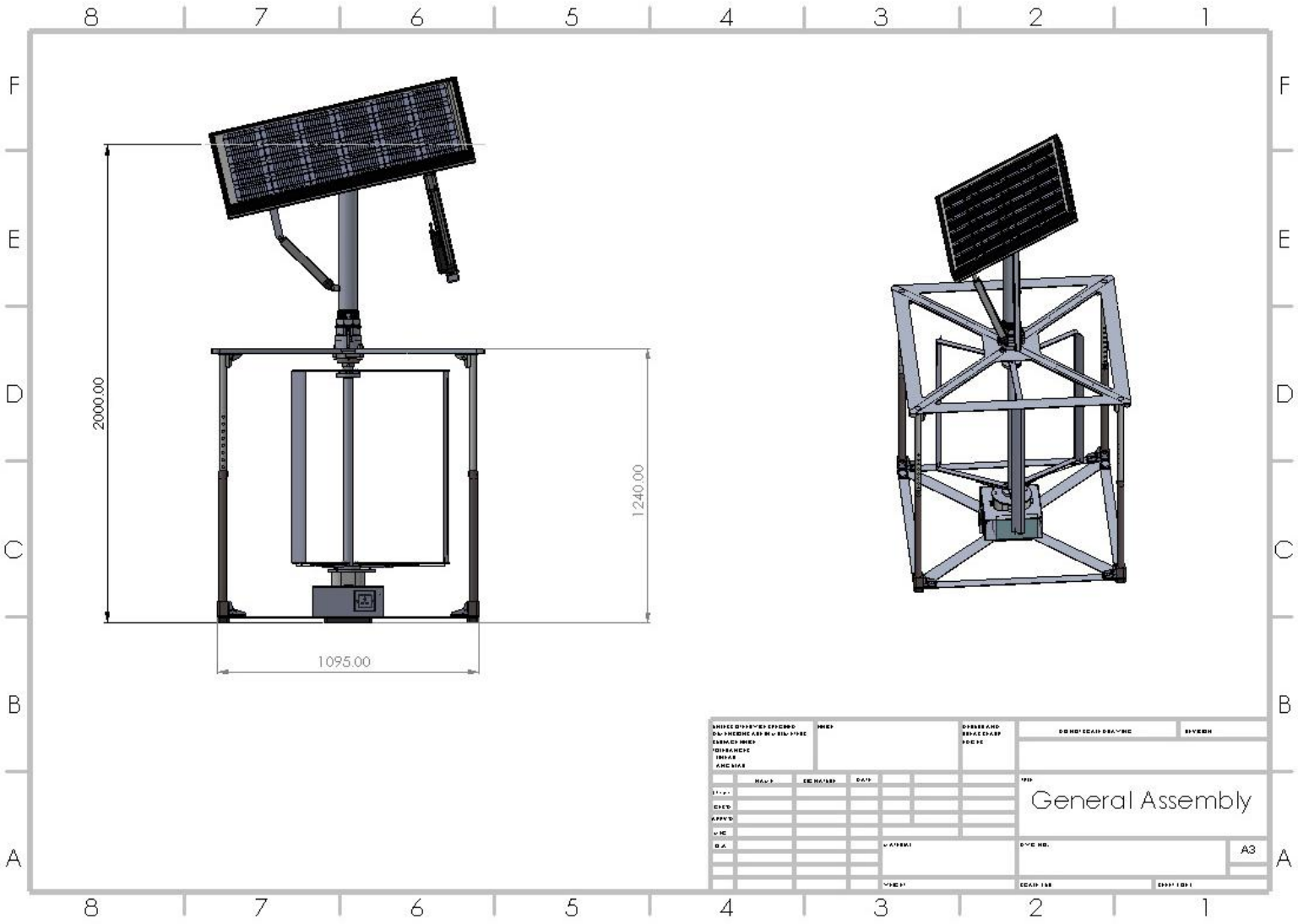

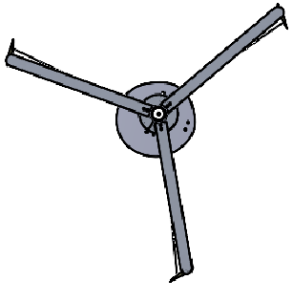

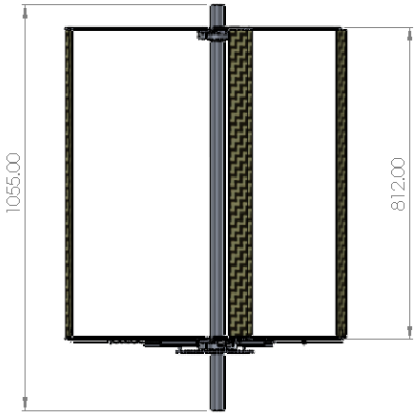

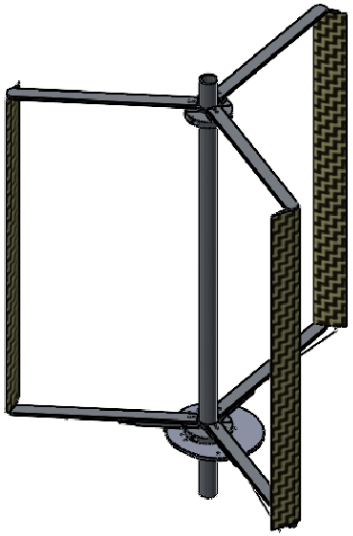

UNLESS OTHERWISE SPECIFIED: DIMENSIONS ARE IN MILLIMETERS SURFACE FINISH: TOLERANCES: LINEAR: ANGULAR:	FINISH:		DEBURR AND BREAK SHARP EDGES	DO NOT SCALE DRAWING	REVISION
	NAME	SIGNATURE	DATE	TITLE: Turbine Assembly	
DRAWN					
CHKD					
APPV'D					
MFG					
Q.A			MATERIAL:	DWG NO. Assem1	A3
			WEIGHT:	SCALE:1:20	SHEET 1 OF 1

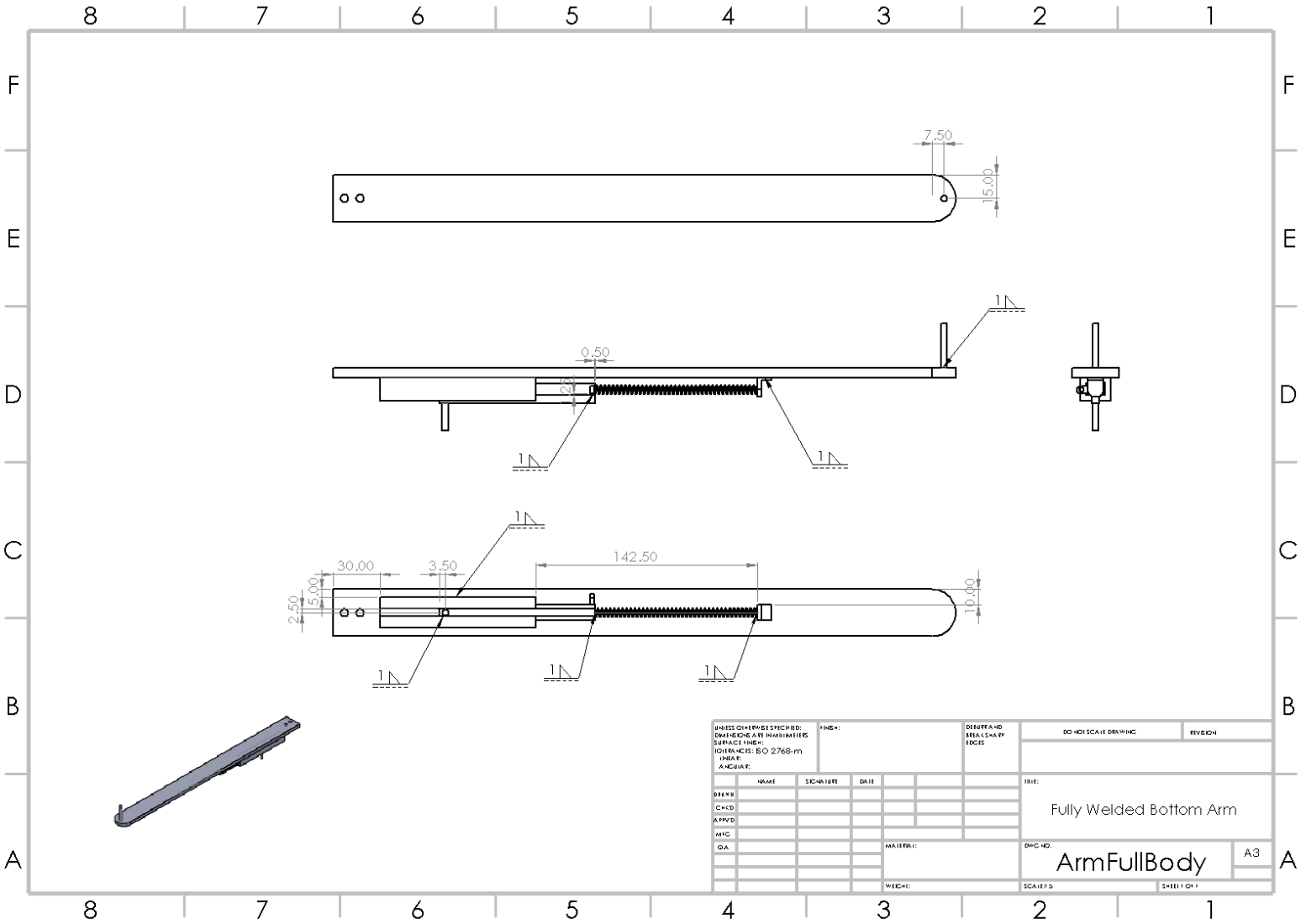
7.50
15.00
0.50
2.00
1
30.00
3.50
142.50
5.00
2.50
10.00
UNLESS OTHERWISE SPECIFIED:
DIMENSIONS ARE IN MILLIMETERS
SURFACE FINISH:
TOLERANCES: ISO 2768-m
LINEAR:
ANGULAR:
FINISH:
DEBURR AND
BREAK SHARP
EDGES
DO NOT SCALE DRAWING
REVISION
NAME
SIGNATURE
DATE
DRAWN
CHKD
APPVD
MFG
Q.A
MATERIAL:
WEIGHT:
TITLE:
Fully Welded Bottom Arm
DWG NO.
ArmFullBody
A3
SCALE:1:5
SHEET 1 OF 1

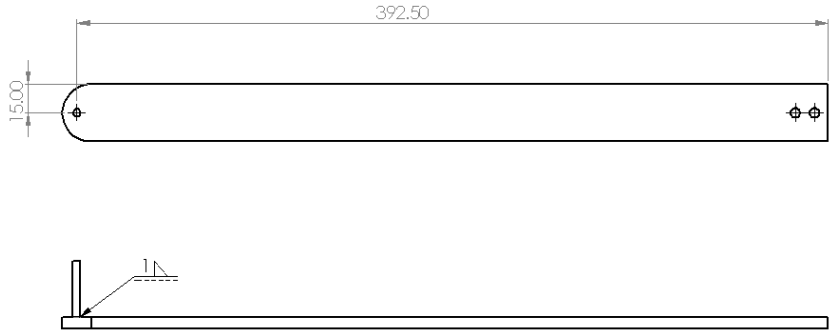

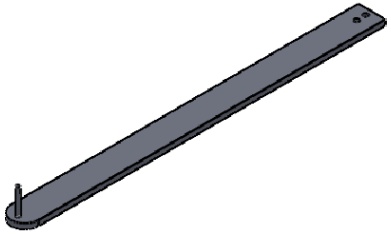

UNLESS OTHERWISE SPECIFIED: DIMENSIONS ARE IN MILLIMETERS SURFACE FINISH: TOLERANCES: ISO 2768-m LINEAR: ANGULAR:	FINISH:		DEBURR AND BREAK SHARP EDGES	DO NOT SCALE DRAWING	REVISION
	NAME	SIGNATURE	DATE	TITLE: Fully Welded Top Arm	
DRAWN					
CHK'D					
APPV'D					
MFG					
Q.A				MATERIAL: Aluminium 6061-T6	DWG NO. ArmTOPI4 A3
				WEIGHT:	SCALE:1:5 SHEET 1 OF 1

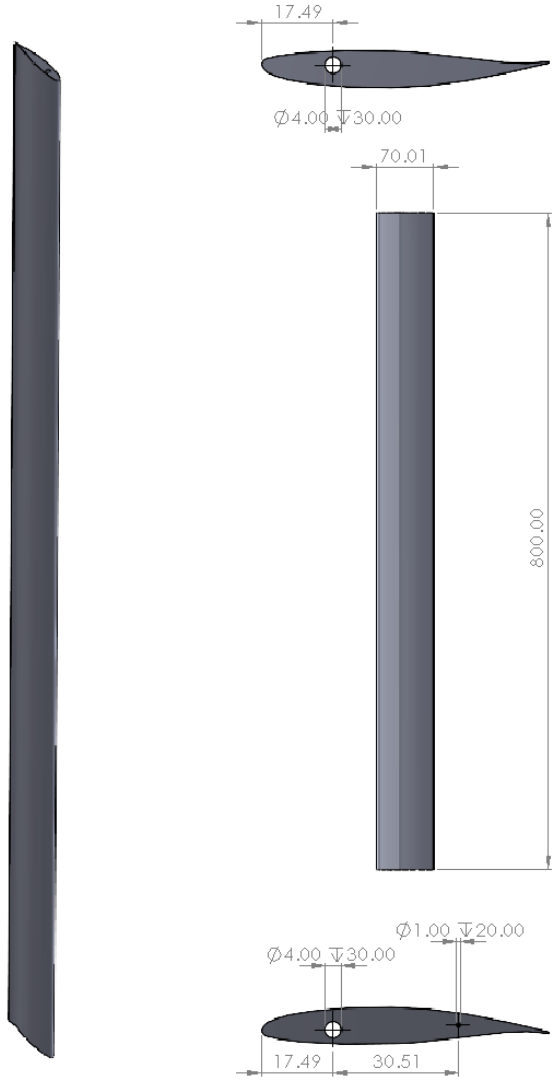

*Blades are the LS(1)-0413 airfoil with 70 mm chord

UNLESS OTHERWISE SPECIFIED: DIMENSIONS ARE IN MILLIMETERS SURFACE FINISH: TOLERANCES: ISO 2768-m LINEAR: ANGULAR:	FINISH:	DEBURR AND BREAK SHARP EDGES	DO NOT SCALE DRAWING / REVISION
	NAME / SIGNATURE / DATE		TITLE: Blade
DRAWN			
CHK'D			
APPV'D			
MFG			
Q.A		MATERIAL: Carbon Fibre Reinforced Polymer	DWG NO. bladel4 / A3
		WEIGHT:	SCALE: 1:5 / SHEET 1 OF 1

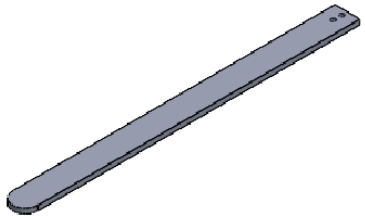

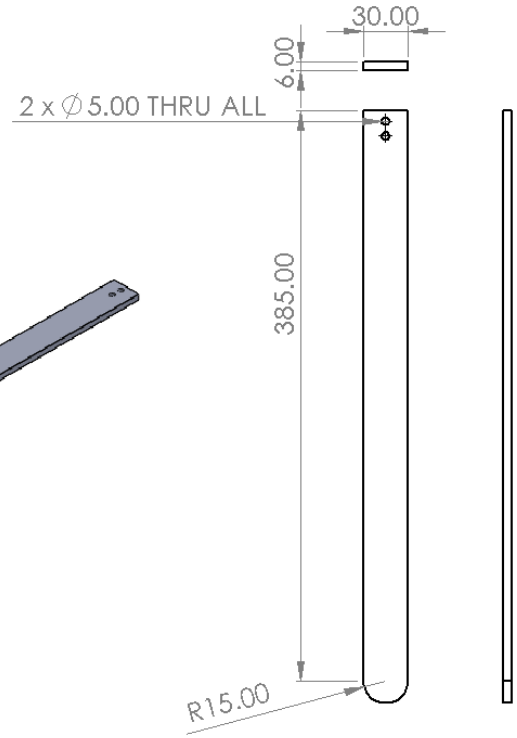

UNLESS OTHERWISE SPECIFIED: DIMENSIONS ARE IN MILLIMETERS SURFACE FINISH: TOLERANCES: ISO 2768-m LINEAR: ANGULAR:	FINISH:			DEBURR AND BREAK SHARP EDGES	DO NOT SCALE DRAWING	REVISION
	NAME	SIGNATURE	DATE		TITLE: Arm Body	
DRAWN						
CHK'D						
APPV'D						
MFG						
Q.A				MATERIAL: Aluminium 6061-T6	DWG NO. ArmTOPBody	A4
				WEIGHT:	SCALE:1:5	SHEET 1 OF 1

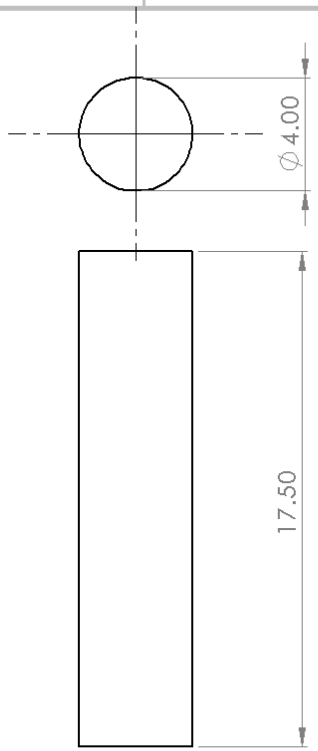

UNLESS OTHERWISE SPECIFIED: DIMENSIONS ARE IN MILLIMETERS SURFACE FINISH: TOLERANCES: ISO 2768-m LINEAR: ANGULAR:	FINISH:		DEBURR AND BREAK SHARP EDGES	DO NOT SCALE DRAWING	REVISION
	NAME	SIGNATURE	DATE	TITLE: Follower	
DRAWN					
CHK'D					
APPV'D					
MFG					
Q.A				MATERIAL: Aluminium 6061-T6	DWG NO. FollowerCam A4
				WEIGHT:	SCALE:5:1 SHEET 1 OF 1

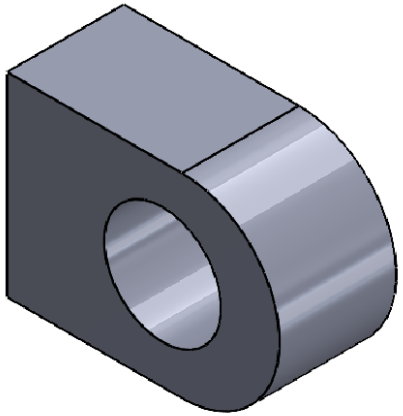

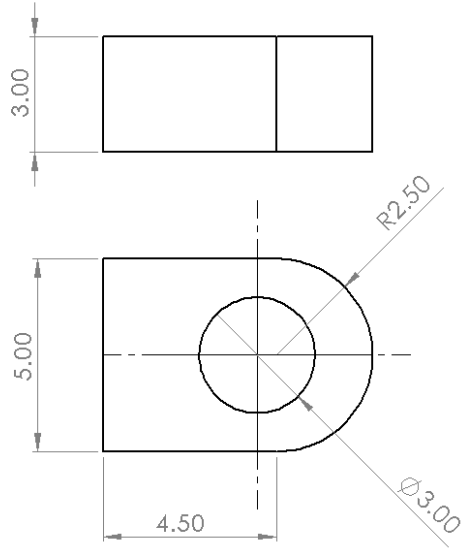

UNLESS OTHERWISE SPECIFIED: DIMENSIONS ARE IN MILLIMETERS SURFACE FINISH: TOLERANCES: ISO 2768-m LINEAR: ANGULAR:	FINISH:		DEBURR AND BREAK SHARP EDGES	DO NOT SCALE DRAWING	REVISION	
	NAME	SIGNATURE	DATE	TITLE: Pull Rod Insert		
DRAWN						
CHK'D						
APPV'D						
MFG						
Q.A				MATERIAL: Aluminium 6061-T6	DWG NO. PullRodInsert	A4
				WEIGHT:	SCALE:10:1	SHEET 1 OF 1

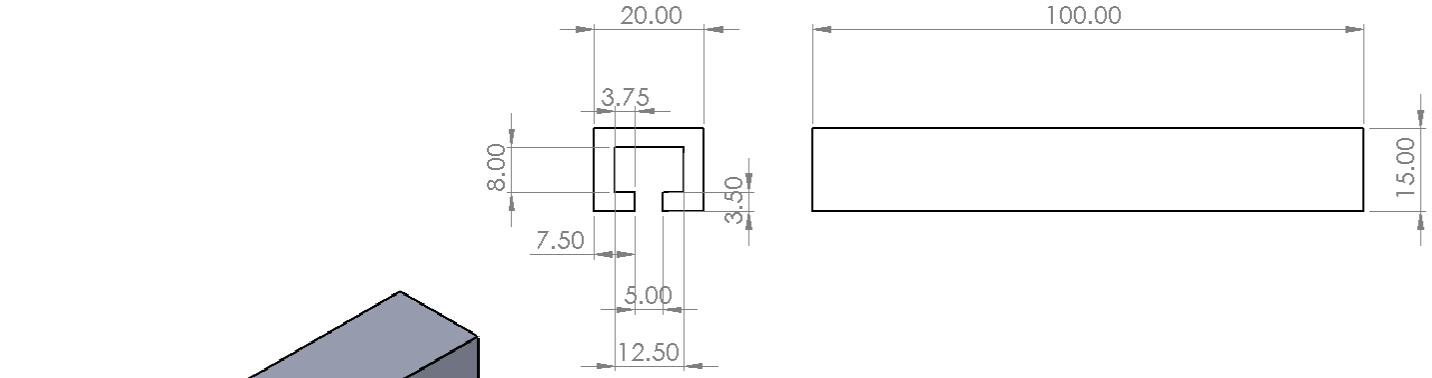

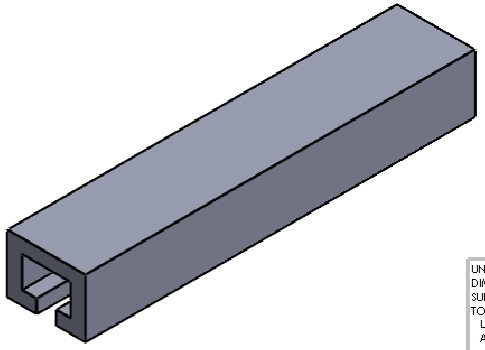

UNLESS OTHERWISE SPECIFIED: DIMENSIONS ARE IN MILLIMETERS SURFACE FINISH: ISO 2768-m TOLERANCES: LINEAR: ANGULAR:	FINISH:		DEBURR AND BREAK SHARP EDGES	DO NOT SCALE DRAWING	REVISION	
	NAME	SIGNATURE	DATE	TITLE: Slider Housing		
DRAWN						
CHK'D						
APPV'D						
MFG						
Q.A				MATERIAL: Aluminium 6061-T6	DWG NO. SliderHousing	A4
				WEIGHT:	SCALE:1:1	SHEET 1 OF 1

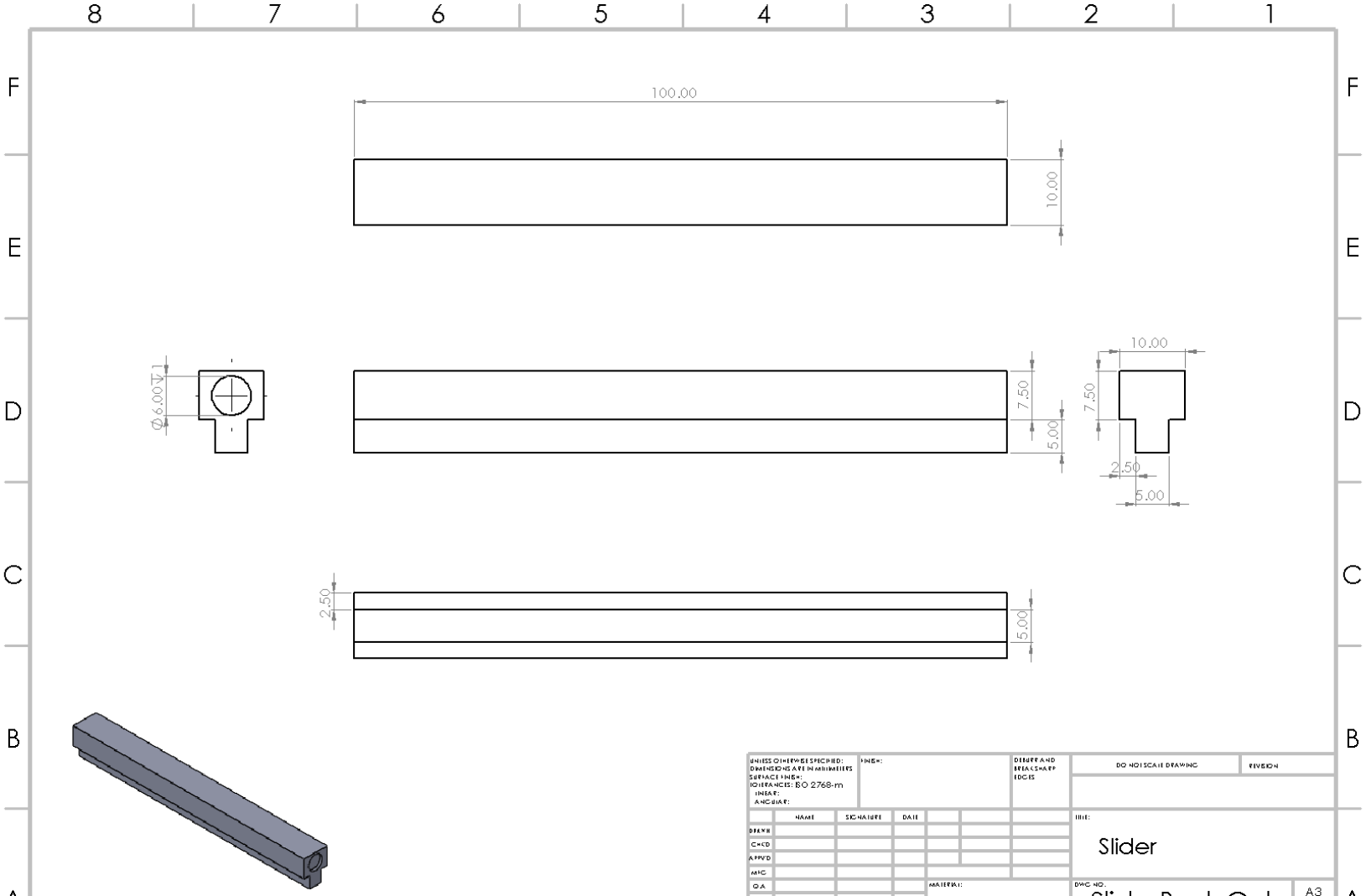

UNLESS OTHERWISE SPECIFIED:
DIMENSIONS ARE IN millimeters
SURFACE FINISH:
TOLERANCES: ISO 2768-m
LINEAR:
ANGULAR:

FINISH:

DEBURR AND BREAK SHARP EDGES

DO NOT SCALE DRAWING

REVISION

	NAME	SIGNATURE	DATE
DRAWN			
CHK'D			
APPV'D			
MFG			
Q.A			

TITLE:

Slider

MATERIAL:

Aluminium 6061-T6

WEIGHT:

DWG NO.

SliderBodyOnly

A3

SCALE:1:1

SHEET 1 OF 1

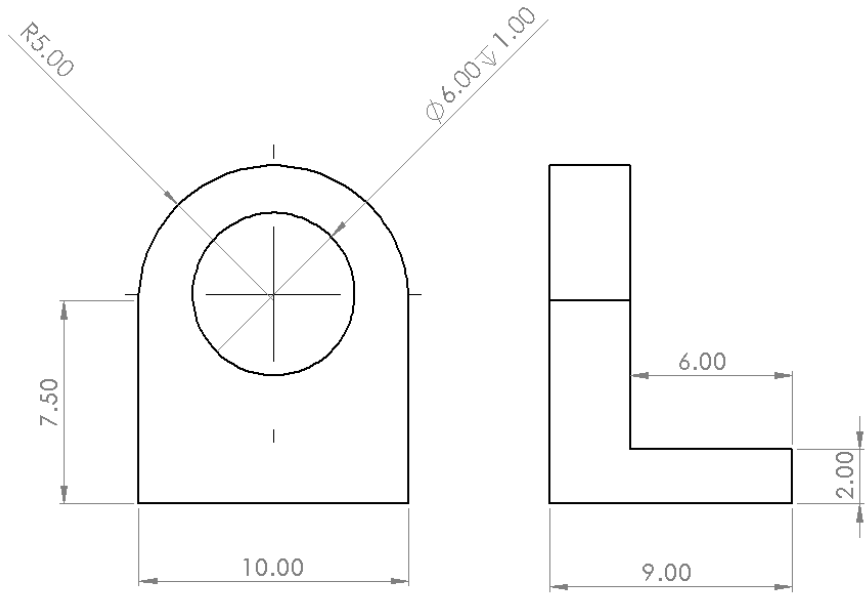

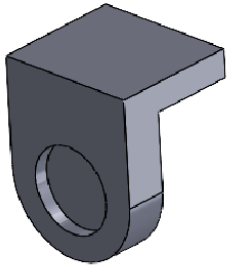

UNLESS OTHERWISE SPECIFIED: DIMENSIONS ARE IN MILLIMETERS SURFACE FINISH: TOLERANCES: ISO 2768-m LINEAR: ANGULAR:	FINISH:		DEBURR AND BREAK SHARP EDGES	DO NOT SCALE DRAWING	REVISION	
	NAME	SIGNATURE	DATE	TITLE:		
DRAWN				Spring Attachment		
CHK'D						
APPV'D						
MFG						
Q.A				MATERIAL:	DWG NO.	A4
				Aluminium 6061-T6	SpringAttachment14	
				WEIGHT:	SCALE:5:1	SHEET 1 OF 1

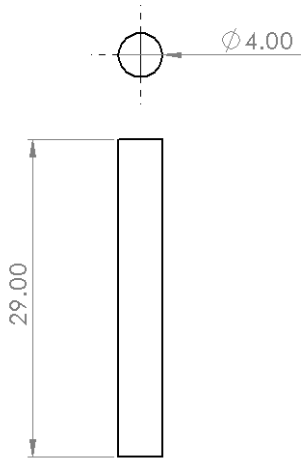

UNLESS OTHERWISE SPECIFIED: DIMENSIONS ARE IN MILLIMETERS SURFACE FINISH: TOLERANCES: ISO 2768-m LINEAR: ANGULAR:	FINISH:			DEBURR AND BREAK SHARP EDGES	DO NOT SCALE DRAWING	REVISION
	NAME	SIGNATURE	DATE		TITLE: Arm-Blade Insert	
DRAWN						
CHK'D						
APPV'D						
MFG						
Q.A				MATERIAL: Aluminium 6061-T6	DWG NO. ArmTOPExtrusion	A4
				WEIGHT:	SCALE:2:1	SHEET 1 OF 1

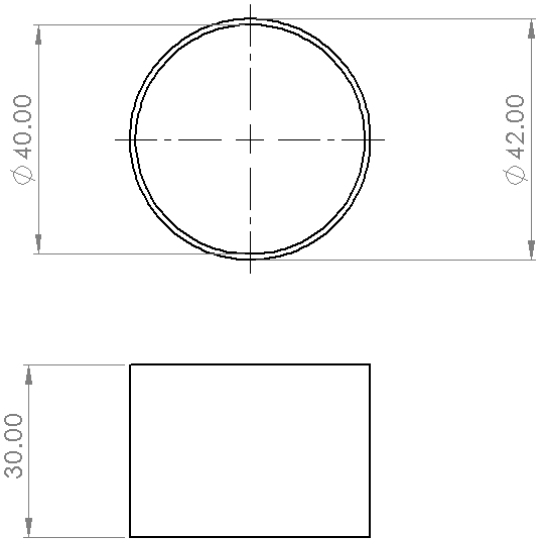

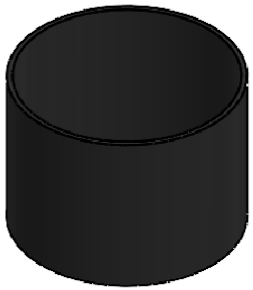

UNLESS OTHERWISE SPECIFIED: DIMENSIONS ARE IN MILLIMETERS SURFACE FINISH: TOLERANCES: ISO 2768-m LINEAR: ANGULAR:	FINISH:			DEBURR AND BREAK SHARP EDGES	DO NOT SCALE DRAWING	REVISION
	NAME	SIGNATURE	DATE		TITLE: Rubber Clamp	
DRAWN						
CHK'D						
APPV'D						
MFG						
Q.A				MATERIAL: Rubber	DWG NO. RubberClamp	A4
				WEIGHT:	SCALE:1:1	SHEET 1 OF 1

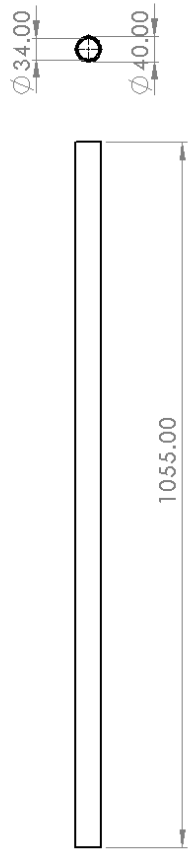

UNLESS OTHERWISE SPECIFIED: DIMENSIONS ARE IN MILLIMETERS SURFACE FINISH: TOLERANCES: ISO 2768-m LINEAR: ANGULAR:	FINISH:		DEBURR AND BREAK SHARP EDGES	DO NOT SCALE DRAWING	REVISION	
	NAME	SIGNATURE	DATE	TITLE: Shaft		
DRAWN						
CHK'D						
APPV'D						
MFG						
Q.A				MATERIAL: Aluminium 6061-T6	DWG NO. Shaft4	A4
				WEIGHT:	SCALE:1:10	SHEET 1 OF 1

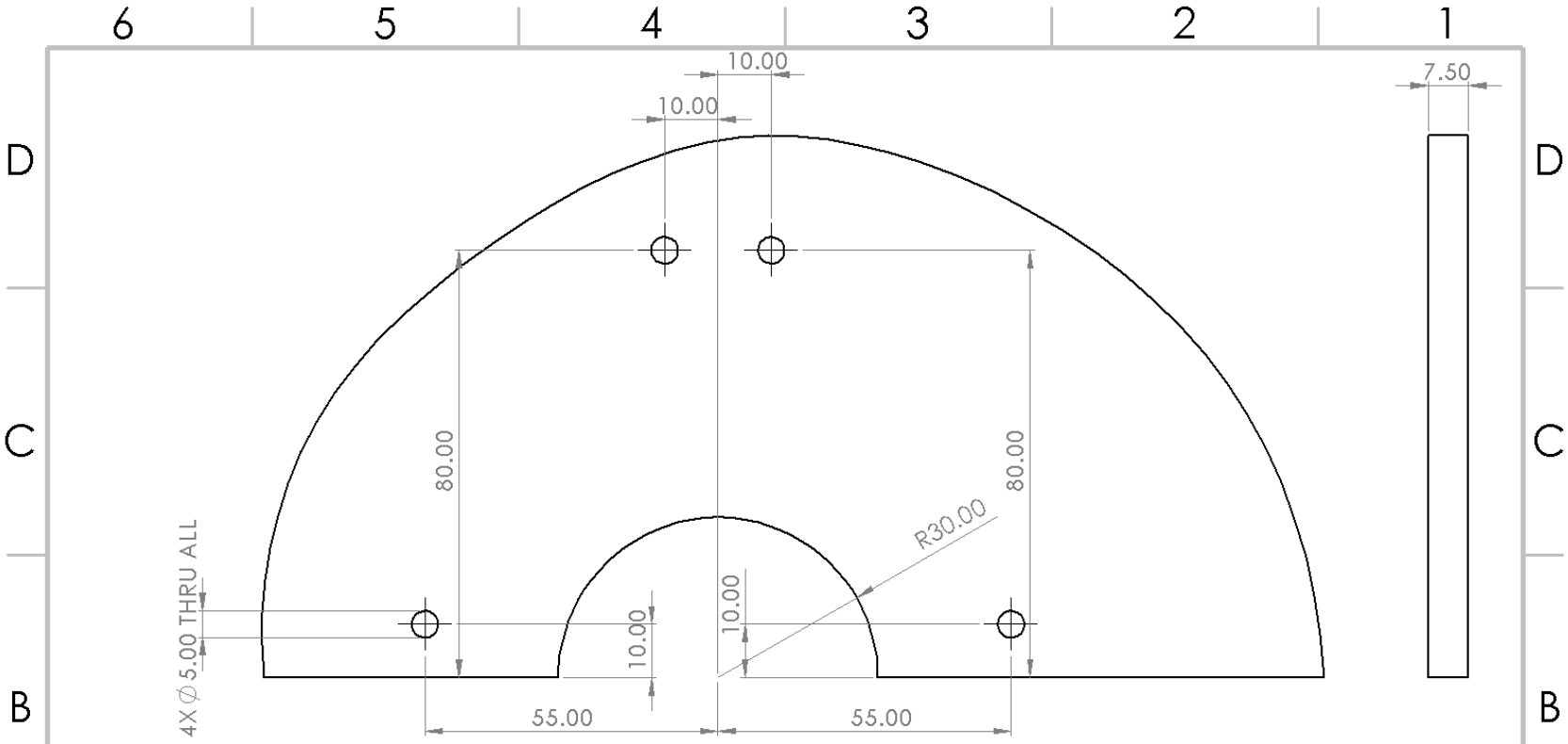

UNLESS OTHERWISE SPECIFIED: DIMENSIONS ARE IN MILLIMETERS SURFACE FINISH: TOLERANCES: ISO 2768-m LINEAR: ANGULAR:	FINISH:		DEBURR AND BREAK SHARP EDGES	DO NOT SCALE DRAWING	REVISION
				*Cam Shape is 1:1	
	NAME	SIGNATURE	DATE	TITLE:	
DRAWN				Cam Part 1	
CHK'D					
APPV'D					
MFG					
Q.A			MATERIAL: Aluminium 6061-T6	DWG NO. Camedited14D	A4
			WEIGHT:	SCALE:1:2	SHEET 1 OF 1

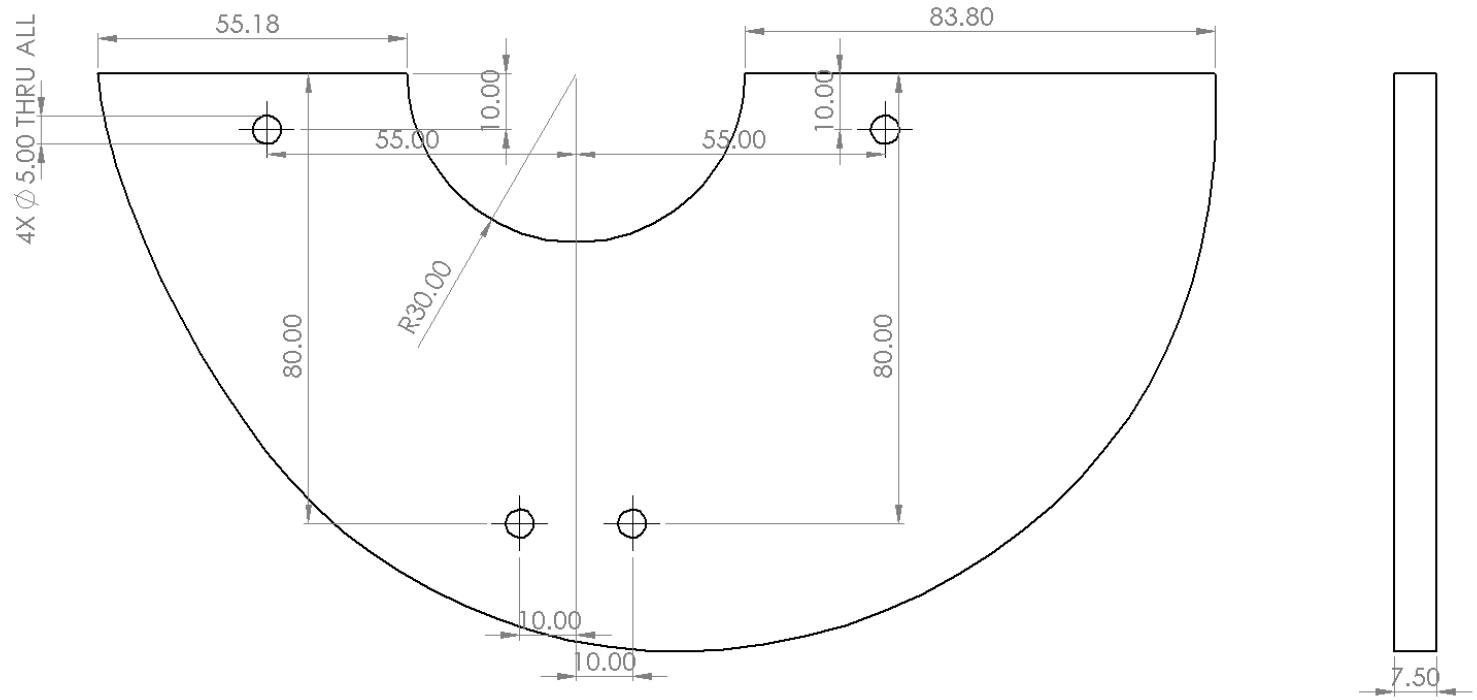

UNLESS OTHERWISE SPECIFIED: DIMENSIONS ARE IN MILLIMETERS SURFACE FINISH: TOLERANCES: LINEAR: ISO 2768-m ANGULAR:	FINISH:		DEBURR AND BREAK SHARP EDGES	DO NOT SCALE DRAWING	REVISION
				*Cam Shape is 1:1	
	NAME	SIGNATURE	DATE	TITLE: Cam Part 2	
DRAWN					
CHK'D					
APPV'D					
MFG					
Q.A			MATERIAL: Aluminium 6061-T6	DWG NO. Camedited4D2	A4
			WEIGHT:	SCALE:1:2	SHEET 1 OF 1

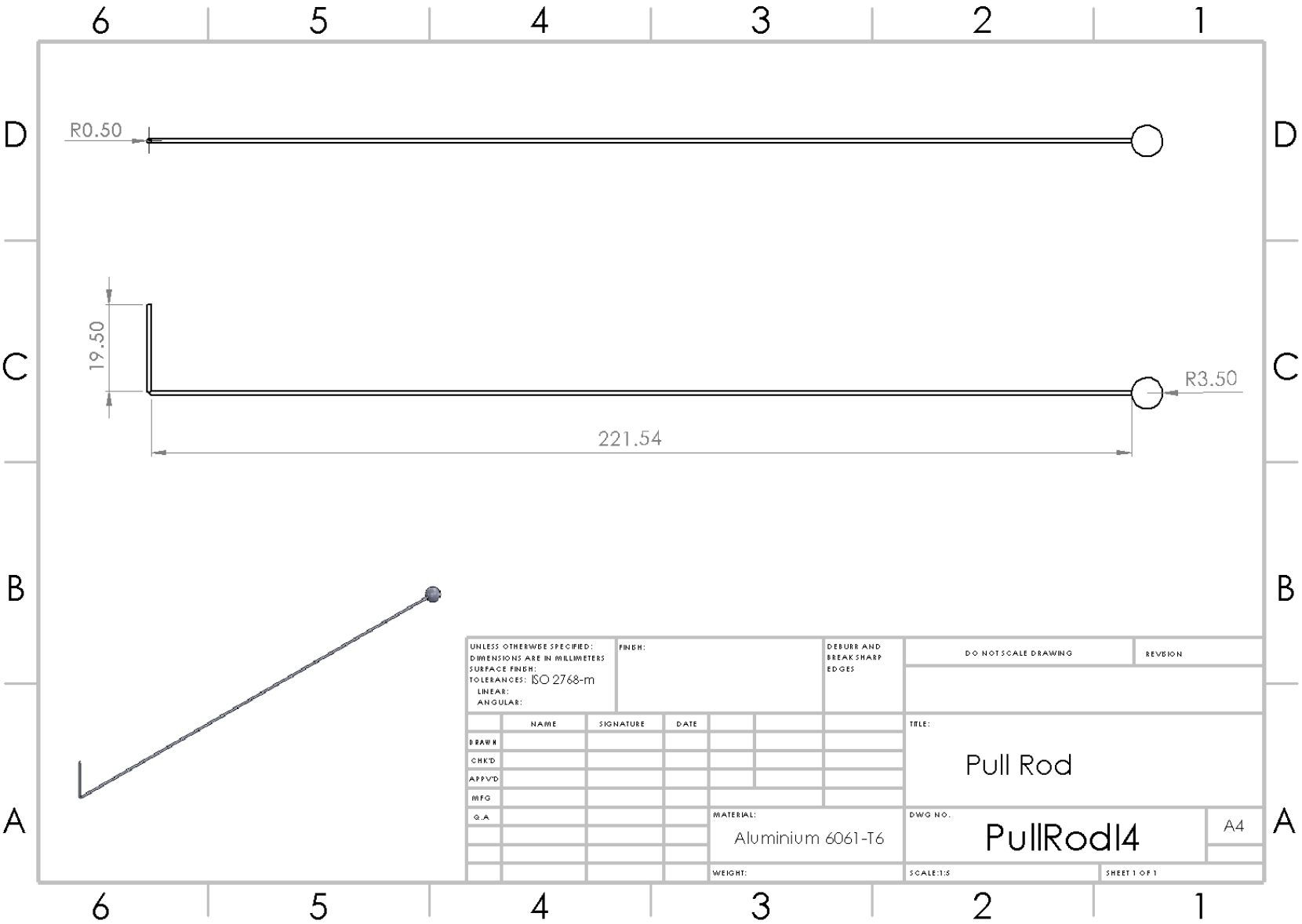
R0.50
19.50
R3.50
221.54
UNLESS OTHERWISE SPECIFIED:
DIMENSIONS ARE IN MILLIMETERS
SURFACE FINISH:
TOLERANCES: ISO 2768-m
LINEAR:
ANGULAR:
FINISH:
DEBURR AND BREAK SHARP EDGES
DO NOT SCALE DRAWING
REVISION
NAME
SIGNATURE
DATE
DRAWN
CHK'D
APPV'D
MFG
Q.A
TITLE:
Pull Rod
MATERIAL:
Aluminium 6061-T6
DWG NO.
PullRod14
A4
WEIGHT:
SCALE:1:5
SHEET 1 OF 1

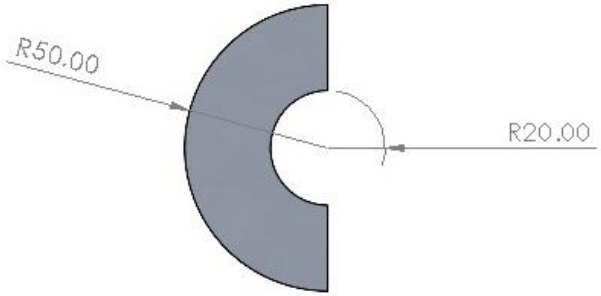

Top view

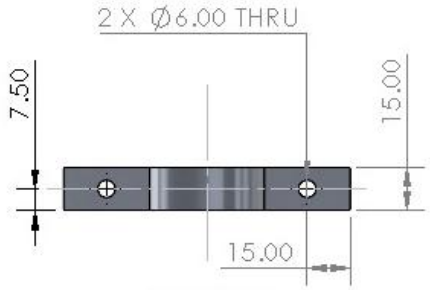

Right view

Left view

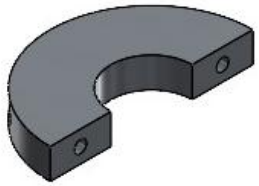

UNLESS OTHERWISE SPECIFIED: DIMENSIONS ARE IN MILLIMETERS SURFACE FINISH: TOLERANCES: ISO 2768-m LINEAR: ANGULAR:	FINISH: Mill finish			DEBURR AND BREAK SHARP EDGES	DO NOT SCALE DRAWING	REVISION
	NAME	SIGNATURE	DATE		TITLE: Clamp A	
DRAWN						
CHK'D						
APPV'D						
MFG						
Q.A				MATERIAL: Aluminium 6061-T6	DWG NO.	A4
				WEIGHT: 0.12kg	SCALE: 1:1	SHEET 1 OF 1

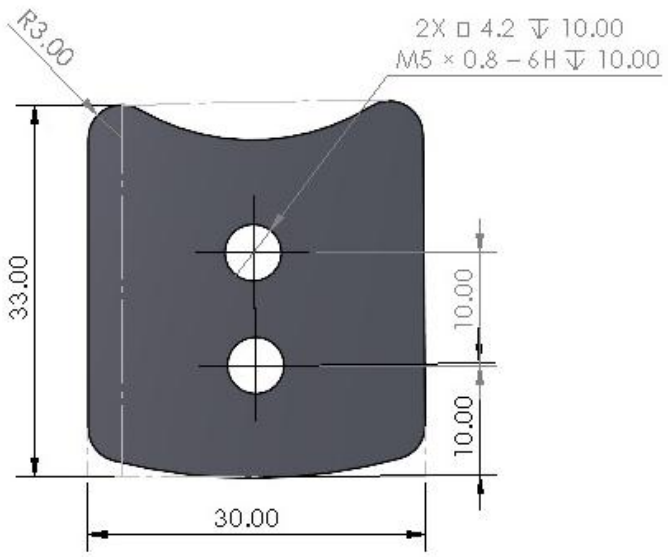

Top view

Side view

UNLESS OTHERWISE SPECIFIED: DIMENSIONS ARE IN MILLIMETERS SURFACE FINISH: TOLERANCES: ISO 2768-m LINEAR: ANGULAR:	FINISH: Mill finish	DEBURR AND BREAK SHARP EDGES	DO NOT SCALE DRAWING / REVISION
NAME / SIGNATURE / DATE			TITLE: Shaft Attachment
DRAWN			
CHK'D			
APPV'D			
MFG			
Q.A	MATERIAL: Aluminium 6061-T6		DWG NO. A4
	WEIGHT: 0.2kg		SCALE: 2:1 / SHEET 1 OF 1

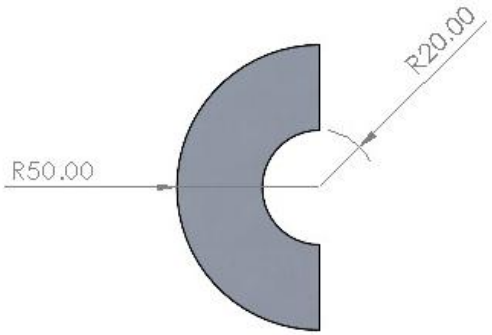

Top view

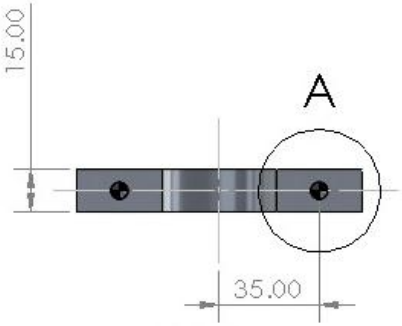

Side view

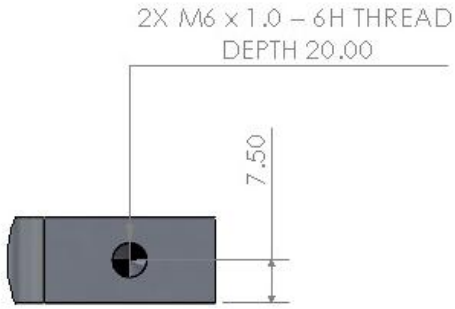

DETAIL A

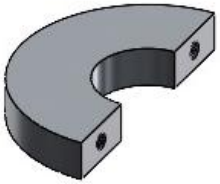

UNLESS OTHERWISE SPECIFIED: DIMENSIONS ARE IN MILLIMETERS SURFACE FINISH: TOLERANCES: ISO 2768-m LINEAR: ANGULAR:	FINISH: Mill finish			DEBURR AND BREAK SHARP EDGES	DO NOT SCALE DRAWING	REVISION
	NAME	SIGNATURE	DATE		TITLE: Clamp B	
DRAWN						
CHK'D						
APPV'D						
MFG						
Q.A				MATERIAL: Aluminium 6061-T6	DWG NO.	A4
				WEIGHT: 0.19kg	SCALE: 1:1	SHEET 1 OF 1

Weld all three attachment blocks to their respective clamp segments using fillet welds on both sides.
The clamp assembly remains detachable via M6 socket head cap screws.
Ensure welds do not interfere with clamp-mating surfaces or bolt access.

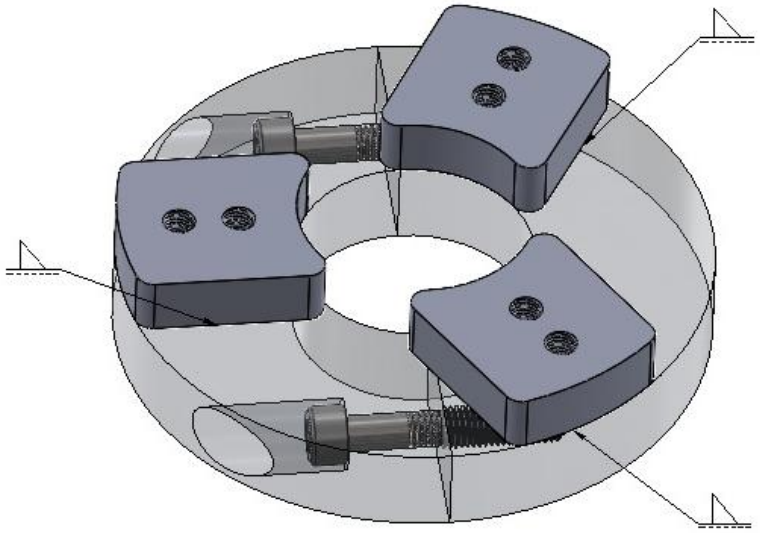

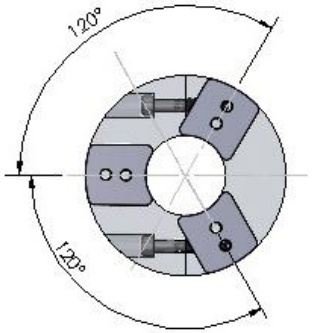

N/A

Welded Shaft Attachment, Clamp A and Clamp B

A3

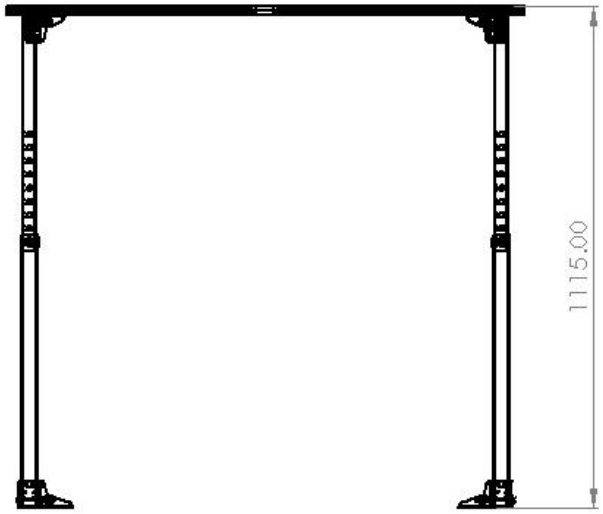

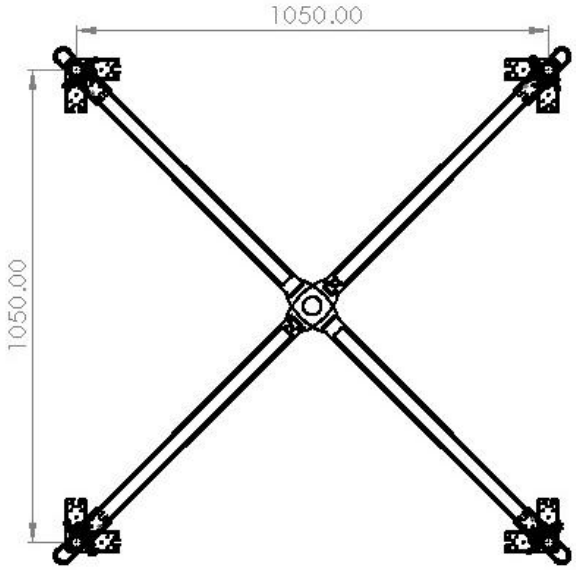

UNLESS OTHERWISE SPECIFIED: DIMENSIONS ARE IN MILLIMETERS SURFACE FINISH: TOLERANCES: LINEAR: ANGULAR:	FINISH:			DEBURR AND BREAK SHARP EDGES	DO NOT SCALE DRAWING	REVISION
	NAME	SIGNATURE	DATE		TITLE:	
DRAWN						
CHK'D						
APPV'D						
MFG						
Q.A				MATERIAL:	DWG NO. leg and scissor	A4
				WEIGHT:	SCALE:1:50	SHEET 1 OF 1

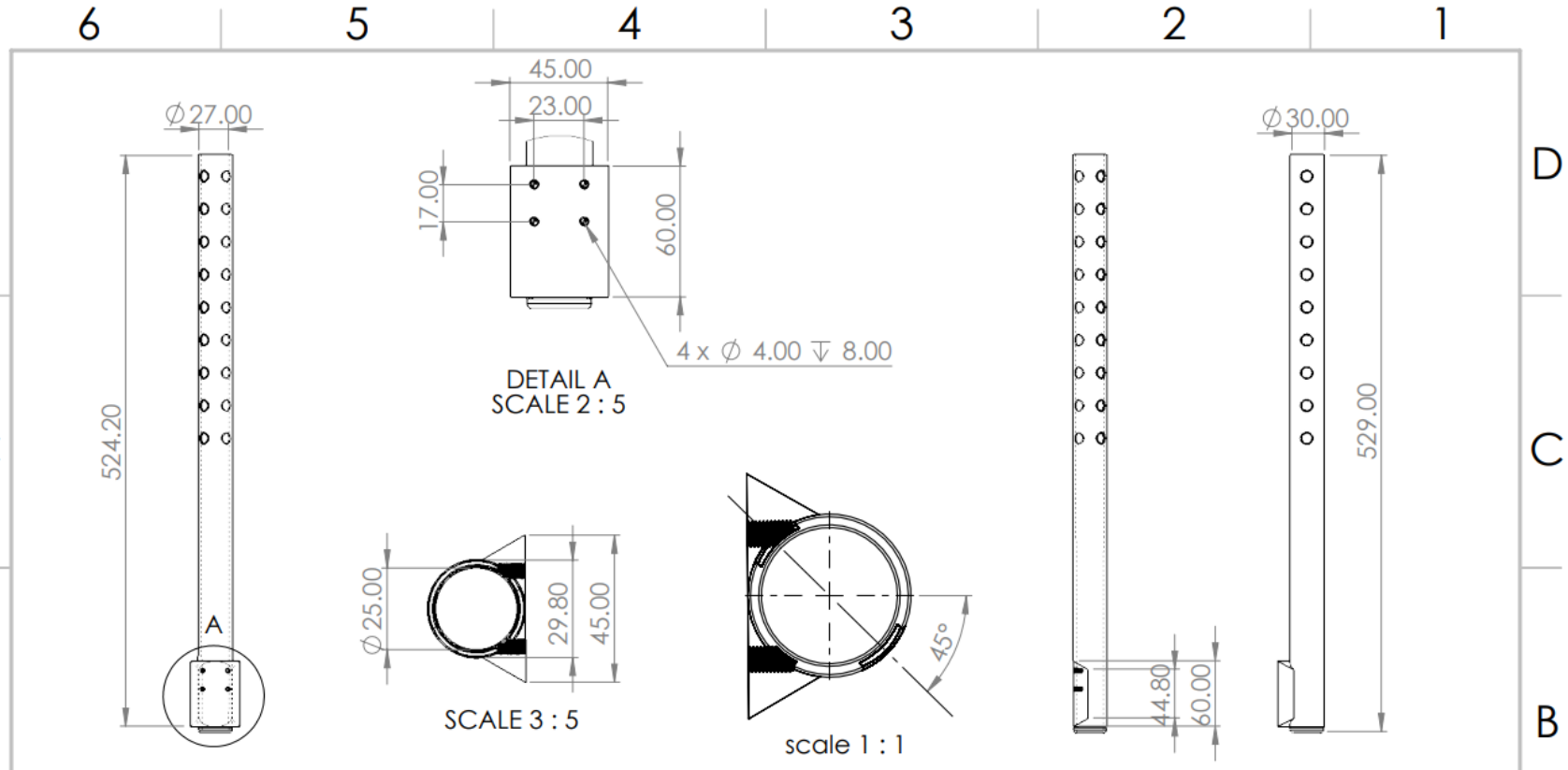

UNLESS OTHERWISE SPECIFIED: DIMENSIONS ARE IN MILLIMETERS SURFACE FINISH: TOLERANCES: ISO 2768 -m LINEAR: ANGULAR:	FINISH:		DEBURR AND BREAK SHARP EDGES	DO NOT SCALE DRAWING		REVISION	
	NAME	SIGNATURE	DATE	TITLE:			
DRAWN							
CHK'D							
APPV'D							
MFG							
Q.A				MATERIAL: ALUMINIUM 6061 - T6	DWG NO. Top Cage leg		A4
				WEIGHT:	SCALE:1:5	SHEET 1 OF 1	

SOLIDWORKS Educational Product. For Instructional Use Only.

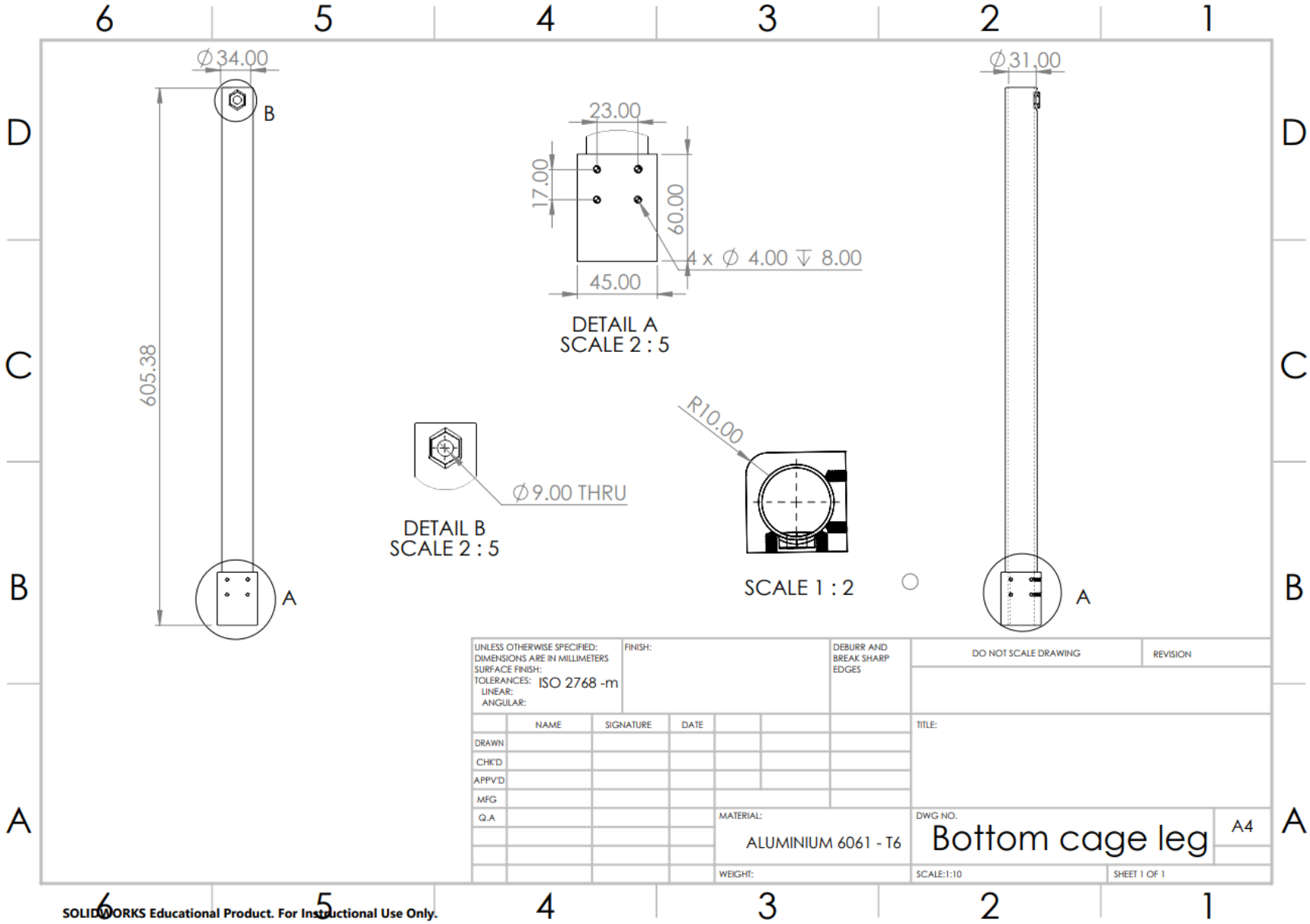

SOLIDWORKS Educational Product. For Instructional Use Only.

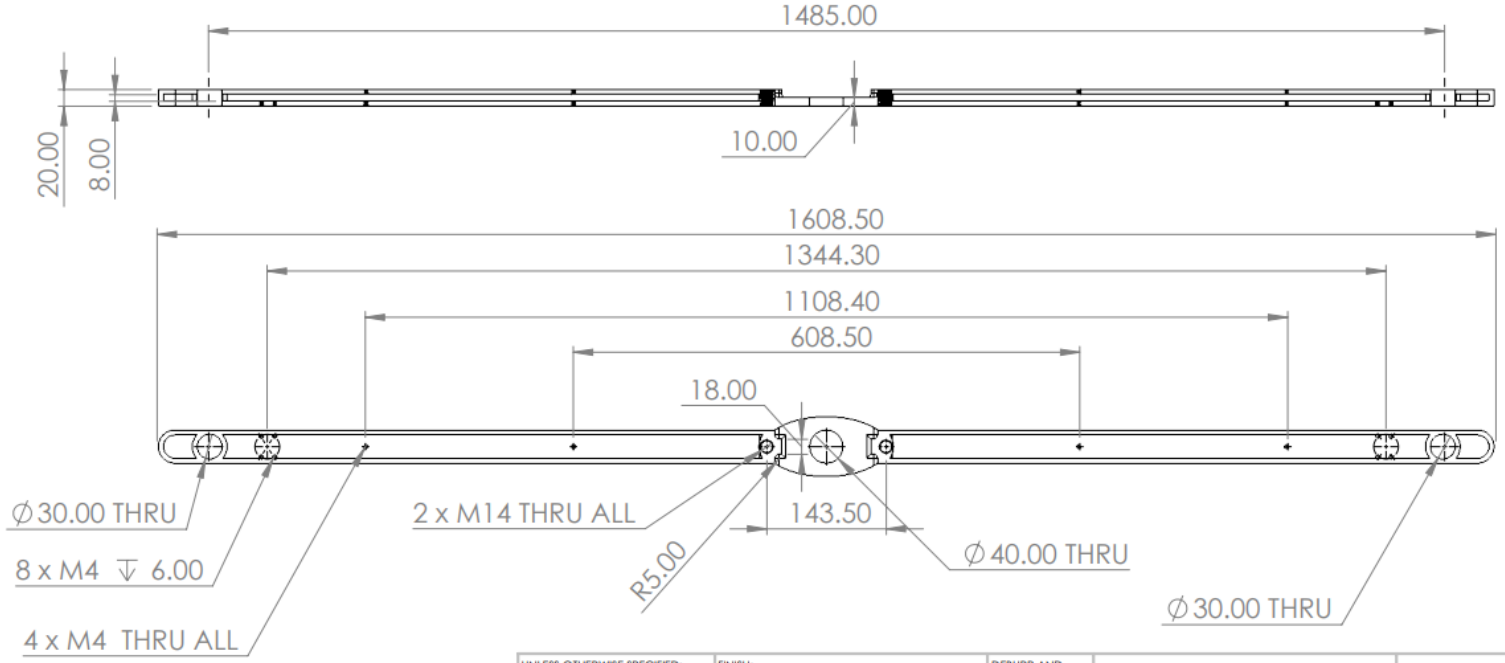

UNLESS OTHERWISE SPECIFIED: DIMENSIONS ARE IN MILLIMETERS SURFACE FINISH: TOLERANCES: LINEAR: ISO 2768 -m ANGULAR:	FINISH:		DEBURR AND BREAK SHARP EDGES	DO NOT SCALE DRAWING	REVISION	
	NAME	SIGNATURE	DATE	TITLE:		
DRAWN						
CHK'D						
APPV'D						
MFG						
Q.A				MATERIAL: ALUMINIUM 6061 - T6	DWG NO. scissor strut A	A4
				WEIGHT:	SCALE 1 : 7	SHEET 1 OF 1

SOLIDWORKS Educational Product. For Instructional Use Only.

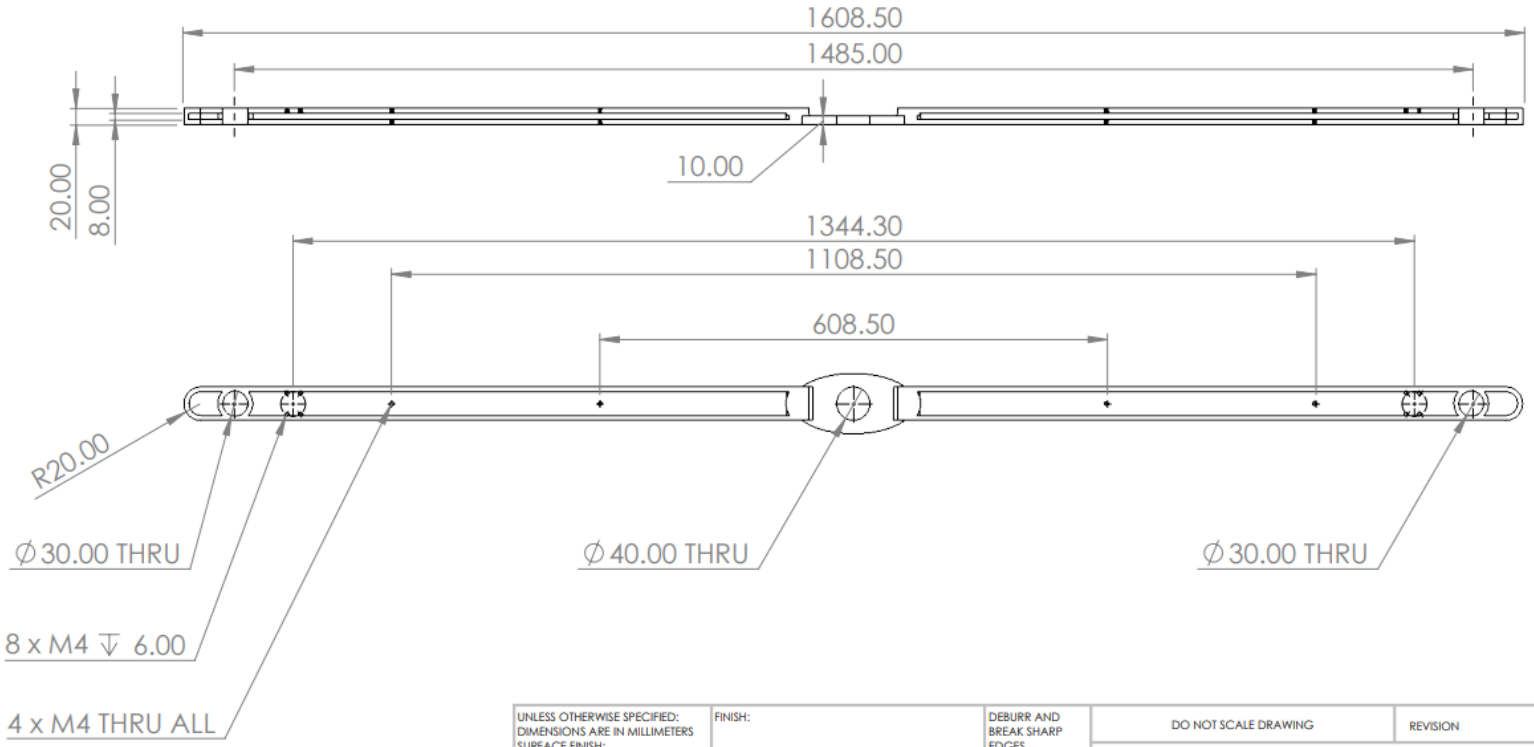

UNLESS OTHERWISE SPECIFIED: DIMENSIONS ARE IN MILLIMETERS SURFACE FINISH: TOLERANCES: LINEAR: ISO 2768 -m ANGULAR:	FINISH:		DEBURR AND BREAK SHARP EDGES	DO NOT SCALE DRAWING	REVISION	
	NAME	SIGNATURE	DATE	TITLE:		
DRAWN						
CHK'D						
APPV'D						
MFG						
Q.A				MATERIAL: ALUMINIUM 6061 - T6	DWG NO. scissor strut B	A4
				WEIGHT:	SCALE:1 : 7	SHEET 1 OF 1

SOLIDWORKS Educational Product. For Instructional Use Only.

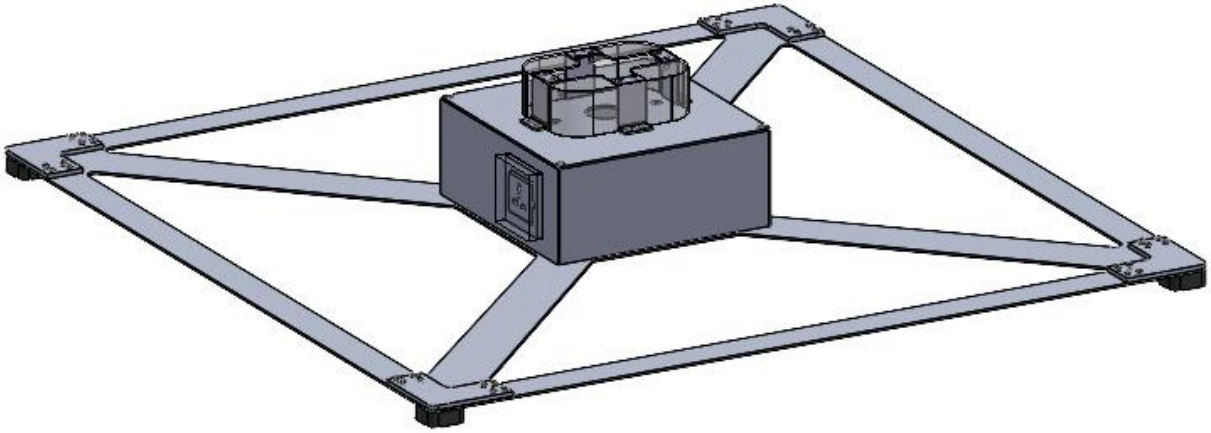

Base Assembly

A3

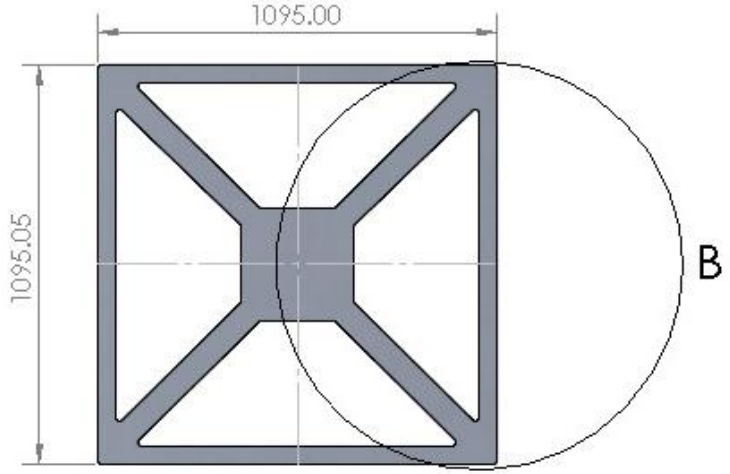

Top view

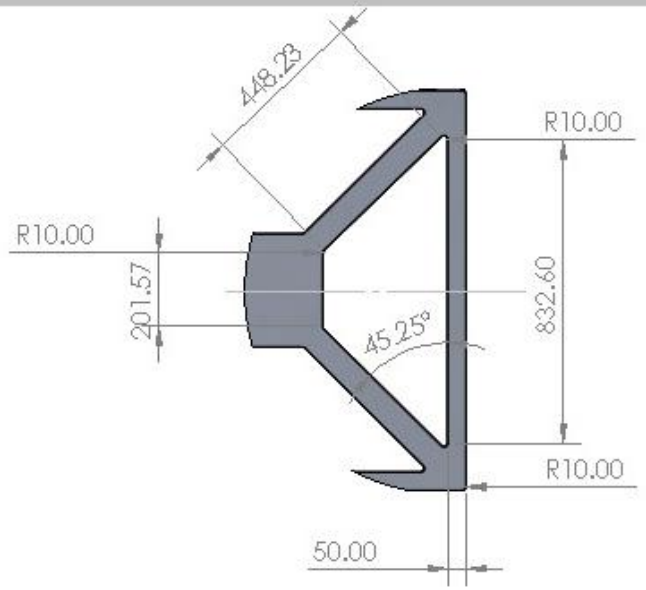

DETAIL B

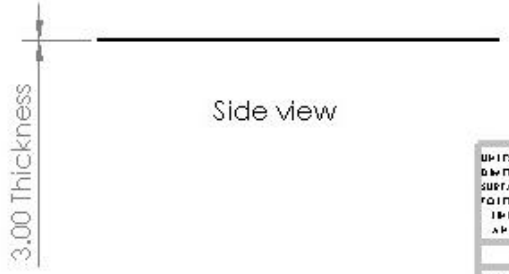

Side view

UNLESS OTHERWISE SPECIFIED: DIMENSIONS ARE IN MILLIMETERS SURFACE FINISH: TOLERANCES: ISO 2768-m LINEAR: ANGULAR:	FINISH: Mill Finish	DEBURR AND BREAK SHARP EDGES	DO NOT SCALE DRAWING / REVISION
NAME / SIGNATURE / DATE			TITLE: Base
DRAWN / CHK'D / APPV'D / MFG / Q.A	MATERIAL: Aluminium 6061-T6		DWG NO / A4
	WEIGHT: 5kg		SCALE: 1:1 / SHEET 1 OF 1

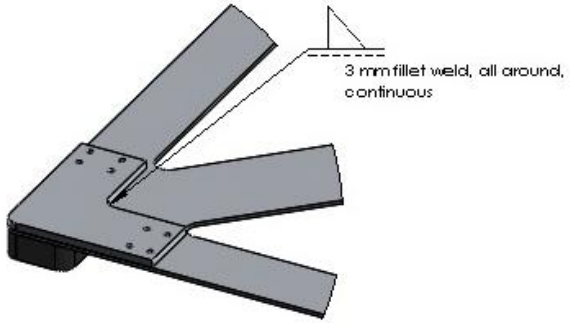

DETAIL B

SCALE 1 : 4

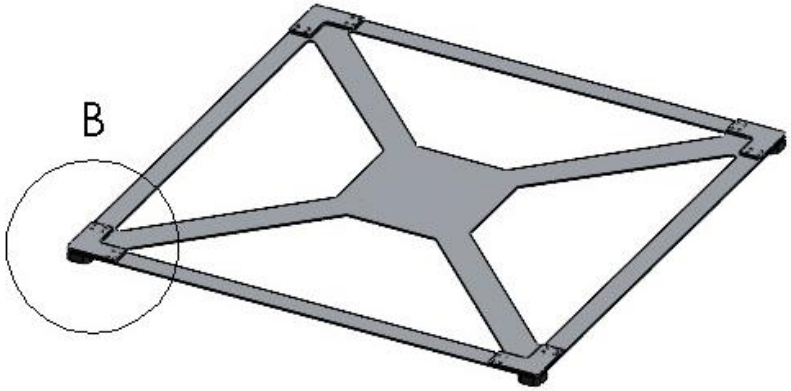

UNLESS OTHERWISE SPECIFIED: DIMENSIONS ARE IN MILLIMETERS SURFACE FINISH: TOLERANCES: LINEAR: ANGULAR:	FINISH: All L-brackets welded to base using continuous fillet weld, unless otherwise specified.	DEBURR AND BREAK SHARP EDGES	DO NOT SCALE DRAWING	REVISION	
	NAME	SIGNATURE	DATE	TITLE: Base Plate Welded Assembly	
DRAWN					
CHK'D					
APPV'D					
MFG					
Q.A				MATERIAL:	DWG NO. A4
				WEIGHT:	SCALE: 1:16 SHEET 1 OF 1

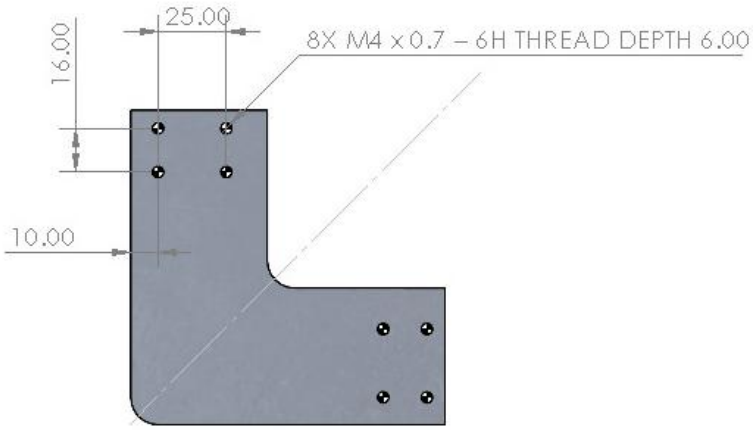

Top view

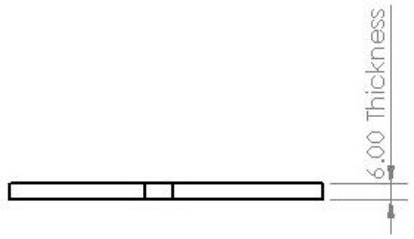

Side view

UNLESS OTHERWISE SPECIFIED: DIMENSIONS ARE IN MILLIMETERS SURFACE FINISH: TOLERANCES: ISO 2768-m LINEAR: ANGULAR:	FINISH: mill finish			DEBURR AND BREAK SHARP EDGES	DO NOT SCALE DRAWING	REVISION
	NAME	SIGNATURE	DATE		TITLE: Corner Base Plate	
DRAWN						
CHK'D						
APPV'D						
MFG						
Q.A				MATERIAL: Aluminium 6061- T6	DWG NO.	A4
				WEIGHT: 0.18kg	SCALE: 1:2	SHEET 1 OF 1

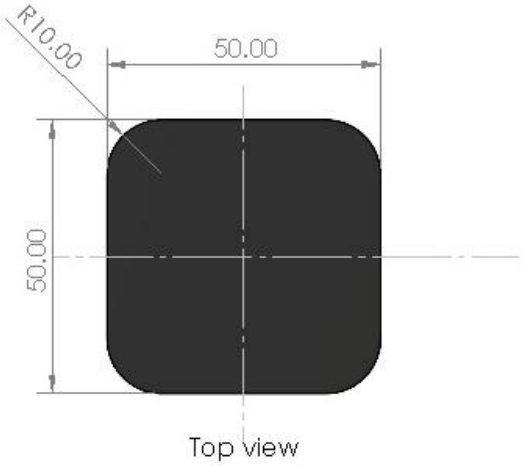

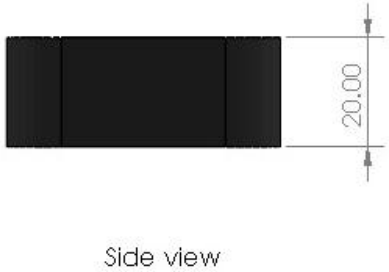

UNLESS OTHERWISE SPECIFIED: DIMENSIONS ARE IN MILLIMETERS SURFACE FINISH: TOLERANCES: ISO 2768-mK LINEAR: ANGULAR:	FINISH: As molded	DEBURR AND BREAK SHARP EDGES	DO NOT SCALE DRAWING / REVISION
			TITLE: Rubber Padding Corner
MATERIAL: EPDM Rubber			DWG NO. A4
WEIGHT:			SCALE: 1:1 / SHEET 1 OF 1

	NAME	SIGNATURE	DATE
DRAWN			
CHK'D			
APPV'D			
MFG			
Q.A			

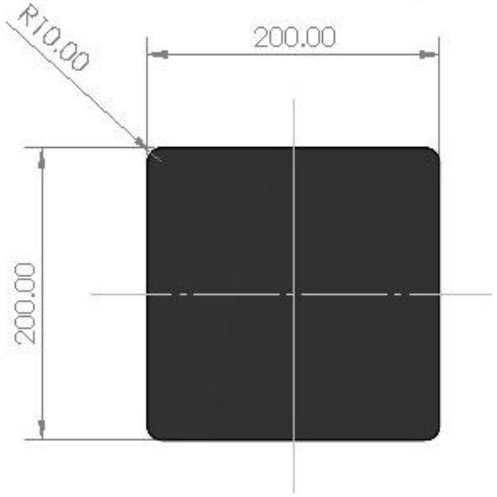

Top view

Side view

UNLESS OTHERWISE SPECIFIED: DIMENSIONS ARE IN MILLIMETERS SURFACE FINISH: TOLERANCES: LINEAR: ISO 2768-mK ANGULAR:	FINISH: As molded	DEBURR AND BREAK SHARP EDGES	DO NOT SCALE DRAWING	REVISION	
	NAME	SIGNATURE	DATE	TITLE: Bottom Base Center Padding	
DRAWN					
CHK'D					
APPV'D					
MFG					
Q.A				MATERIAL: EPDM Rubber	DWG NO. A4
				WEIGHT:	SCALE: 1:4 SHEET 1 OF 1

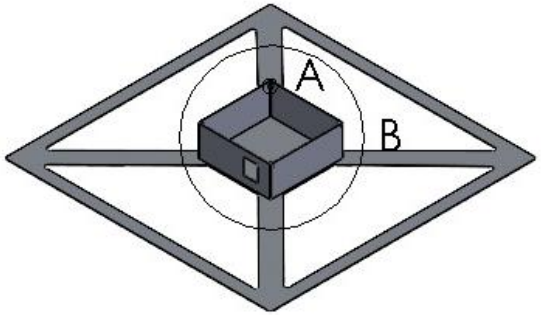

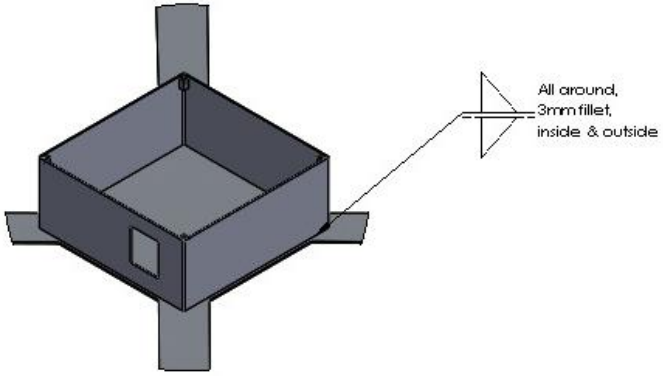

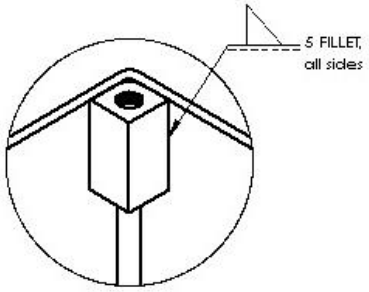

DETAIL B

SCALE 1 : 8

UNLESS OTHERWISE SPECIFIED: DIMENSIONS ARE IN MILLIMETERS SURFACE FINISH: TOLERANCES: LINEAR: ANGULAR:	FINISH: Welds per symbols, fillet welds unless noted. Clean weld spatter. Remove sharp edges.			DEBURR AND BREAK SHARP EDGES	DO NOT SCALE DRAWING	REVISION
	NAME	SIGNATURE	DATE		TITLE: Base Welded	
DRAWN						
CHK'D						
APPV'D						
MFG						
Q.A				MATERIAL:	DWG NO.	A4
				WEIGHT:	SCALE: 1:16	SHEET 1 OF 1

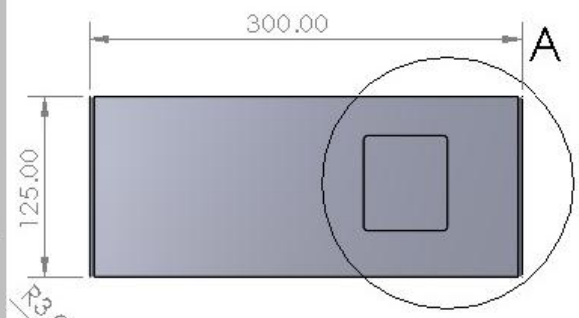

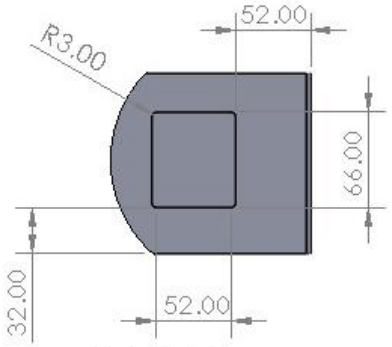

DETAIL A

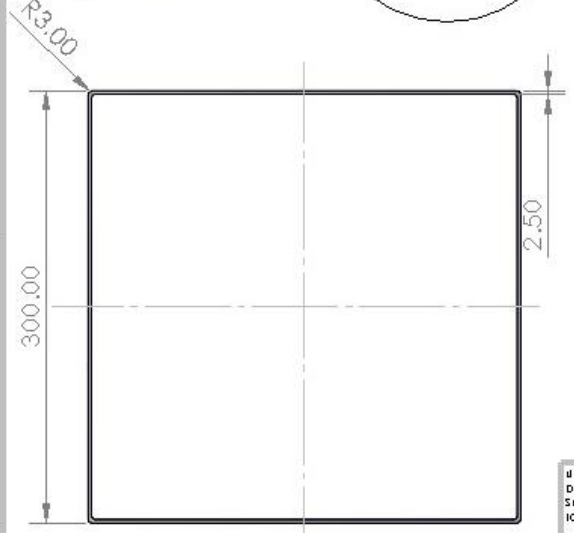

Top view

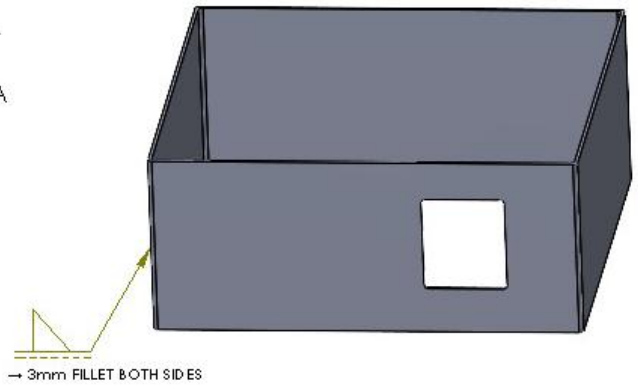

UNLESS OTHERWISE SPECIFIED: DIMENSIONS ARE IN MILLIMETERS SURFACE FINISH: TOLERANCES: ISO 2768-m LINEAR: ANGULAR:	FINISH: Mill finish	DEBURR AND BREAK SHARP EDGES	DO NOT SCALE DRAWING	REVISION	
	NAME	SIGNATURE	DATE	TITLE: Base Box	
DRAWN					
CHK'D					
APPV'D					
MFG					
Q.A				MATERIAL: Aluminium 6061-T6	DWG NO. A4
				WEIGHT: 0.9kg	SCALE: 2:1 SHEET 1 OF 1

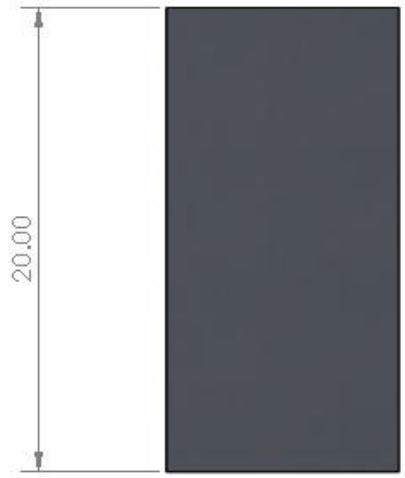

Side view

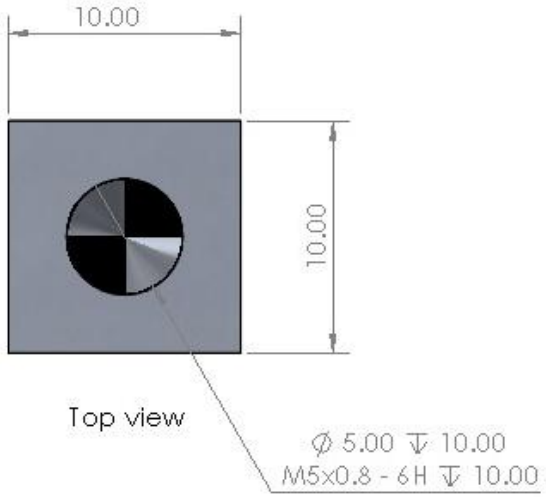

Top view

UNLESS OTHERWISE SPECIFIED: DIMENSIONS ARE IN MILLIMETERS SURFACE FINISH: TOLERANCES: ISO 2768-m LINEAR: ANGULAR:	FINISH: Milling finish	DEBURR AND BREAK SHARP EDGES	DO NOT SCALE DRAWING / REVISION
	NAME / SIGNATURE / DATE		TITLE: Lid Threaded Corner Block
DRAWN			
CHK'D			
APPV'D			
MFG			
Q.A		MATERIAL: Aluminium 6061 - T6	DWG NO. A4
		WEIGHT:	SCALE:2:1 / SHEET 1 OF 1

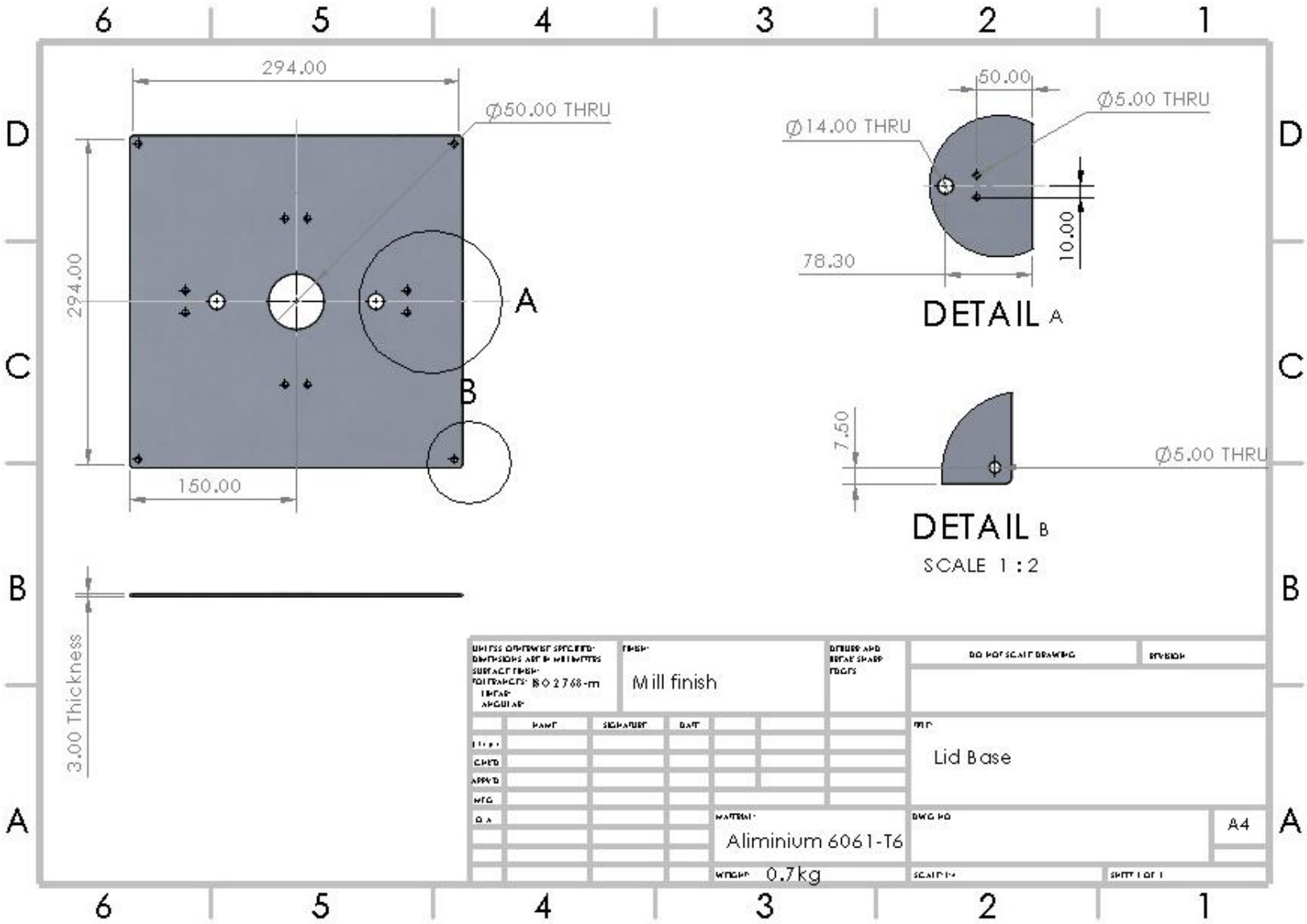
294.00
⌀50.00 THRU
294.00
150.00
A
B
50.00
⌀5.00 THRU
⌀14.00 THRU
10.00
78.30
DETAIL A
7.50
⌀5.00 THRU
DETAIL B
SCALE 1 : 2
3.00 Thickness
Mill finish
DO NOT SCALE DRAWING
REVISION
Lid Base
Aliminium 6061-T6
A4
0.7kg

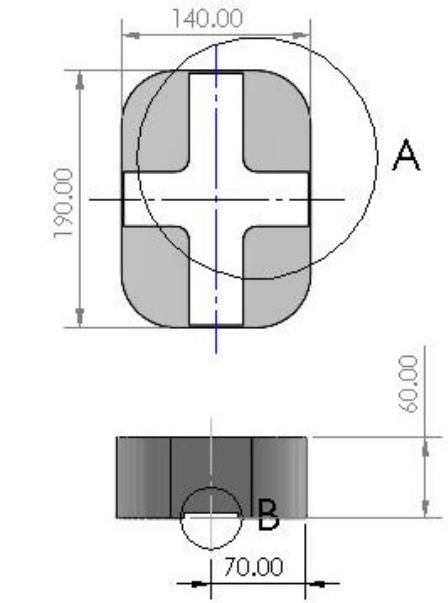

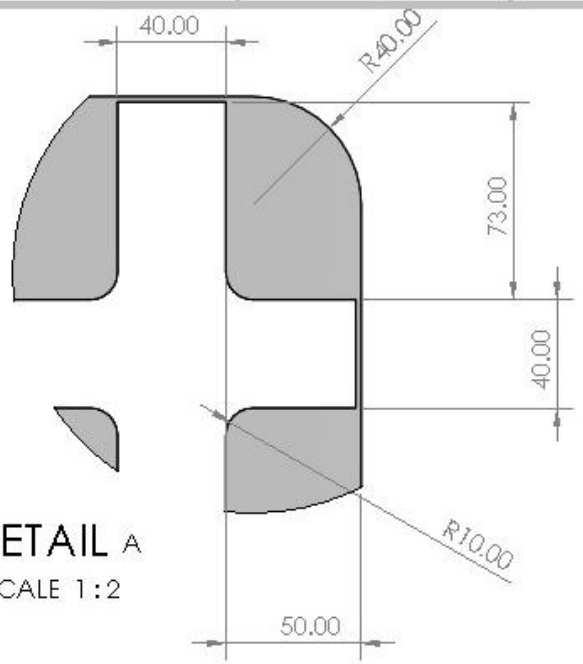

DETAIL A

SCALE 1:2

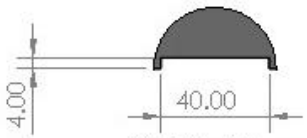

DETAIL B

SCALE 1:2

UNLESS OTHERWISE SPECIFIED: DIMENSIONS ARE IN MILLIMETERS SURFACE FINISH: TOLERANCES: ISO 2768-mK LINEAR: ANGULAR:	FINISH: As moulded	DEBURR AND BREAK SHARP EDGES	DO NOT SCALE DRAWING	REVISION	
NAME / SIGNATURE / DATE			TITLE: Bearing Casing		
DRAWN					
CHK'D					
APPV'D					
MFG					
Q.A			MATERIAL: ABS	DWG NO.	A4
			WEIGHT:	SCALE: 1:1	SHEET 1 OF 1

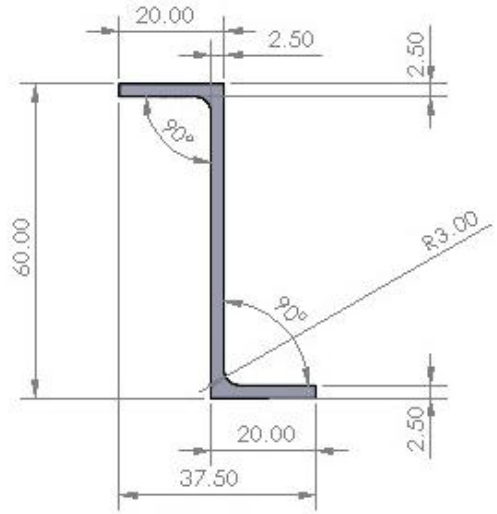

Side view

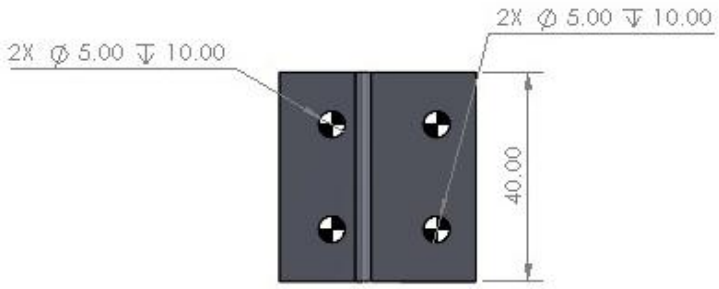

Top view

UNLESS OTHERWISE SPECIFIED:
DIMENSIONS ARE IN MILLIMETERS
SURFACE FINISH:
TOLERANCES: ISO 2768-m
LINEAR:
ANGULAR:

FINISH: Mill finish

DEBURR AND BREAK SHARP EDGES

DO NOT SCALE DRAWING

REVISION

	NAME	SIGNATURE	DATE
DRAWN			
CHK'D			
APPV'D			
MFG			
Q.A			

TITLE: CAM Bracket

MATERIAL: Aluminium 6061-T6

WEIGHT: 0.05kg

DWG NO.

A4

SCALE: 1:1

SHEET 1 OF 1

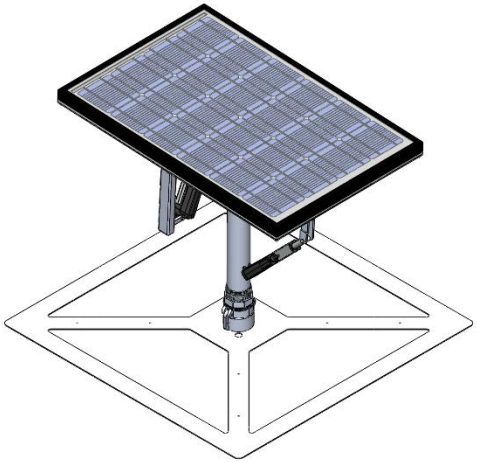

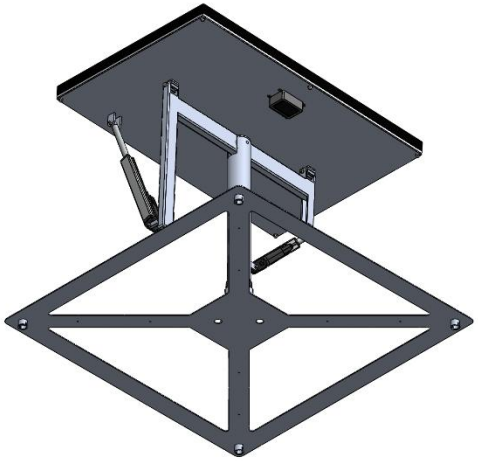

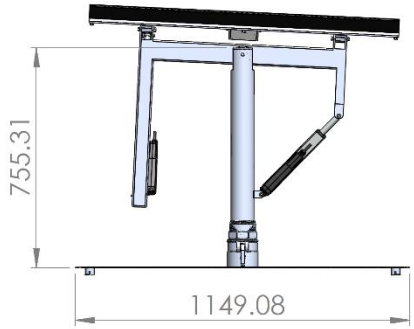

UNLESS OTHERWISE SPECIFIED: DIMENSIONS ARE IN MILLIMETERS SURFACE FINISH: TOLERANCES: LINEAR: ANGULAR:	FINISH:			DEBURR AND BREAK SHARP EDGES	DO NOT SCALE DRAWING	REVISION
	NAME	SIGNATURE	DATE		TITLE: Solar Assembly	
DRAWN						
CHK'D						
APPV'D						
MFG						
Q.A				MATERIAL:	DWG NO. Assembly	A4
				WEIGHT:	SCALE:1:20	SHEET 1 OF 1

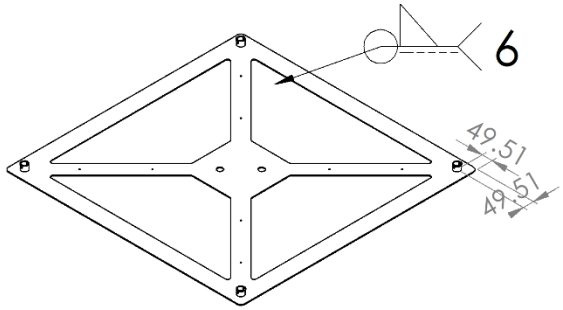

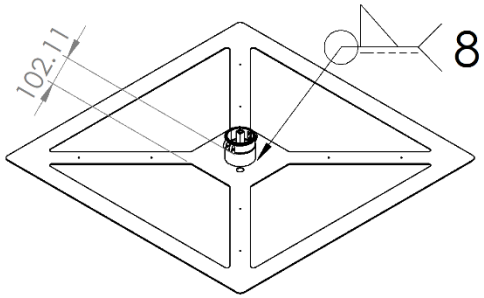

Shaft Attachment is weld at center of the base plate

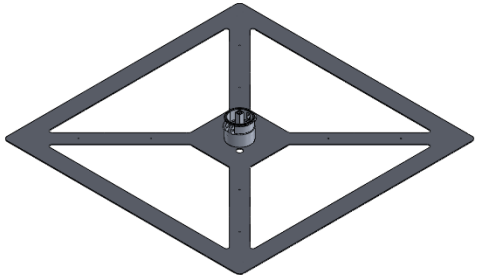

UNLESS OTHERWISE SPECIFIED: DIMENSIONS ARE IN MILLIMETERS SURFACE FINISH: TOLERANCES: LINEAR: ANGULAR:	FINISH:			DEBURR AND BREAK SHARP EDGES	DO NOT SCALE DRAWING	REVISION
	NAME	SIGNATURE	DATE		TITLE: Solar Assembly Plate	
DRAWN						
CHK'D						
APPV'D						
MFG						
Q.A				MATERIAL:	DWG NO. Top_Plate	A4
				WEIGHT:	SCALE:1:20	SHEET 1 OF 1

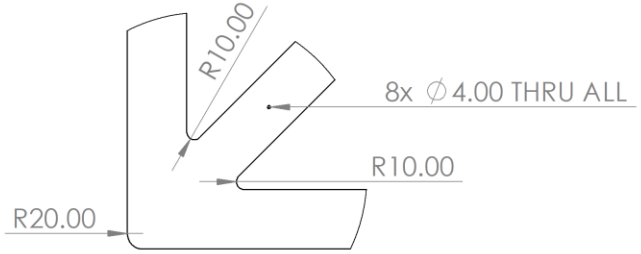

DETAIL A

SCALE 2 : 15

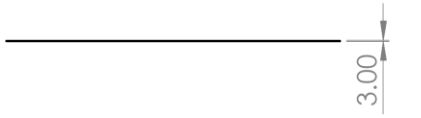

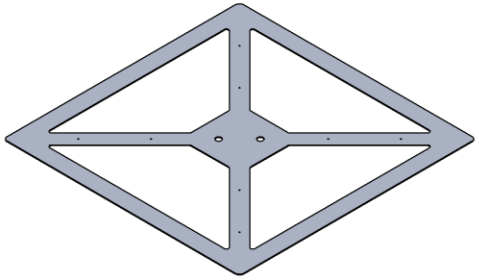

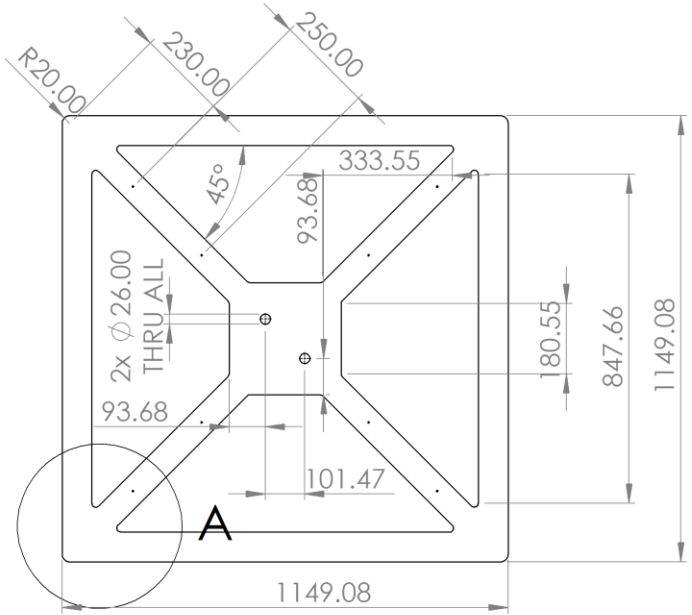

*Square plate with holes equidistant to each corner, except for 2 in center

UNLESS OTHERWISE SPECIFIED: DIMENSIONS ARE IN MILLIMETERS SURFACE FINISH: TOLERANCES: ISO 2768-m LINEAR: ANGULAR:	FINISH: Mill Finish		DEBURR AND BREAK SHARP EDGES	DO NOT SCALE DRAWING	REVISION
	NAME	SIGNATURE	DATE	TITLE: Solar Assembly Plate Base	
DRAWN					
CHK'D					
APPV'D					
MFG					
Q.A			MATERIAL: Aluminium 6061	DWG NO. Top_Plate_Plate	A4
			WEIGHT:	SCALE:1:20	SHEET 1 OF 1

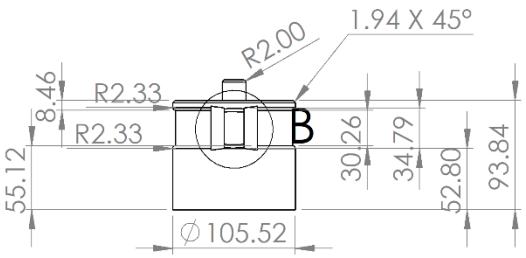

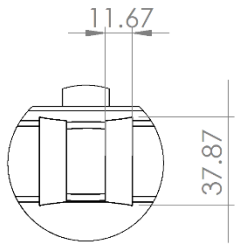

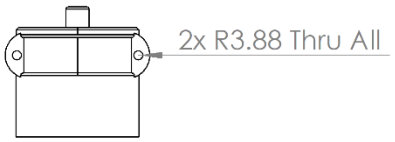

DETAIL B

SCALE 2 : 5

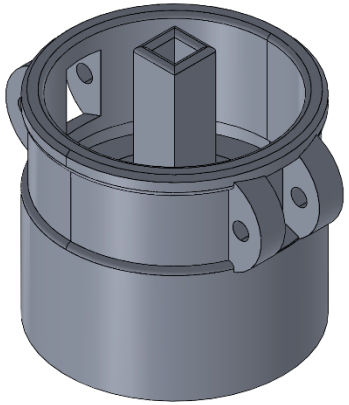

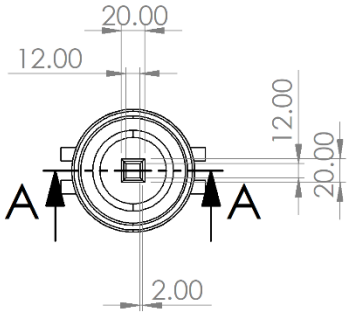

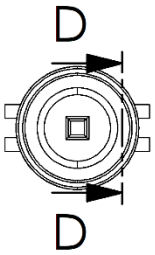

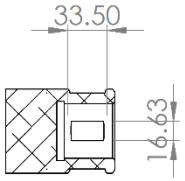

SECTION D-D

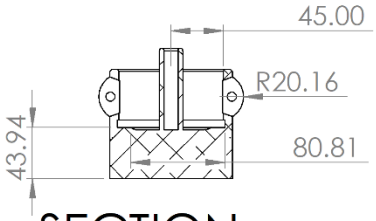

SECTION A-A

UNLESS OTHERWISE SPECIFIED: DIMENSIONS ARE IN MILLIMETERS SURFACE FINISH: TOLERANCES: ISO 2768-m LINEAR: ANGULAR:	FINISH: Mill Finish		DEBURR AND BREAK SHARP EDGES	DO NOT SCALE DRAWING	REVISION
	NAME	SIGNATURE	DATE	TITLE: Solar Assembly Plate Shaft	
DRAWN					
CHK'D					
APPV'D					
MFG					
Q.A			MATERIAL: Aluminium 6061	DWG NO. Top_Plate_Shaft	A4
			WEIGHT:	SCALE:1:5	SHEET 1 OF 1

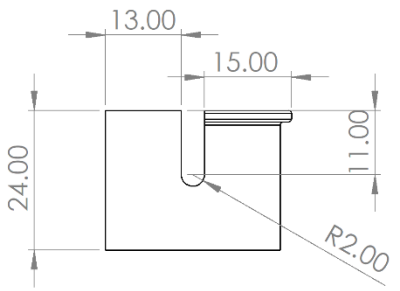

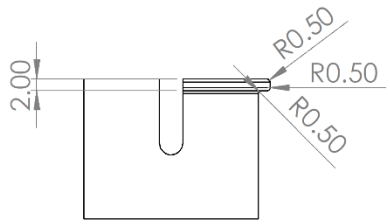

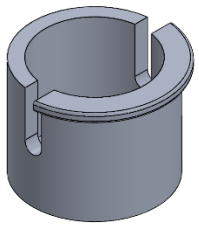

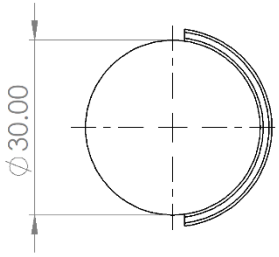

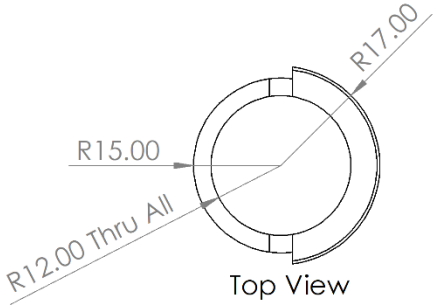

UNLESS OTHERWISE SPECIFIED: DIMENSIONS ARE IN MILLIMETERS SURFACE FINISH: TOLERANCES: ISO 2768-m LINEAR: ANGULAR:	FINISH: Mill Finish			DEBURR AND BREAK SHARP EDGES	DO NOT SCALE DRAWING	REVISION
	NAME	SIGNATURE	DATE		TITLE: Solar Assembly Plate Technic Pins	
DRAWN						
CHK'D						
APPV'D						
MFG						
Q.A				MATERIAL: Aluminium	DWG NO. Top_Plate_Techpins	A4
				WEIGHT:	SCALE:1:1	SHEET 1 OF 1

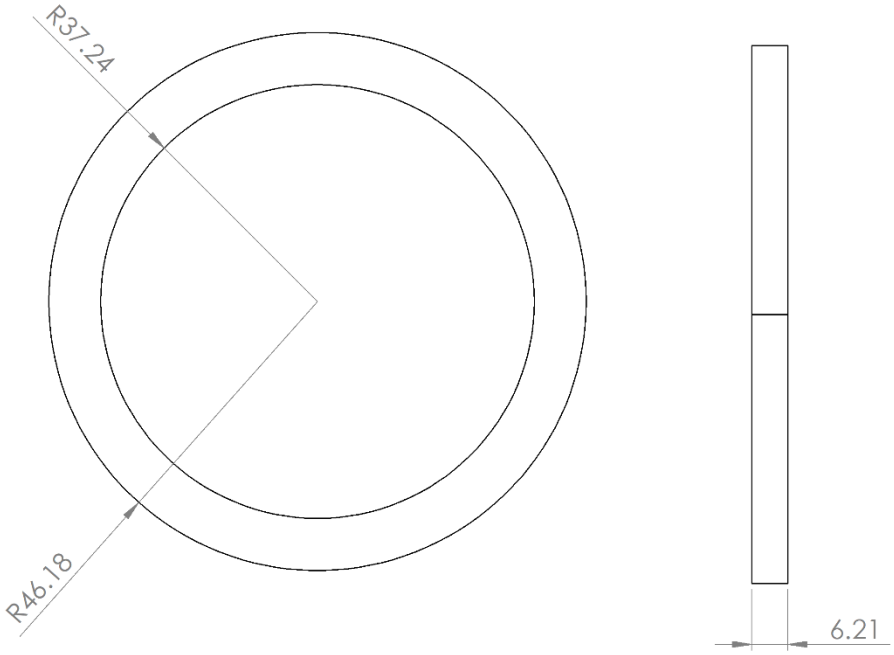

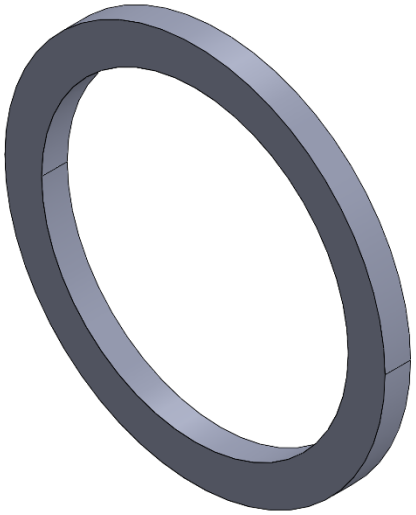

UNLESS OTHERWISE SPECIFIED: DIMENSIONS ARE IN MILLIMETERS SURFACE FINISH: TOLERANCES: ISO 2768-m LINEAR: ANGULAR:	FINISH: As Molded			DEBURR AND BREAK SHARP EDGES	DO NOT SCALE DRAWING	REVISION
	NAME	SIGNATURE	DATE		TITLE: Solar Assembly Plate Pressure Ring	
DRAWN						
CHK'D						
APPV'D						
MFG						
Q.A				MATERIAL: EPDM (Ethylene Propylene Diene Monomer) Shore A 60 ±5	DWG NO. Pressure_Ring	A4
				WEIGHT:	SCALE:1:1	SHEET 1 OF 1

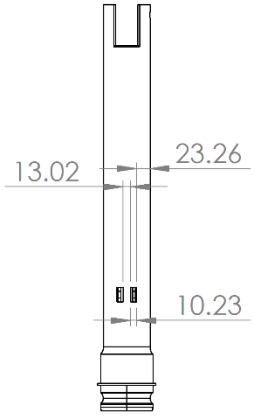

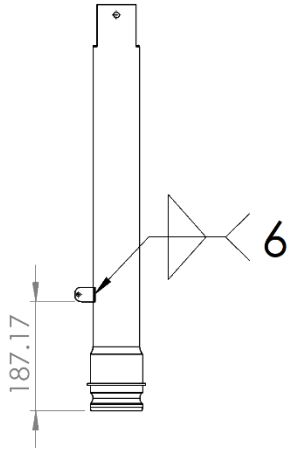

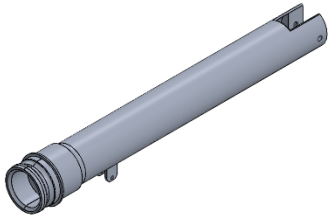

Weld actuator supports on either ends

UNLESS OTHERWISE SPECIFIED: DIMENSIONS ARE IN MILLIMETERS SURFACE FINISH: TOLERANCES: LINEAR: ANGULAR:	FINISH: Mill Finish		DEBURR AND BREAK SHARP EDGES	DO NOT SCALE DRAWING	REVISION
	NAME	SIGNATURE	DATE	TITLE: Solar Assembly Shaft	
DRAWN					
CHK'D					
APPV'D					
MFG					
Q.A			MATERIAL: Aluminium 6061	DWG NO. Shaft	A4
			WEIGHT:	SCALE:1:10	SHEET 1 OF 1

6

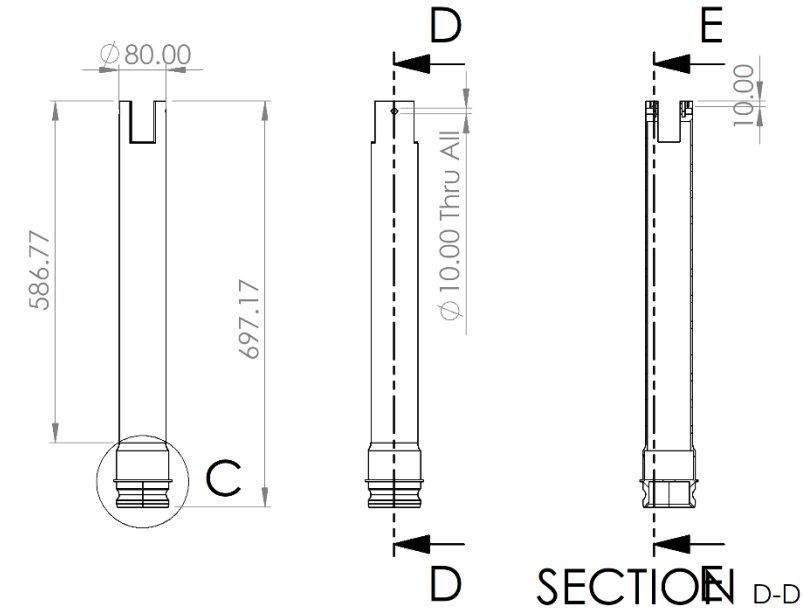

UNLESS OTHERWISE SPECIFIED: DIMENSIONS ARE IN MILLIMETERS SURFACE FINISH: TOLERANCES:ISO 2768-m LINEAR: ANGULAR:	FINISH: Mill Finish		DEBURR AND BREAK SHARP EDGES	DO NOT SCALE DRAWING	REVISION
	NAME	SIGNATURE	DATE	TITLE: Solar Assembly Shaft Main	
DRAWN					
CHK'D					
APPV'D					
MFG					
Q.A			MATERIAL: Aluminium 6061	DWG NO. Shaft Main	A4
			WEIGHT:	SCALE:1:10	SHEET 1 OF 1

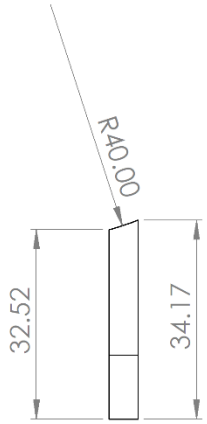

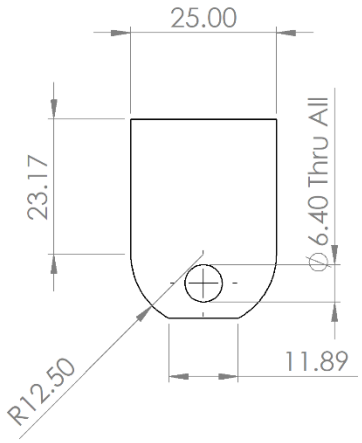

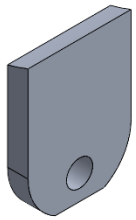

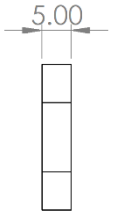

UNLESS OTHERWISE SPECIFIED: DIMENSIONS ARE IN MILLIMETERS SURFACE FINISH: TOLERANCES: ISO 2768-m LINEAR: ANGULAR:	FINISH: Mill Finish	DEBURR AND BREAK SHARP EDGES	DO NOT SCALE DRAWING / REVISION

	NAME	SIGNATURE	DATE
DRAWN			
CHK'D			
APPV'D			
MFG			
Q.A			

MATERIAL: Aluminium 6061

WEIGHT:

TITLE:

Solar Assembly Shaft Attachment

DWG NO. Shaft_Attach Attachment

A4

SCALE:1:1

SHEET 1 OF 1

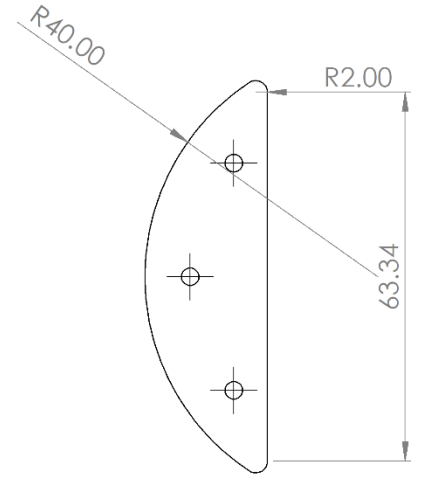

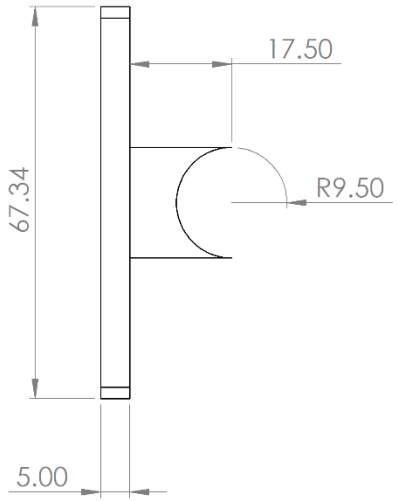

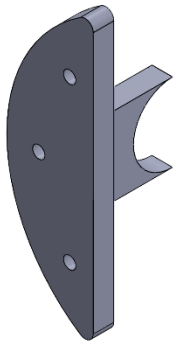

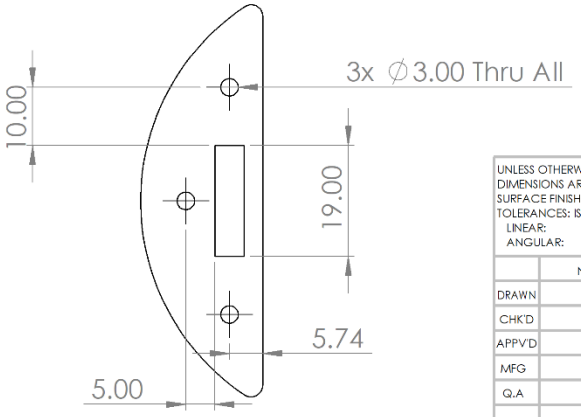

UNLESS OTHERWISE SPECIFIED: DIMENSIONS ARE IN MILLIMETERS SURFACE FINISH: TOLERANCES: ISO 2768-m LINEAR: ANGULAR:	FINISH: As Moulded	DEBURR AND BREAK SHARP EDGES	DO NOT SCALE DRAWING / REVISION

	NAME	SIGNATURE	DATE
DRAWN			
CHK'D			
APPV'D			
MFG			
Q.A			

MATERIAL: ABS

WEIGHT:

TITLE:

Solar Assembly Shaft Bearing Cap

DWG NO. Bearing Cap

A4

SCALE:1:1

SHEET 1 OF 1

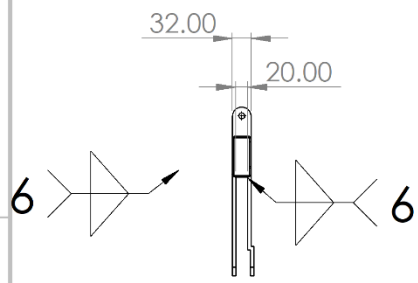

SECTION A-A

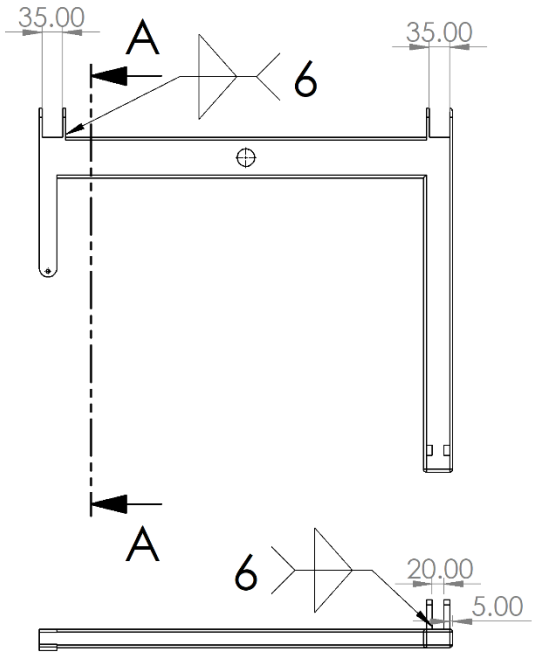

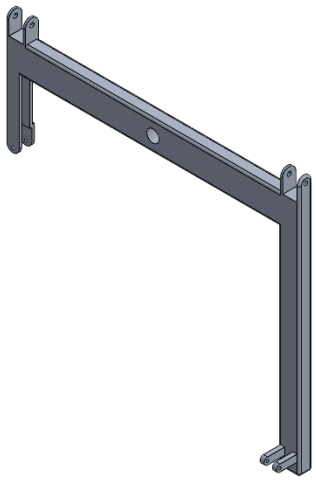

UNLESS OTHERWISE SPECIFIED: DIMENSIONS ARE IN MILLIMETERS SURFACE FINISH: TOLERANCES: ISO-2678-m LINEAR: ANGULAR:	FINISH: Mill Finish		DEBURR AND BREAK SHARP EDGES	DO NOT SCALE DRAWING	REVISION
	NAME	SIGNATURE	DATE	TITLE: Solar Assembly Support	
DRAWN					
CHK'D					
APPV'D					
MFG					
Q.A			MATERIAL: Aluminium 6061	DWG NO. Support	A4
			WEIGHT:	SCALE:1:10	SHEET 1 OF 1

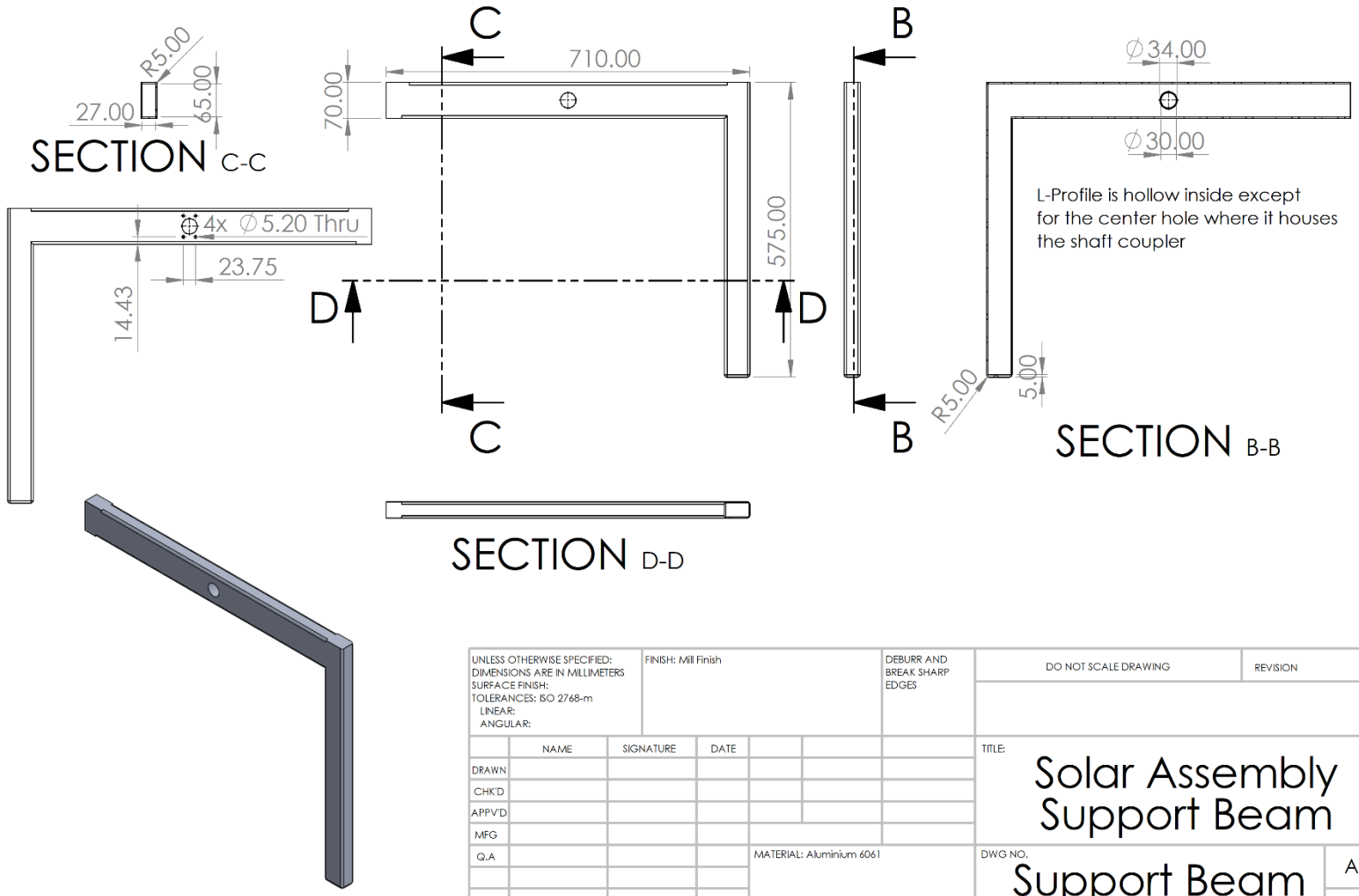

UNLESS OTHERWISE SPECIFIED: DIMENSIONS ARE IN MILLIMETERS SURFACE FINISH: TOLERANCES: ISO 2768-m LINEAR: ANGULAR:	FINISH: Mill Finish		DEBURR AND BREAK SHARP EDGES	DO NOT SCALE DRAWING	REVISION
	NAME	SIGNATURE	DATE	TITLE: Solar Assembly Support Beam	
DRAWN					
CHK'D					
APPV'D					
MFG					
Q.A			MATERIAL: Aluminium 6061	DWG NO. Support Beam	A4
			WEIGHT:	SCALE:1:10	SHEET 1 OF 1

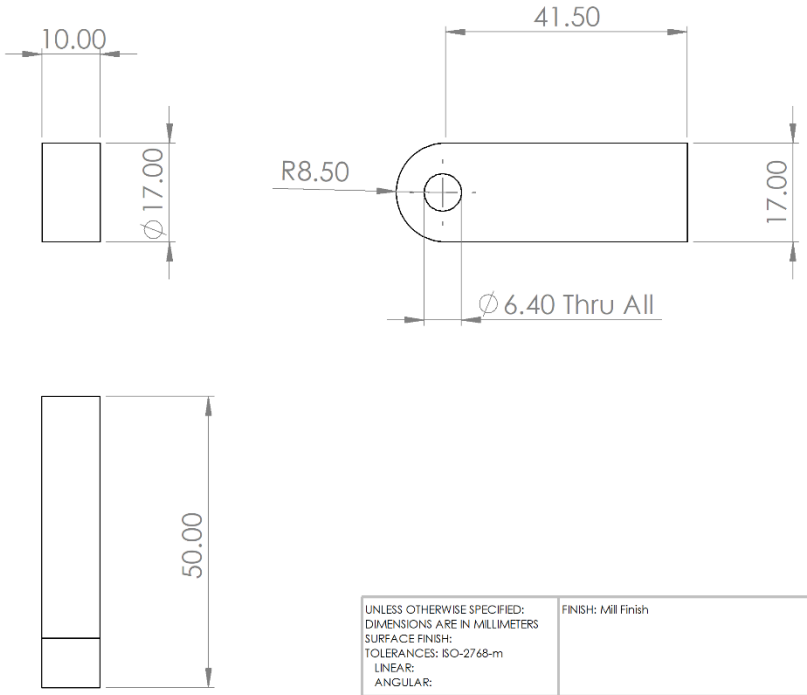

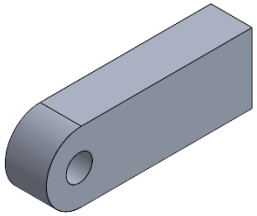

UNLESS OTHERWISE SPECIFIED: DIMENSIONS ARE IN MILLIMETERS SURFACE FINISH: TOLERANCES: ISO-2768-m LINEAR: ANGULAR:	FINISH: Mill Finish		DEBURR AND BREAK SHARP EDGES	DO NOT SCALE DRAWING	REVISION
	NAME	SIGNATURE	DATE	TITLE: Support Beam Panel	
DRAWN					
CHK'D					
APPV'D					
MFG					
Q.A			MATERIAL: Aluminium 6061	DWG NO. Support Beam_Panel	A4
			WEIGHT:	SCALE:1:1	SHEET 1 OF 1

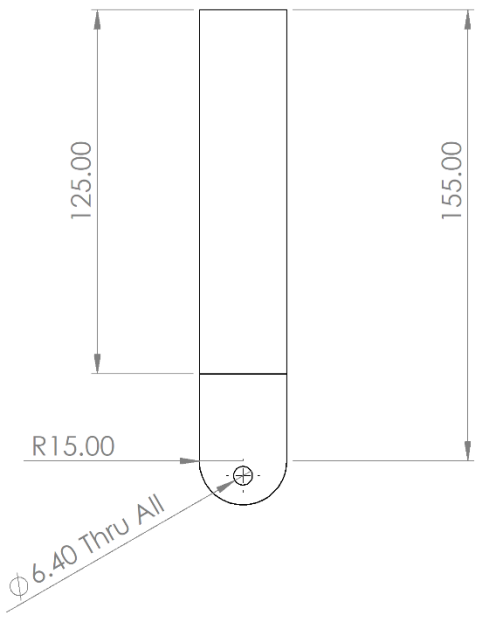

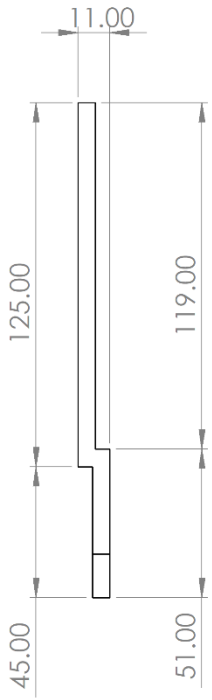

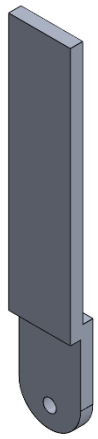

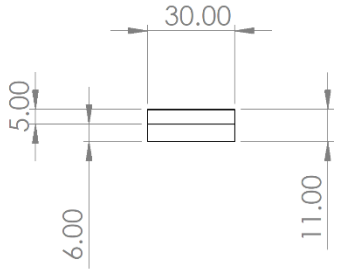

UNLESS OTHERWISE SPECIFIED: DIMENSIONS ARE IN MILLIMETERS SURFACE FINISH: TOLERANCES: ISO 2678-m LINEAR: ANGULAR:	FINISH: Mill Finish		DEBURR AND BREAK SHARP EDGES	DO NOT SCALE DRAWING	REVISION
	NAME	SIGNATURE	DATE	TITLE: Support Beam Linear Actuator 1	
DRAWN					
CHK'D					
APPV'D					
MFG					
Q.A				MATERIAL: Aluminium 6061	DWG NO. Support Beam_Linear1 A4
				WEIGHT:	SCALE:1:2 SHEET 1 OF 1

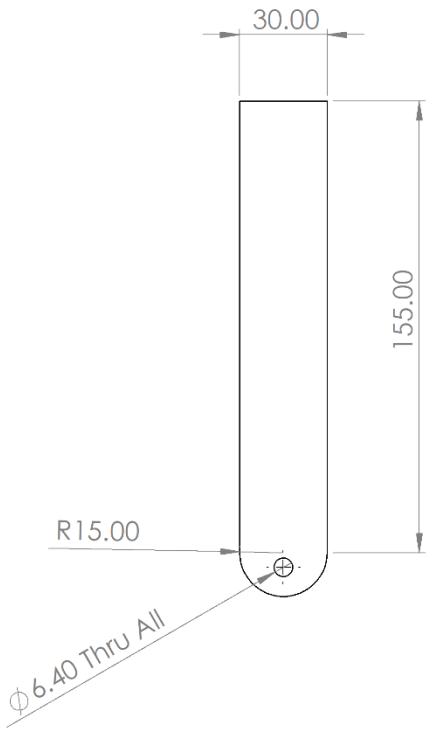

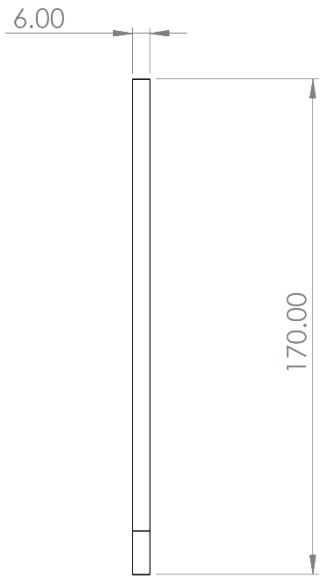

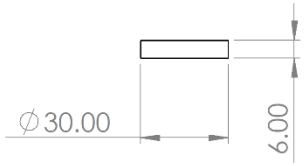

UNLESS OTHERWISE SPECIFIED: DIMENSIONS ARE IN MILLIMETERS SURFACE FINISH: TOLERANCES: ISO 2678-m LINEAR: ANGULAR:	FINISH: Mill Finish		DEBURR AND BREAK SHARP EDGES	DO NOT SCALE DRAWING	REVISION
	NAME	SIGNATURE	DATE	TITLE: Support Beam Linear Actuator 2	
DRAWN					
CHK'D					
APPV'D					
MFG					
Q.A				MATERIAL: Aluminium 6061	DWG NO. Support Beam_Linear2 A4
				WEIGHT:	SCALE:1:2 SHEET 1 OF 1

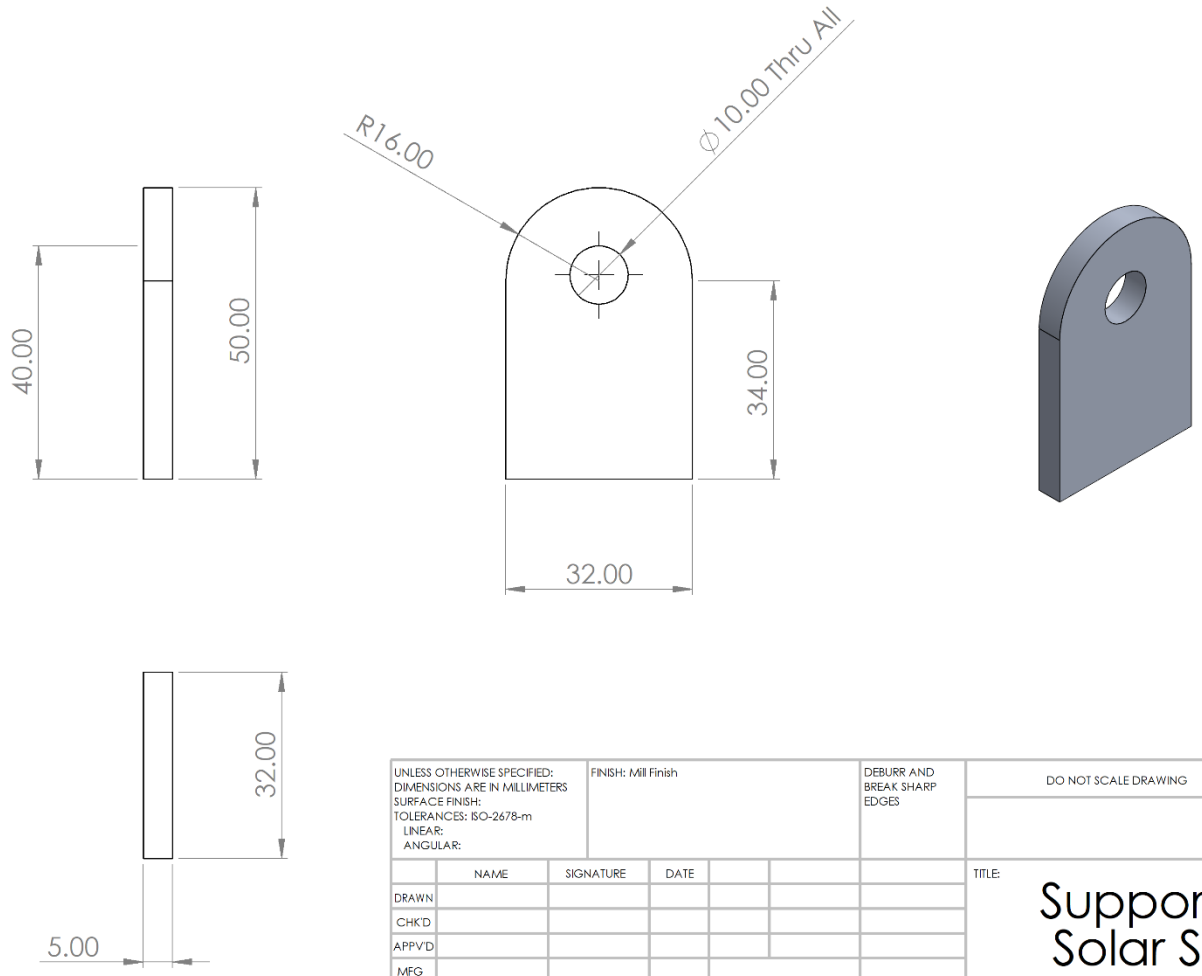

UNLESS OTHERWISE SPECIFIED:
DIMENSIONS ARE IN MILLIMETERS
SURFACE FINISH:
TOLERANCES: ISO-2678-m
LINEAR:
ANGULAR:

FINISH: Mill Finish

DEBURR AND BREAK SHARP EDGES

DO NOT SCALE DRAWING

REVISION

	NAME	SIGNATURE	DATE
DRAWN			
CHK'D			
APPV'D			
MFG			
Q.A			

TITLE:

Support Beam Solar Support

MATERIAL: Aluminium-6061

DWG NO.

Support Beam_Solar

A4

WEIGHT:

SCALE:1:1

SHEET 1 OF 1

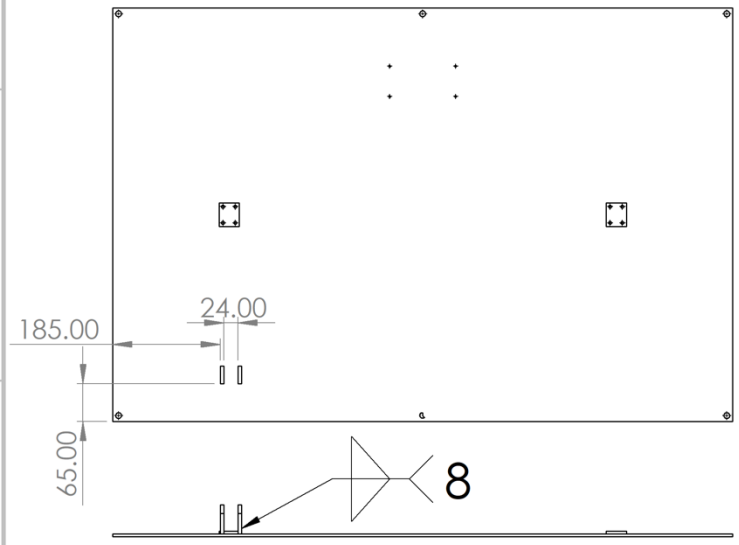

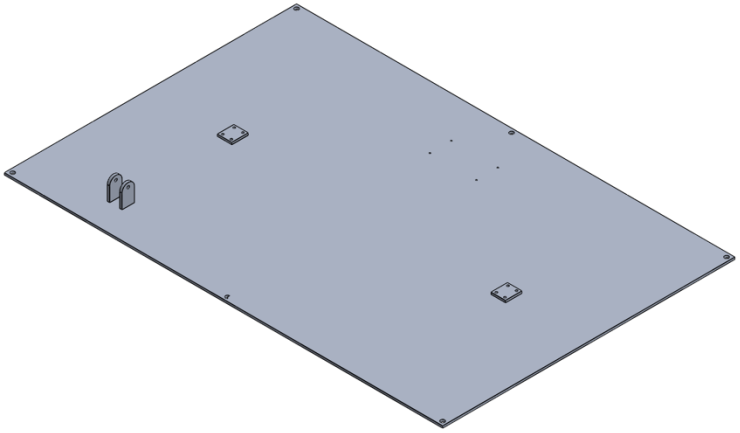

UNLESS OTHERWISE SPECIFIED: DIMENSIONS ARE IN MILLIMETERS SURFACE FINISH: TOLERANCES: ISO 2678-m LINEAR: ANGULAR:	FINISH: Mill Finish			DEBURR AND BREAK SHARP EDGES	DO NOT SCALE DRAWING	REVISION
	NAME	SIGNATURE	DATE		TITLE: Solar Assembly Solar Plate	
DRAWN						
CHK'D						
APPV'D						
MFG						
Q.A				MATERIAL: Aluminium 6061	DWG NO. Solar Plate1	A4
				WEIGHT:	SCALE:1:20	SHEET 1 OF 1

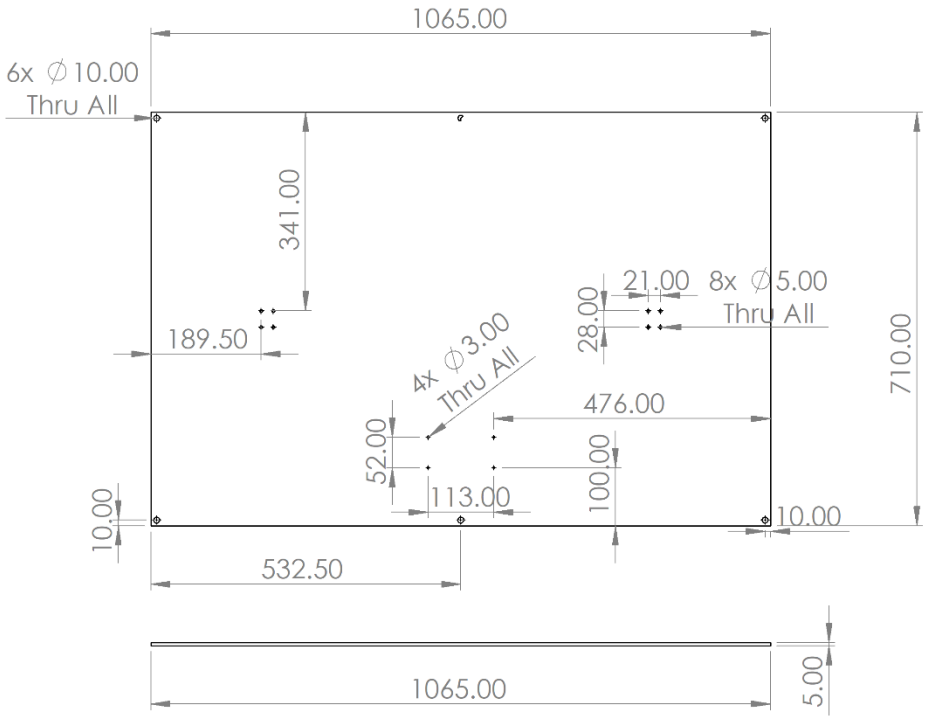

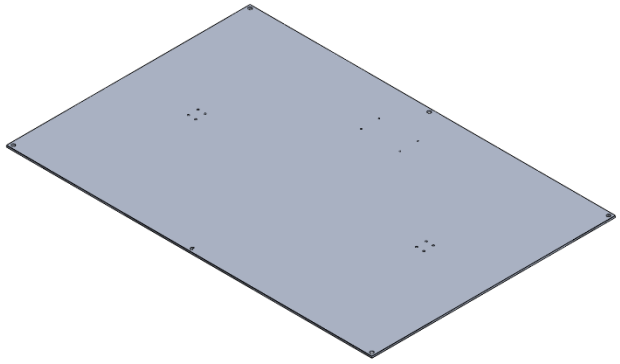

UNLESS OTHERWISE SPECIFIED: DIMENSIONS ARE IN MILLIMETERS SURFACE FINISH: TOLERANCES: ISO 2678-m LINEAR: ANGULAR:	FINISH: Mill Finish		DEBURR AND BREAK SHARP EDGES	DO NOT SCALE DRAWING	REVISION
	NAME	SIGNATURE	DATE	TITLE: Solar Assembly Solar Plate Base	
DRAWN					
CHK'D					
APPV'D					
MFG					
Q.A				MATERIAL: Aluminium 6061	DWG NO. Solar Plate A4
				WEIGHT:	SCALE:1:20 SHEET 1 OF 1

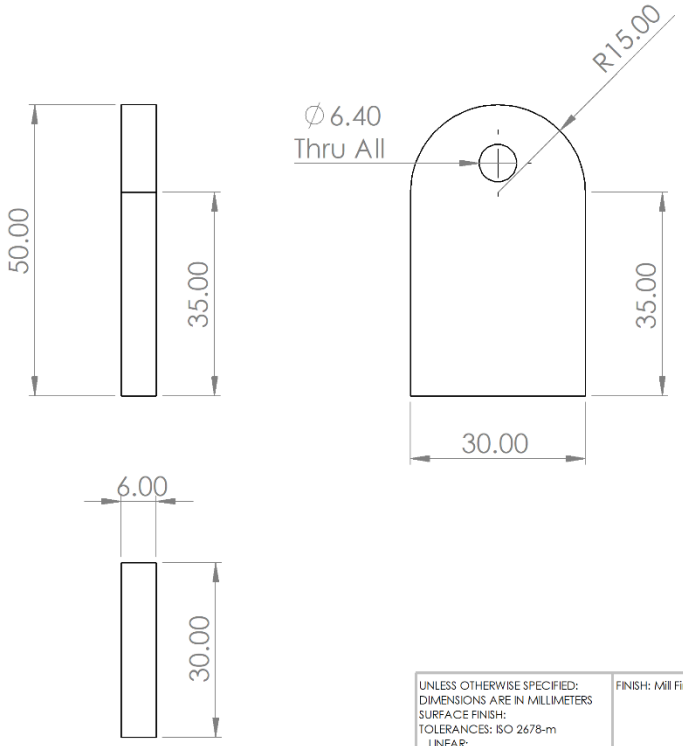

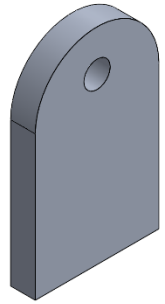

UNLESS OTHERWISE SPECIFIED: DIMENSIONS ARE IN MILLIMETERS SURFACE FINISH: TOLERANCES: ISO 2678-m LINEAR: ANGULAR:	FINISH: Mill Finish		DEBURR AND BREAK SHARP EDGES	DO NOT SCALE DRAWING	REVISION
	NAME	SIGNATURE	DATE	TITLE: Solar Assembly Solar Plate Support	
DRAWN					
CHK'D					
APPV'D					
MFG					
Q.A				MATERIAL: Aluminium 6061	DWG NO. Solar Plate_Support A4
				WEIGHT:	SCALE:1:1 SHEET 1 OF 1

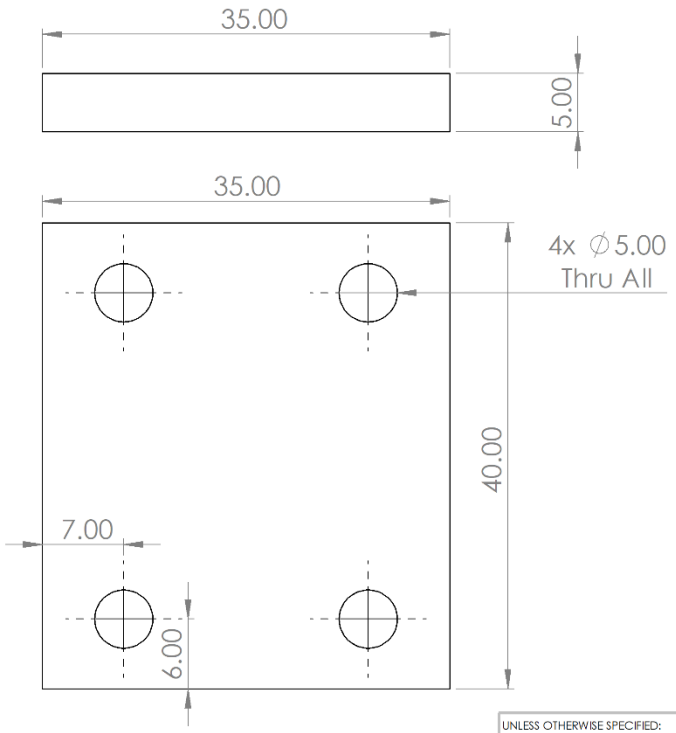

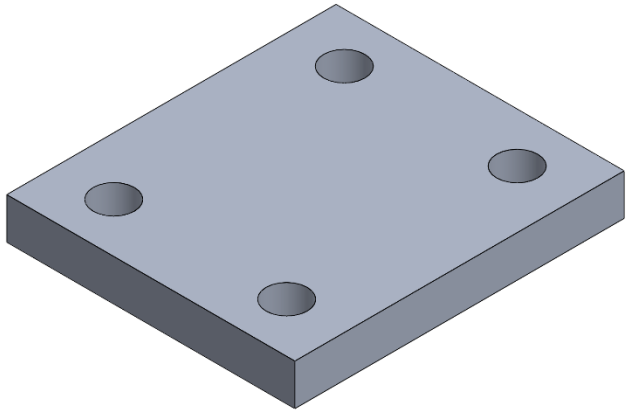

UNLESS OTHERWISE SPECIFIED: DIMENSIONS ARE IN MILLIMETERS SURFACE FINISH: TOLERANCES: ISO 2678-m LINEAR: ANGULAR:	FINISH: Mill Finish	DEBURR AND BREAK SHARP EDGES	DO NOT SCALE DRAWING / REVISION

	NAME	SIGNATURE	DATE
DRAWN			
CHK'D			
APPV'D			
MFG			
Q.A			

MATERIAL: Aluminium 6061

WEIGHT:

TITLE:

Solar Assembly
Solar Plate Bearing

DWG NO. Solar Plate_Bearing

A4

SCALE:2:1

SHEET 1 OF 1

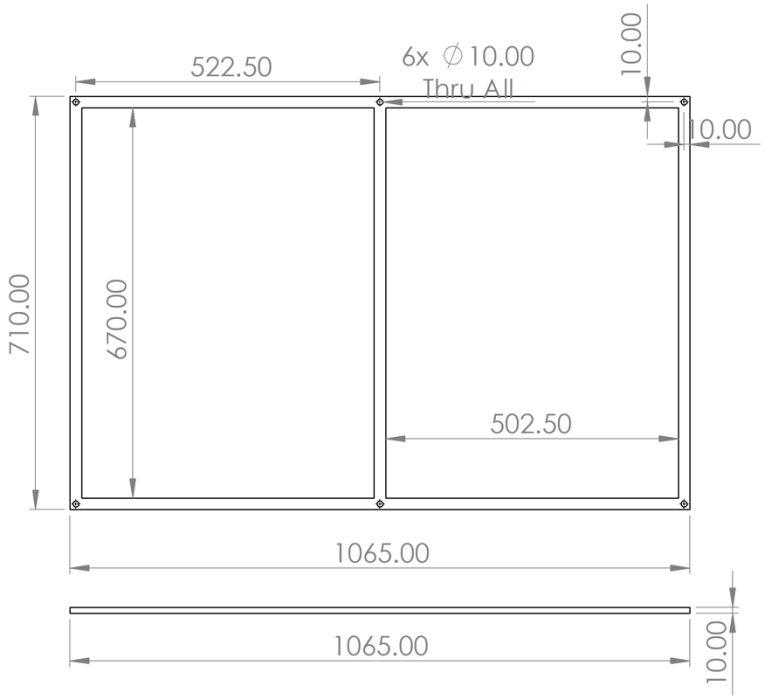

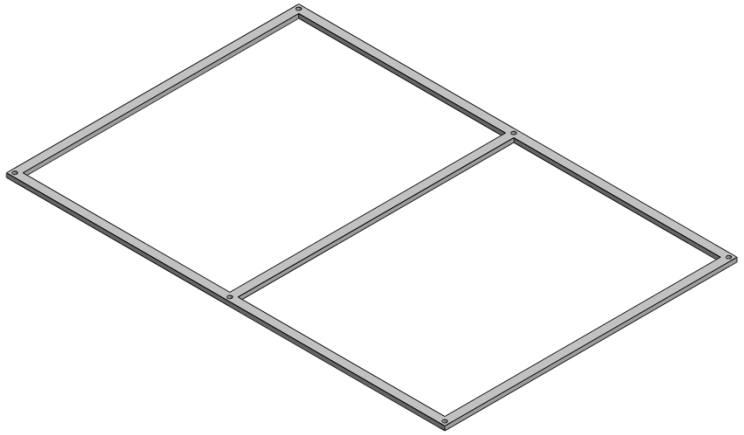

UNLESS OTHERWISE SPECIFIED: DIMENSIONS ARE IN MILLIMETERS SURFACE FINISH: TOLERANCES: ISO 2678-m LINEAR: ANGULAR:	FINISH: Mill Finish		DEBURR AND BREAK SHARP EDGES	DO NOT SCALE DRAWING	REVISION
	NAME	SIGNATURE	DATE	TITLE: Solar Assembly Solar Platform	
DRAWN					
CHK'D					
APPV'D					
MFG					
Q.A			MATERIAL: Aluminium 6061	DWG NO. Solar Platform	A4
			WEIGHT:	SCALE:1:20	SHEET 1 OF 1

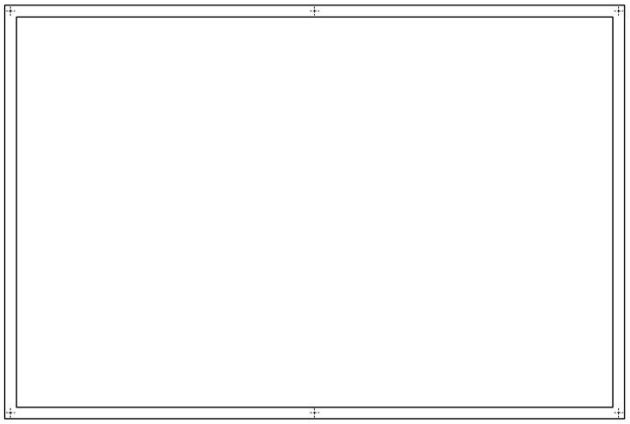

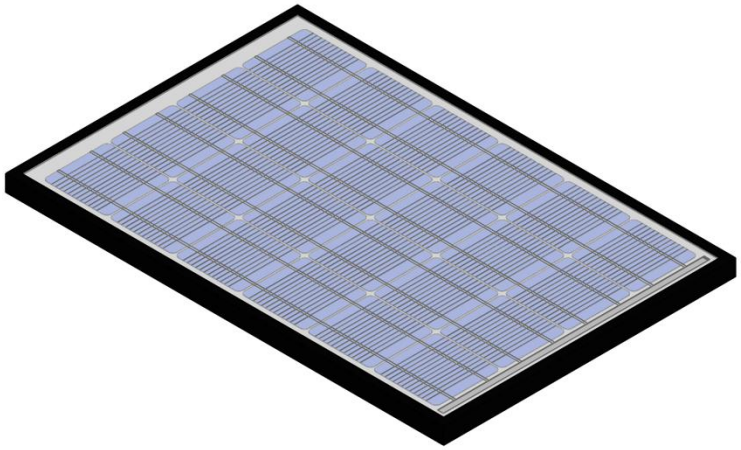

UNLESS OTHERWISE SPECIFIED: DIMENSIONS ARE IN MILLIMETERS SURFACE FINISH: TOLERANCES: LINEAR: ANGULAR:	FINISH:			DEBURR AND BREAK SHARP EDGES	DO NOT SCALE DRAWING	REVISION
	NAME	SIGNATURE	DATE		TITLE: Solar Panel	
DRAWN						
CHK'D						
APPV'D						
MFG						
Q.A				MATERIAL:	DWG NO. Solar Panel	A4
				WEIGHT:	SCALE:1:20	SHEET 1 OF 1

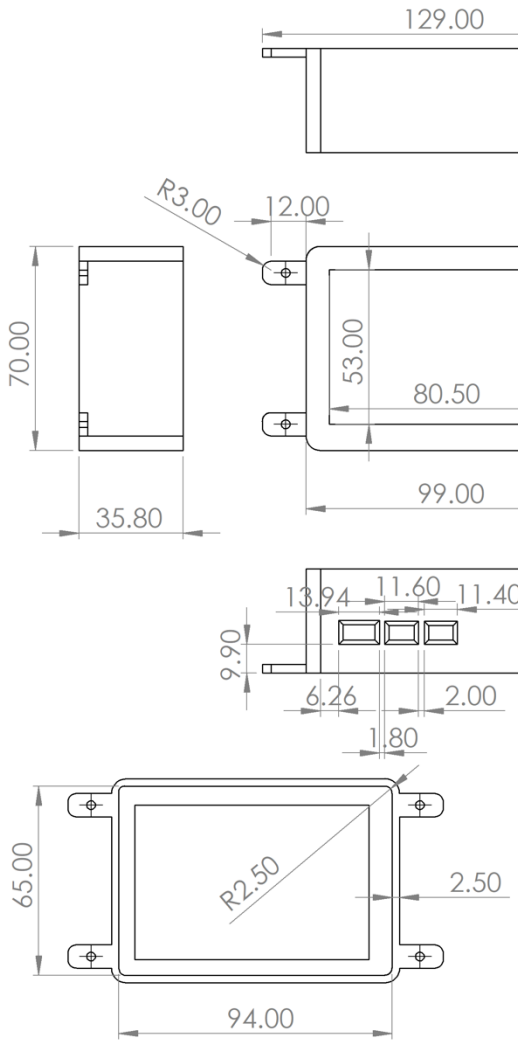

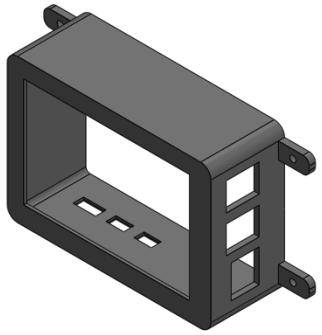

UNLESS OTHERWISE SPECIFIED: DIMENSIONS ARE IN MILLIMETERS SURFACE FINISH: TOLERANCES: ISO 2678-m LINEAR: ANGULAR:	FINISH: 3D Printed As Moulded	DEBURR AND BREAK SHARP EDGES	DO NOT SCALE DRAWING	REVISION	
	NAME	SIGNATURE	DATE	TITLE: Solar Assembly Sensor Housing	
DRAWN					
CHK'D					
APPV'D					
MFG					
Q.A			MATERIAL: PETG	DWG NO. Housing	A4
			WEIGHT:	SCALE:1:2	SHEET 1 OF 1

5. Team Professional Practice Statement

TEAM PROFESSIONAL REFLECTIVE STATEMENT TEMPLATE
Deliverable 6

This document is required for Deliverable 6. You will submit **one** completed reflective statement **per group.**

[redacted]

SECTION A: TEAM NEEDS ANALYSIS (max. 300 words)
In this section describe where the team is starting from with regard to their professional competences. See page 4 of Professional Practice Outline v8 – available on Blackboard. **You will need to note the evidence that informs your judgements.** Consider your areas of strength and areas that you have noticed that require development.

At the start of our hybrid renewable energy project, our team demonstrated strong emotional intelligence and a shared understanding of individual development needs (P2). This was reflected in our initial Buddycheck assessment (October 2024), where scores in *Emotional Awareness* and *Awareness of Needs* were consistently high. These early results likely reflected the team's initial optimism and respectful caution, as we were still unfamiliar with each other's working styles. Even so, this awareness helped us collaboratively set SMART goals, aligning personal development with team objectives (T1, T2).
As we progressed, the second Buddycheck review (March 2025) provided more nuanced insight. Categories such as *Providing Advice (C3)* and *Responding to Feedback (T4)* remained lower in comparison, reflecting growing honesty in peer assessments. Our team became more open to constructive criticism during technical disagreements, and we consistently acted with mutual respect and integrity (P1, P5, T3, T5). This created a space where challenges were addressed collaboratively and productively.
Despite strengths in face-to-face communication, we identified issues with coordination and planning—particularly linked to our reliance on WhatsApp. Difficulties in scheduling meetings and tracking documents negatively impacted workflow and created frustrations during busy phases (P4, T2). This confirmed earlier reflections in our NAAP, where digital communication and task tracking were highlighted as development priorities.
Additionally, role repetition early in the project—where the same individuals led meetings and updates—limited opportunities for wider skill development (T2, C4). This was addressed mid-project through intentional rotation of responsibilities.
Moving forward, improving coordination systems and embedding feedback processes will be vital to maximising both team performance and individual growth.

SECTION B: TEAM GOALS
In this section state the team goals that you have decided upon, based on Section A. Identify no less than 2 goals and no more than 4. You should consider selecting across the 3 areas of professional competences as outlined in Professional Practice Outline v8.

By the end of the project the team will have improved in their group ability to:
Enhance coordination and project planning across all phases (T1, T2, P4):
To address early challenges with communication and task tracking, the team will adopt clearer planning processes. This includes the use of a shared OneDrive structure with consistent file naming, and weekly meetings focused on short-term planning and progress checks. Roles such as meeting chair and note-

taker will be rotated to encourage flexibility and reduce dependency on individual members. These steps aim to support smoother collaboration and reduce bottlenecks during high-pressure weeks.
Strengthen feedback processes and peer-to-peer support (C3, T4):
To make feedback more effective, the team will encourage open, specific peer input following presentations, design reviews, and GTA meetings. Feedback will be briefly discussed as a group, and actions resulting from it will be assig ned to individuals with deadlines. This approach will ensure that constructive criticism leads to measurable improvement, and that all team members remain engaged with each other's contributions.
Improve consistency and professionalism in external communication and documentation (C2, T2):
The team will streamline how external communications—such as GTA follow-ups and deliverable drafts—are produced and shared. Agreed standards for formatting, file naming, and collaborative editing will be used to reduce confusion and delays. A simple checklist and shared timeline will help ensure that documentation and correspondence remain timely and consistent throughout the project.
Foster shared responsibility and skill development through active role rotation (P5, T2):
To avoid repetition of roles and stagnation, the team will formally rotate leadership, presentation, and documentation duties. This will help build confidence in less experienced members and ensure all individuals have the opportunity to develop a broad range of technical and interpersonal skills during the course of the project.

SECTION C: TEAM ACTION PLANNING

In this section consider the actions your team will take to achieve the goals above. Consider where you will source new information and guidance, how you will upskill within the areas of competence you have focused on, how you may try out new ideas and feedback to each other. You should list as many actions in the table below as you consider relevant. It will be important to distribute roles within the team and consider the deadlines that you will work to across the year. It would be expected that doing and reviewing Buddycheck Team Assessments will form part of this list of actions.

Team actions targeted to achieve the goals	*Who?*	*Start-end dates*
HM actively facilitated the organisation of team workflows by assigning tasks during meetings, setting deadlines, and ensuring accountability. HM led the effort to structure the shared OneDrive folder using a consistent and intuitive naming convention, improving accessibility and version control across all project documents. These actions align with competencies T2 (Teamwork Planning), C2 (Presenting & Reporting), and C3 (Providing Advice), by enhancing team clarity, communication, and operational efficiency. HM's contributions directly supported the team's productivity and ability to meet both technical and professional practice milestones on schedule.	*HM*	*23/09/2024 – End of Project*
T3, T4, T5 – BGP consistently provide feedback during initial and ongoing project meetings, ensuring active contribution to idea generation and acknowledge my groupmates inquiries and suggestions. Developing and communicating clear design and operation recommendations based on group discussion and feedback.	*BGP*	*23/09/2024 – End of Project*
P5, T1, T3 – RK acted as the primary liaison between group members, ensuring smooth collaboration by addressing concerns and mediating conflicts when they arose. By being the go-to person for resolving issues, RK helped maintain productive working relationships and ensured consistent team cohesion throughout the project. RK took on the responsibility of reviewing all proposed designs from team members, providing a	*RK*	*23/09/2024 – End of Project*

critical assessment and ultimately deciding which design options aligned best with our collective objectives. This centralised decision-making process kept the project on track and maintained alignment with agreed deliverables. RK consistently reviewed teammates' work, offering constructive feedback and posing key questions regarding feasibility and optimisation. RK's feedback focused on improving both individual outputs and our broader project goals, encouraging continuous development across the group.		
P4, T2 – AND demonstrated flexibility by adjusting to changes in the team's workflow and responsibilities, particularly during the prototype assembly stage. When unexpected issues occurred, such as delays in component delivery, I adjusted my tasks and offered support to teammates, even when it meant stepping outside my assigned role. My willingness to shift and contribute necessary helped sustain collaborative environment, which is crucial for keeping the project on schedule.	*AND*	*23/09/2024 – End of Project*
T5, C2 - MY collaborated closely with HM to enhance the design of the turbine arm, ensuring that the revised version met the necessary criteria for commercial viability, including considerations for manufacturability, cost-effectiveness, and structural integrity. MY was responsible for drafting multiple components of the design, including detailed technical drawings that were essential for the development of the commercially viable version of the product, ensuring accuracy and alignment with engineering standards.	*MY*	*23/09/2024 – End of Project*
P5, C3, C4 – MB supported a collaborative team environment by maintaining positive and constructive working relationships. MB emphasized coordination and clarity when merging subassemblies, helping resolve interface issues calmly and efficiently, and encouraging open, respectful discussions during integration and design evaluations. MB regularly provided technical advice on component modeling and drawing accuracy, suggesting improvements to ensure assemblies were realistic and manufacturable. This included reviewing others' designs and offering constructive guidance to enhance compatibility and robustness. MB upheld professional standards by ensuring that his work—FEA, modeling, and final drawings—met engineering accuracy and safety requirements. MB was transparent about limitations and committed to collective success over individual preference, especially when coordinating complex assembly integrations.	*MB*	*23/09/2024 – End of Project*

T1, C1, C2 – MS supported team coordination by booking collaborative spaces, maintaining a shared meeting log, and ensuring everyone had access to weekly updates. This helped sustain consistent momentum across different project stages and kept the group aligned on evolving priorities. MS was responsible for capturing detailed records of team meetings, which included technical decisions, design updates, and task allocations. These logs became essential references during integration and report compilation, ensuring design consistency and accountability. MS contributed significantly to the written output of the project by drafting the introduction, assembly description, and parts of the optimisation report. This written work helped establish the technical narrative and also ensured the team's achievements were accurately represented in the final documentation and NAAP.	*MS*	*23/09/2024 – End of Project*

Books, publications and resources

List below identified texts, papers, articles and/or resources (with hyperlinks if appropriate) that you will use to support your development as a team. At least 3 references should be provided at minimum.

McGuier, E.A., Kolko, D.J., Aarons, G.A., Schachter, A., Klem, M.L., Diabes, M.A., Weingart, L.R., Salas, E. and Wolk, C.B. (2024). Teamwork and implementation of innovations in healthcare and human service settings: a systematic review. Implementation Science : IS, [online] 19(19), p.49. doi:https://doi.org/10.1186/s13012-024-01381-9.

De Jong, B.A., Dirks, K.T. and Gillespie, N. (2016). Trust and team performance: A meta-analysis of main effects, moderators, and covariates. Journal of Applied Psychology, 101(8), pp.1134–1150. doi:https://doi.org/10.1037/apl0000110.

Roberts, A.P.J., Webster, L.V., Salmon, P.M., Flin, R., Salas, E., Cooke, N.J., Read, G.J.M. and Stanton, N.A. (2021). State of science: models and methods for understanding and enhancing teams and teamwork in complex sociotechnical systems. Ergonomics, 65(2), pp.161–187. doi:https://doi.org/10.1080/00140139.2021.2000043.

Lacerenza, C.N., Marlow, S.L., Tannenbaum, S.I. and Salas, E. (2018). Team development interventions: Evidence-based approaches for improving teamwork. American Psychologist, [online] 73(4), pp.517–531. doi:https://doi.org/10.1037/amp0000295.

van Diggele, C., Roberts, C., Burgess, A. and Mellis, C. (2020). Interprofessional education: Tips for Design and Implementation. BMC Medical Education, [online] 20(2), pp.1–6. doi:https://doi.org/10.1186/s12909-020-02286-z.

SECTION D: SUCCESS FORECASTING (max. 300 words)

In this section describe what success will look like, sound like or feel like if the actions you have identified in Section C come to fruition. It is important that you can articulate as a group when you will have considered success to be achieved.

If the actions outlined in our plan are successfully implemented, success will be evident across both the team's working practices and the quality of our project outputs.

From a process perspective, success will look like a well-coordinated, self-directed team. Weekly meetings will run efficiently with clear agendas, rotating leadership, and timely updates on progress. Tasks will be clearly delegated and documented, with accountability shared across the group. The shared drive will be well-organised, making it easy to locate and edit project files. Communication—both internal and external—will be smooth, with fewer misunderstandings or delays in responses, helping maintain momentum throughout busy phases.

Success will also sound like a team that listens actively and supports each other. Constructive feedback will be a normal part of meetings, with team members openly sharing ideas and

responding positively to suggestions. Feedback from GTAs will be discussed promptly and acted upon in

subsequent iterations, showing that the team values continuous improvement and external input. Importantly, success will feel like a collaborative, inclusive environment where everyone contributes meaningfully and feels ownership of the final product. No single person will dominate leadership roles or technical contributions—team members will step outside their comfort zones and gain confidence in areas they were initially unfamiliar with. The group will feel more cohesive and resilient when facing technical or logistical challenges.

In terms of outputs, success will be reflected in a functioning prototype that meets the technical and ethical objectives of the project. The design will demonstrate thoughtful consideration of user needs and the documentation will be clear, professional, and aligned with engineering standards.

Ultimately, we will consider the project a success if we have not only delivered a well-functioning renewable energy device, but also grown individually and collectively as emerging professional engineers.

SECTION E: EVIDENCING WITHIN YOUR TEAM PORFOLIO

In this section list and describe the ways in which the team will evidence their impact within their portfolio. What records of activity or impact will you keep? How will you save key information related to your progress.

Our team has compiled a comprehensive portfolio to document both our technical progress and professional development throughout the project. The following evidence captures how we addressed our goals and adapted our practices over time:

- **Weekly Meeting Logs**: We recorded structured agendas, action points, and task allocations. These logs tracked our decision-making process, highlighted changes in direction, and helped monitor individual and team responsibilities. This documentation supported the development of competencies such as project coordination (T1), meeting management (C1), and team planning (T2).
- **BuddyCheck Assessments**: Conducted at two key stages, these assessments provided insight into how each team member perceived contribution levels and group dynamics. The feedback prompted important changes in task distribution and role clarity mid-project. Our improvement in peer collaboration is reflected in stronger scores for team relationships (P5), giving feedback (T3), and responding to feedback (T4).
- **Engineering Professional Competency Chart (Final Review)**: This team self-assessment reflects our progress across the full range of UoM professional competencies. By Review Point 4, we had improved in nearly every area, with multiple categories reaching a level 4. This includes flexibility (P4), team relationships (P5), presenting and reporting (C2), and feedback integration (T4), confirming the depth and breadth of our development.

SECTION F: REFLECTION ON ACTION AND IMPACT (750 words max)

In this section you should bring together your learning across the Professional Practice aspect of the course. You should describe and be reflective in reviewing the progress you have made during the project. You should update and refresh Sections A-E based on the reality of what happened. Refer to the Assessment Rubric on page 8 of Professional Practice Outline v8.

Our hybrid wind and solar energy project challenged us technically, but also gave us a valuable opportunity to grow in professional practice. At the start of the year, our Needs Analysis and Action Plan (NAAP) helped us identify four key areas we wanted to develop. These were structured project management, clearer communication, technical upskilling in CAD and simulation, and building a more inclusive and collaborative team culture. These goals gave us a strong direction, but the reality of the project meant we had to constantly adapt, re-evaluate, and reflect on how we were actually working together.

One of our biggest early challenges was in task ownership and planning. Although we had discussed structured project management as a priority, we didn't stick to it effectively at first. Tasks overlapped, roles weren't clear, and we experienced deadline pressure. Our first BuddyCheck made this obvious. There were comments about uneven contributions and people not knowing exactly what was expected of them. In response, we introduced clear subsystem leads, a shared task tracker, and properly structured weekly meetings. From Week 4 onwards, our meeting logs showed real improvement. We started recording action points, following up on tasks, and creating a

rhythm to our work. These changes helped us become more accountable and confident in managing both time and resources, and brought our project management skills much closer to what we had set out to achieve.
Communication was another area where we had to make a shift. At first, we relied heavily on WhatsApp messages, which worked socially but not professionally. As the project became more complex and we had to justify technical decisions—especially when integrating electronics and mechanics—things started getting lost. The feedback from our GTA in Week 5 helped a lot. They pointed out that our report lacked clarity in materials justification. We took that seriously and made big improvements. We started using proper meeting minutes, reviewing each other's work more formally, and providing feedback in writing. This made our deliverables clearer, helped us respond to criticism better, and improved the way we communicated both internally and externally.
When it came to technical development, our NAAP had set a goal of improving simulation and CAD skills. While we did follow through, we learned that upskilling didn't happen in isolation. For example, one teammate took the lead on the SPH simulations, but ended up running mini walkthroughs for others so we could understand the data and use it to inform design decisions. Similarly, when the MTTF and MTTR section wasn't initially understood, the group came together to workshop the idea and reshape it into something more valuable. What we thought would be solo learning turned into shared, peer-led development. That process not only made us more competent but also made the final work stronger because more of us could contribute meaningfully.
One of the most unexpected things we learned was about leadership and inclusion. Originally, we thought leadership would naturally fall into place based on roles. But we found the project worked better when leadership rotated. Different members took the lead depending on the milestone—for example, one led the DFA analysis, another took ownership of electronics testing, and so on. This allowed everyone to contribute in a way that played to their strengths. It also made a big difference for some of our international teammates. In early meetings, we realised that language barriers were stopping people from speaking up. So, we started using translated notes, clearer visuals, and more simplified communication tools. These changes helped everyone participate more fully, and it was reflected in how much more balanced our second BuddyCheck feedback was.
Over time, our definition of success changed. At the start, we imagined success as hitting deadlines and producing technically strong work. While those things still mattered, we began to understand that resilience and adaptability were just as important. We had supply delays, late tool access, and unexpected testing issues. But instead of falling behind, we changed direction when needed, shifted focus between subsystems, and supported each other through tight spots. One example was when we had to redesign a subsystem late in the project. Instead of panicking, we reorganised tasks and still met our submission goals. Those experiences made us more confident and more flexible, which we now see as essential professional skills.
We've collected plenty of evidence along the way—meeting logs, BuddyCheck reports, feedback responses, and design iteration records—all of which show how we adapted and improved. Looking back, what stands out most is that professional practice was not something we did separately from the technical work. It was embedded in everything, from how we assigned tasks to how we learned from each other. We now see that things like giving feedback, managing time, and including everyone in the process are not just soft skills—they are what make engineering projects actually work. This project helped us build those habits, and we'll carry them forward into whatever we do next, both in university and beyond.

6 Conclusions and Recommendations

The integration of Fault Tree Analysis (FTA) into the design refinement process provided a clear, systematic framework for identifying and mitigating the root causes of power generation failure across the system. This optimisation strategy enabled a top-down investigation of functional reliability and revealed several critical failure modes that had previously been overlooked in early design phases. Notably, FTA drew attention to mechanical vulnerabilities in the VAWT subsystem, inadequacies in solar tracking hardware, and environmental factors such as excessive wind load and corrosion—each of which posed significant risks to the unit's long-term functionality and energy output.

As a result of this structured fault analysis, the design team implemented targeted upgrades to key components. Foam blades were replaced with reinforced composites to improve aerodynamic stability and durability under wind shear. The aluminium hollow shaft was redesigned with higher wall thickness, improving resistance to torsional deformation and shaft misalignment—previously identified as a high-probability failure. Bolted connections and bearing mounts were enhanced with vibration-damping materials and self-locking mechanisms to mitigate loosening under cyclical loading. In the solar subsystem, motors were replaced with sealed, lower-torque alternatives better suited to outdoor conditions, and the MPPT control unit was reconfigured with improved thermal management and refined sensor calibration to enhance electrical reliability.

One of the main challenges encountered in this process was the limited scope of the current iteration—electrical faults in grid-connected modes and autonomous tracking logic were explicitly excluded. These omissions represent a key learning point: while mechanical and environmental resilience were substantially improved, the broader integration of control and electrical safety systems remains essential for achieving full compliance with energy systems standards such as IEC 61727 or IEC 60364. This underscores the importance of cross-domain fault analysis when designing hybrid renewable systems.

Looking forward, it is recommended that future iterations expand the FTA scope to include both electrical and software fault domains, ideally incorporating a modular logic structure that can account for interdependencies between physical failures and digital control faults. Professionally, adopting a more iterative testing protocol—where fault simulations inform hardware updates in real time—could reduce development cycles and produce more robust systems. Additionally, collaboration with industry partners for validation of weatherproofing and electronic subsystem resilience would ensure the deployable unit meets both safety and operational reliability benchmarks under diverse environmental conditions. These measures would support the delivery of a compliant, field-ready renewable energy solution capable of reliable off-grid operation.

The Design for Assembly (DFA) optimisation provided one of the most significant turning points in the transition from an experimental prototype to a practical deployable product. Through systematic analysis of the structural and solar assembly processes, this approach directly tackled the challenges that arose during initial build and testing phases—chiefly, excessive assembly time, high part count,

and reliance on specialised tools. In the structural system, the prototype's bracket-heavy, screw-dependent design often resulted in long, error-prone construction phases that made repeatability and user-friendliness difficult to guarantee. By implementing collapsible scissor struts and telescopic legs secured with detent pins, the redesign eliminated much of the bespoke fabrication previously required, while vastly improving portability. Equally, the reduction in fastener diversity and the slotting mechanism for blade attachment simplified the build process, enabling intuitive, tool-light assembly without sacrificing structural performance. The impact was clearly quantifiable: part count was nearly halved, unique components dropped by over 40%, and total assembly time was reduced from an hour to just 15 minutes.

The second phase of DFA optimisation focused on the solar subsystem, where earlier designs had suffered from slow and tool-intensive panel attachment procedures. The introduction of camlock bases and snap-fit pins, inspired by modular industrial products, streamlined this process. These modifications not only sped up assembly and disassembly—allowing even inexperienced users to complete the solar setup within minutes—but also reduced the potential for alignment errors and overtightening damage, improving long-term system reliability. Importantly, this re-engineered solar mounting strategy reflects a broader systems-thinking approach: that a deployable product must be not just technically functional, but operable under real-world constraints such as time pressure, remote installation, and non-specialist user input.

From a professional standpoint, the lessons from DFA reinforce the value of early-stage assembly analysis in product lifecycle planning. While the original prototype served well as a proof-of-concept, the deployable iteration shows how deliberate design simplification can yield products that are safer, faster to set up, and easier to maintain—all key to achieving real-world impact. Future improvements should continue to prioritise multi-functional components and passive alignment strategies to further improve robustness. Additionally, integrating more rapid prototyping and modular testing during the design cycle could help validate DFA decisions earlier in development. Overall, this work demonstrates how assembly-focused thinking can directly support safe, compliant, and reliable deployment in field environments.

One of the key outcomes of this project was the refinement of the design through targeted FMEA optimisation. By systematically identifying and addressing high-risk failure modes, we not only reduced the likelihood of failure in several critical components but also improved the overall structural efficiency of the deployable unit. The redesign successfully moved away from an overly conservative, overengineered frame to a more balanced structure, where a calculated reduction in safety redundancy enabled significant improvements in portability, ease of maintenance, and user assembly without compromising operational integrity. The shift to lighter, more purpose-built structural members demonstrated a marked improvement in the strength-to-weight ratio—an essential performance metric for deployable systems.

This process highlighted the value of iterative, risk-driven design thinking, particularly when aiming to meet real-world constraints such as field deployment, user handling, and manufacturing feasibility. A major lesson from this optimisation phase was the importance of balancing analytical risk metrics (such as RPN scores) with practical considerations like accessibility and structural simplicity. While the second design retains a safety margin well within aluminium 6061’s yield capabilities, it is clear that future development should focus on standardising the FMEA process across

components to avoid comparative skew and possibly integrating load case-specific failure mode libraries to refine criticality assessments.

For improved practice, it is recommended that future iterations adopt a modular FMEA template early in the design stage, to better harmonise component-level risk scoring. Additionally, incorporating real-time load testing alongside digital simulations would provide richer validation data, especially in dynamic or fatigue-sensitive applications. Professionally, fostering closer collaboration between risk analysts, structural designers, and assembly technicians during design reviews could yield further performance and usability gains. These approaches would help ensure that future systems are not only structurally sound and safe, but also practical, compliant, and aligned with user needs in operational environments.

The DFRaM optimisation strategy was central to improving system uptime by enhancing both the durability and maintainability of critical subsystems. By systematically addressing the root causes of premature failure and field repair difficulty, this approach directly supported the deployability of the hybrid energy unit in remote, weather-exposed environments. Key upgrades included the replacement of fatigue-prone foam blades with CFRP and leading-edge coatings, the introduction of dual-support bearings to reduce shaft misalignment, and the adoption of sealed, modular electronics enclosures for improved environmental resilience. Each intervention was guided by RAM metrics and informed by practical failure scenarios and stress modelling. These design changes not only raised subsystem MTTF but also significantly reduced MTTR through modular interfaces, standardised fasteners, and accessible layouts. With average availability now exceeding 95%, the final design aligns with reliability targets and demonstrates how uptime-driven engineering can produce robust, service-ready systems suitable for real-world deployment.

7 References

AZO Materials. (2001). *"ASA"*. Available at: https://www.azom.com/article.aspx?ArticleID=335

AZO Materials. (2016). *"A4-grade stainless steel (316)"*. Available at: https://www.azom.com/article.aspx?ArticleID=2868

Bai, J. (2023). *"Fiber-reinforced Polymer Types and Properties"*. Available at: https://doi.org/10.101/6B978-0-12-820346-0.00014-9

Balduzzi, F., Marten, D., Bianchini, A., Drofelnik, J., Ferrari, L., Campobasso, M.S., Pechlivanoglou, G., Nayeri, C.N., Ferrara, G. and Paschereit, C.O. (2017). Three-Dimensional Aerodynamic Analysis of a Darrieus Wind Turbine Blade Using Computational Fluid Dynamics and Lifting Line Theory. *Journal of Engineering for Gas Turbines and Power*, 140(2). https://doi.org/10.1115/1.4037750

Belden Inc. (2023). *Cable Shielding Techniques and EMI Mitigation*. Belden Technical White Paper. Available at: https://www.belden.com/blog/smart-building/cable-shielding-to-reduce-emi

Campbell, F.C. (2010). *Structural Composite Materials*. Materials Park, OH: ASM International.

Chang, K. (2015). *"Design Optimisation"*. Available at: https://doi.org/10.1016/B978-0-12-398512-5.00003-7

Chowdhury, S., Saha, H. and Das, D. (2016). *'A Review on MPPT Algorithms for Solar PV Systems'*. *International Journal of Electrical Engineering*, 3(4), pp. 23–31.

Composites Construction UK. (2021). *"CFRP: Pros & Cons"*. Available at: https://www.fibrwrap-ccuk.com/blog/carbon-fibre-reinforced-polymer-pros-cons/

CompositesWorld. *"Resin Transfer Molding"*. Available at: https://www.compositesworld.com/topics/rtm

Davis, J.R. (1993). *Aluminum and Aluminum Alloys*. Materials Park, OH: ASM International.

Essentra Components. (2018). *"The Pros and Cons of Nylon Fasteners"*. Available at: https://www.essentracomponents.com/en-gb/news/solutions/fastening-components/the-pros-and-cons-of-nylon-fasteners

Europlas. *"About ASA Plastic"*. Available at: https://europlas.com.vn/en-US/blog-1/about-asa-plastic-what-is-it

Europlas. *"GFRP: Pros and Cons"*. Available at: https://europlas.com.vn/en-US/blog-1/glass-fiber-reinforced-plastic-definition-and-pros-cons

Exim Wind. (n.d.). *Practical Rotor Coupling and Shaft Isolation Solutions*. Available at: https://eximwind.com/coupling/

Gay, D., Hoa, S.V. and Tsai, S.W. (2002). *Composite Materials: Design and Applications*. Boca Raton: CRC Press.

Genta, G. (2005). *Dynamics of Rotating Systems*. Springer.

Ha, K. (2020). *'Reduction of Stress Concentration Factor (SCF) on the Bolted Joint Connection for a Large Wind Turbine Rotor Blade through Various Design Modifications'*. *Applied Sciences*, 10(18), p. 6588. https://doi.org/10.3390/app10186588

Harper, C.A. (2002). *Handbook of Plastics, Elastomers, and Composites*. 4th ed. New York: McGraw-Hill.
Hoorenwell. (2024). *"Advantages and Disadvantages of ASA Materials"*. Available at: https://www.hoorenwell.com/news/240-en.html
IAEI. (2020). *'Sunlight Resistant Requirement and Choices for Enforcement'*. *IAEI Magazine*. Available at: https://iaeimagazine.org/magazine/2020/03/01/sunlight-resistant-requirement-and-choices-for-enforcement/
IEEE. (2012). *IEEE Standard 1143-2012: EMI Shielding for Communication Systems*. Institute of Electrical and Electronics Engineers. Available at: https://standards.ieee.org/standard/1143-2012.html
ISO. (2018). *ISO 12944: Paints and Varnishes – Corrosion Protection of Steel Structures by Protective Paint Systems*. International Organization for Standardization.
Juang, H.-M. and Radharamanan, R. (2023). *'Design of a Solar Tracking System for Renewable Energy'*. *Journal of Solar Energy Engineering*, 145(4).
Kalpakjian, S. and Schmid, S.R. (2014). *Manufacturing Engineering and Technology*. 7th ed. Pearson.
Katche, D., Khoucha, F.A. and Kessal, A. (2023). *'A Comprehensive Review of Maximum Power Point Tracking (MPPT) Techniques Used in Solar PV Systems'*. *Solar Energy*, 256, pp. 1012–1037.
Kaufman, J.G. (2000). *Introduction to Aluminum Alloys and Tempers*. Materials Park, OH: ASM International.
Keegan, M.H., Nash, D.H. and Stack, M.M. (2013). *'On Erosion Issues Associated with the Leading Edge of Wind Turbine Blades'*. *Journal of Physics D: Applied Physics*, 46(38), p. 383001. https://doi.org/10.1088/0022-3727/46/38/383001
Lee, J. et al. (2019). *"Effect of Thermoplastic Resin Transfer Molding Process and Flame Surface Treatment on Mechanical Properties of Carbon Fiber Reinforced Polyamide 6 Composite"*. Available at: https://4spepublications.onlinelibrary.wiley.com/doi/abs/10.1002/pc.25445
Logan, P.E. and Raichle, B.W. (2012). *Performance Comparison of Fixed, Single, and Dual Axis Tracking Systems for Small Photovoltaic Systems with Measured Direct Beam Fraction*. Appalachian State University.
Mallick, P.K. (2007). *Fiber-Reinforced Composites*. 3rd ed. Boca Raton: CRC Press.
Martinez-Luengo, M., Kolios, A. and Wang, L. (2016). *'Structural Health Monitoring of Offshore Wind Turbines: A Review through the Statistical Pattern Recognition Paradigm'*. *Renewable and Sustainable Energy Reviews*, 64, pp. 91–105.
May, A., McMillan, D. and Thöns, S. (2015). *'Economic Analysis of Condition Monitoring Systems for Offshore Wind Turbine Sub-systems'*. *IET Renewable Power Generation*, 9(8), pp. 900–907.
Mistri, R.K., Singh, K., Kumar, U., Bharti, P. and Kumari, P. (2018). *Solar Tracker Using LDR*. *International Journal for Research in Applied Science and Engineering Technology (IJRASET)*, 6(5), pp. 2242–2244. https://doi.org/10.22214/ijraset.2018.5365
Mark, J.E. and Gaylord, N.G. (1982). *Encyclopedia of Polymer Science and*

Technology. New York: Wiley-Interscience.
MDPI. (2023). *'Fatigue Design and Shaft-Bearing Configurations for Renewable Systems'*. *Machines*, 11(7), 681. Available at: https://www.mdpi.com/2075-1702/11/7/681
Mohamed, M.H., Dessoky, A. and Alqurashi, F. (2019). *Blade Shape Effect on the Behavior of the H-Rotor Darrieus Wind Turbine: Performance Investigation and Force Analysis*. *Energy*, 179, pp. 1217–1234. https://doi.org/10.1016/j.energy.2019.05.069
Muhammad, H. et al. (2023). *'Performance Enhancement of Hybrid Solar Trackers Using Encoder Feedback'*. *Energy Reports*, 9, pp. 1123–1135.
Muszynska, A. (2005). *Rotordynamics*. CRC Press.
NPA. (2023). *"Nylon Screws: A Buyer's Guide"*. Available at: https://www.npa.com.au/nylon-screws-a-buyers-guide
Osswald, T.A. and Hernández-Ortiz, J.P. (2006). *Polymer Processing: Modeling and Simulation*. Munich: Hanser Publishers.
Polmear, I.J. (2006). *Light Alloys: From Traditional Alloys to Nanocrystals*. 4th ed. Oxford: Butterworth-Heinemann.
Patel, D. and Patel, B. (2014). *Low Cost and Robust Solar Tracking System Based on Data of Daily and Seasonal Variation in Sun Position*. *International Journal of Innovative Research in Science, Engineering and Technology*, 3(9), pp. 15888–15893. https://doi.org/10.15680/IJIRSET.2014.0309014
Prince Lund. *"Fiber Reinforced Polymers Characteristics and Behaviors"*. Available at: https://www.princelund.com/fiber-reinforced-polymers.html#gsc.tab=0
Strong, A.B. (2008). *Fundamentals of Composites Manufacturing*. 2nd ed. Dearborn, MI: SME.
QBlade and sphinx-quickstart. (2021). *QBlade Documentation — QBlade Documentation 2.0.4*. Available at: https://docs.qblade.org/
Reda, I. and Andreas, A. (2008). *Solar Position Algorithm for Solar Radiation Applications (Revised)*. Golden, CO: National Renewable Energy Laboratory (NREL/TP-560-34302).
Rezaeiravesh, S. (2024). *Bayesian Optimisation Based on GPR*. University of Manchester. AERO40041 Data-driven Modelling & Simulation Lecture.
Rotar, M. et al. (2023). *'Dependability Assessment of a Dual-Axis Solar Tracking Prototype'*. *Renewable Energy Systems Journal*, 18(2), pp. 55–63.
Simon, J. and Mosey, G. (2013). *Feasibility Study of Economics and Performance of Solar Photovoltaics at the Kerr McGee Site in Columbus, Mississippi*. Golden, CO: National Renewable Energy Laboratory (NREL), NREL/TP-7A30-57251.
Sutherland, H.J. (1999). *'On the Fatigue Analysis of Wind Turbines'*. Sandia National Laboratories Report SAND99-0089.
Timoshenko, S.P. and Goodier, J.N. (1970). *Theory of Elasticity*. McGraw-Hill.
TiMOTION. (n.d.). *MA4 Series - Linear Actuators*. Available at: https://www.timotion.com/en/products/linear-actuators/ma4-series
Toray Group. (2025). *"Carbon Fiber Resin Transfer Molding"*. Available at: https://www.toraycma.com/applications/resin-transfer-molding/

Yoksoulian, L. (2024). *“Researchers Clarify How Soft Materials Fail Under Stress”*. Available at: https://news.illinois.edu/researchers-clarify-how-soft-materials-fail-under-stress/

Vishwa Stainless. (2024). *The Importance of Stainless-Steel Round Bars in Renewable Energy Sector*. Available at: https://www.vishwastainless.com/ss-round-bars-in-renewable-energy-sector/

Yoo, S. (2024). *‘Effect of Conformal Coating on Electrochemical Migration Behavior of Multi-Layer Ceramic Capacitors Based on Water Drop Test’*. *Microelectronics Reliability*, 155. https://www.mdpi.com/2072-666X/10/1/15

Zhao, W., Jiang, Z., Zhang, P. and Huang, X. (2023). *‘Reliability Sensitivity Analysis of Main Shaft Bearings of Wind Turbines Subject to Subsurface Stress’*. *Machines*, 11(7), 681. https://doi.org/10.3390/en14217246

8 Appendix

8.1 Appendix A

Appendix A.1: Blade Optimisation Data

Test	Chord (mm)	Height (mm)	Radius (mm)	Cp
Prototype	200	400	200	0.75554
1	100	800	500	0.51663
2	200	400	100	0.61867
3	200	400	380.16	0.59330
4	200	511.84	213.85	0.77682
5	192.91	997.91	234.86	0.70768
6	200	551.53	227	0.70359
7	200	484.12	215.12	0.77445
8	70	1000	207.3	0.51387
9	148.3	400	220.9	0.70462
10	200	879.64	252.27	0.72921

Figure 8.a: Cp values for optimised blade configurations at peak TSR.

Test	Chord (mm)	Height (mm)	Radius (mm)	Cp_mean
Prototype	200	400	200	-0.09005
1	100	800	500	0.33637
2.1	97.53	804.41	500	0.33894
3.1	200	1000	500	0.26386
4.1	70	1000	500	0.36169
5.1	70	800	500	0.36169

Figure 8.b: Mean Cp Optimisation Results (Across TSR Range)

Appendix A.2: Comparison of Pitch Mechanisms

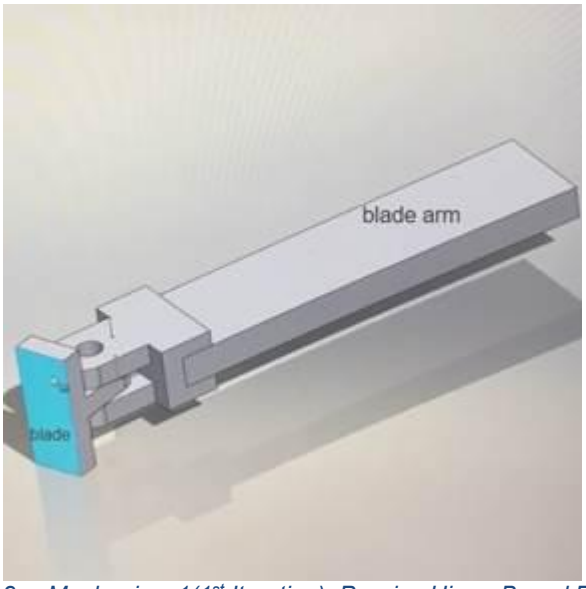

Figure 8.c: Mechanism 1(1st Iteration), Passive Hinge-Based Pitching

Figure 8.c shows a concept sketch of a passive hinge-based pitching that would allow the user to adjust the pitch based on the conditions at a given time. Before starting the turbine, the user would check the wind conditions, setting a higher blade angle for lower wind speeds to provide more lift, and a lower blade angle for high wind to prevent overloading. A user interface would suggest the best pitch angle to the user would need physical access to the turbine. A locking mechanism with built in angle indicators would be utilized.

Advantages:

Mechanically very simple which only includes a locking mechanism and hinges. Would also make it cheaper to manufacture and have a higher reliability with fewer points of failure.

Disadvantages:

- Not adaptive during operation of turbine as the pitch of the blades can only be adjusted when it is static.
- Relies on the judgement of the user to determine wind conditions.
- Suboptimal performance as it is not able to respond to sudden gusts or dynamic loads, leading to stalling or overspeeding.

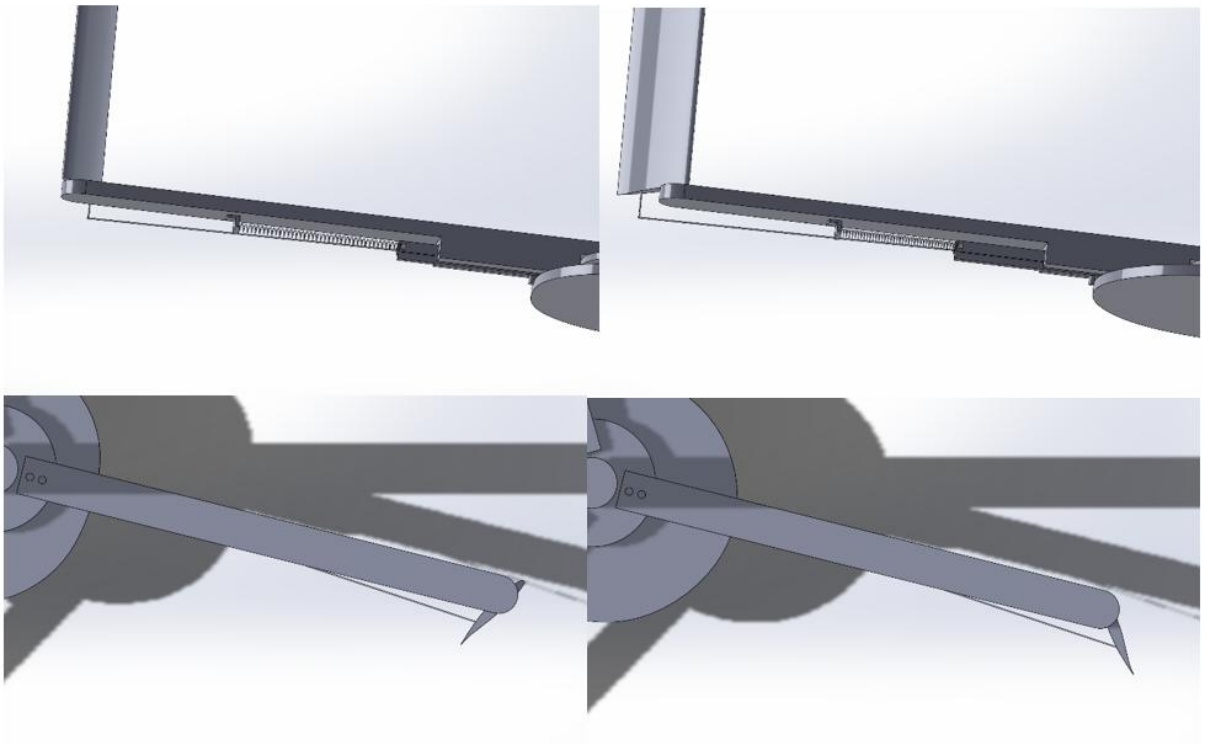

Figure 8.d: Mechanism 2 (2nd Iteration), Cam and Follower Pitching Mechanism

Figure 8.d shows a cam and follower system for the variable pitch blades. Compared to the passive hinge-based pitching system, the user would only need to set up the arms during the initial building phase. Before operation, the user would not need to do any set up regarding the blade pitch. However, the user would need to pick the suitable cam for the environment. The user would also only maybe need to ensure the turbine is free to rotate with proper lubrication. The spring compresses or extends as the followers connected to each blade ride along the cam profile, pulling the blade in at a point of lower radius of the cam and pushing the blade out at a point of higher radius of the cam. The cam is designed to match the angle-of-attack variation simulated in QBlade. There is no need for user intervention, unless if inspection or maintanence is needed.

Advantages:

- Predefined, accurate pitch control at each azimuthal position
- Customisable cam profile using simulation data
- Proven to enhance self-starting and maintain lift during full rotation

Disadvantages:

- Mechanically more complex
- Requires precision machining and spring calibration

This mechanism is selected as the recommended solution for its reliability and ability to suppress stall under varied wind speeds.

Figure 8.e: Scissor-Strut Folding Mechanism

Figure 8.f: Telescopic Adjustable Leg with Detent Pin

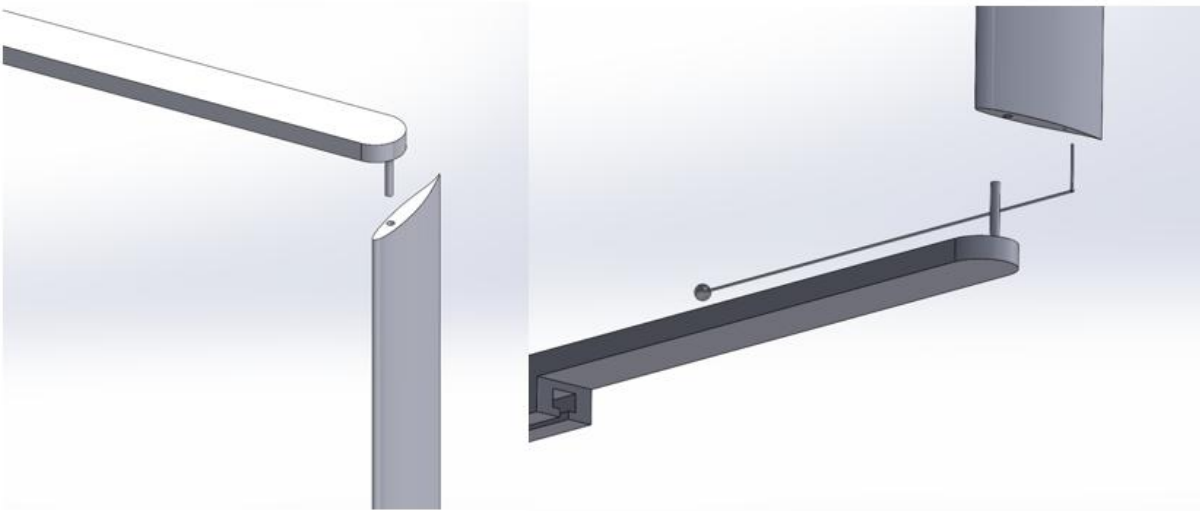

Figure 8.g: Slotting Mechanism for Blade and Arm Connection

Component	Failure Mode	S	O	D	RPN
Corner brackets	Plastic deformation	6	5	4	120
	Fatigue failure	7	3	5	105
	Bolt loosening/shearing	7	3	5	105
	Corrosion	6	1	2	12
	Crack initiation	8	6	4	192
Corner connectors	Shearing at connections	7	1	4	28
	Excessive deflection	6	3	2	36
	Stress concentration failure	8	3	5	120
	Material fatigue	5	2	4	40
	Bolt pull-out	8	2	3	48
Vertical Members	Buckling	9	2	2	36
	Bending deformation	6	2	3	36
	Fatigue failure	8	1	3	24
	Material yielding	8	2	2	32
	Surface wear/corrosion	6	1	2	12
Horizontal Members	Excessive deflection	7	2	2	28
	Shear failure	9	2	3	54
	Brittle fracture	8	1	1	8
	Loosening	7	1	4	28
	Torsional twisting	6	1	2	12
PETG Sheets	Cracking	9	1	3	27
	Fatigue failure	8	3	5	120
	Excessive deflection	8	3	2	48
	UV degradation	6	1	6	36
	Edge failures	7	4	4	112

Figure 8.h - FMEA RPN Scores

Simulation setup (FEA 1)

The simulation model replicated a middle tier of the prototype, as those were the tiers using the corner brackets, consisting of:

- Horizontal aluminium members (460 mm length)
- Vertical aluminium members (700 mm height)
- Corner brackets at each junction

The model was simplified by exploiting symmetry and only included one quadrant of the frame. Each solid body was explicitly defined and joined via bonded contacts to reflect fixed mechanical connections.

Two primary load cases were considered:

- **Vertical weight load:** A uniformly distributed pressure simulating a 5 kg mass resting on the PETG sheet. This load represents components such as the shaft, housing bearings, as well as arms and blades connected to the shaft. The distributed pressure was utilised in order to reduce computational loads, as this meant we didn't have to model the sheet itself. This equated to a pressure of:

$$Pressure = \frac{Force}{Area} = \frac{5 \times 9.81}{36800\ mm^2} = 0.00133\ MPa$$

- **Wind load:** A lateral pressure was applied to the side face of the structure to simulate wind conditions typical for Manchester, UK. Based on peak wind speeds (~25 m/s), the resulting dynamic wind pressure was calculated as:

$$P = 0.5 \times \rho \times v^2 = 0.5 \times 1.225 \times (25)^2 = 382.81 \frac{N}{m^2} = 0.000383\ MPa$$

Material Properties

All components that were modelled are made of Aluminium 6061, and so material selections in the model were done accordingly. The key properties used were:

- Young's Modulus: 68.9 GPa
- Yield Strength: 275 MPa
- Poisson's Ratio: 0.33
- Density: 2.70 g/cm³

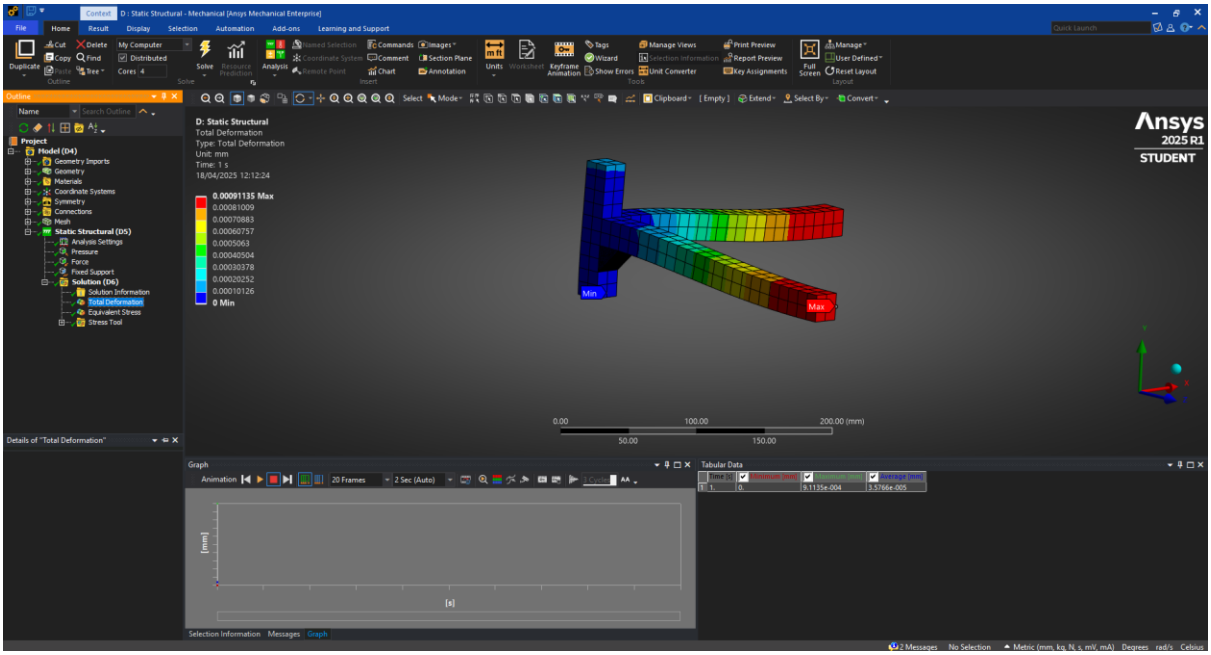

Figure 8.i: FEA 1: Total deformation

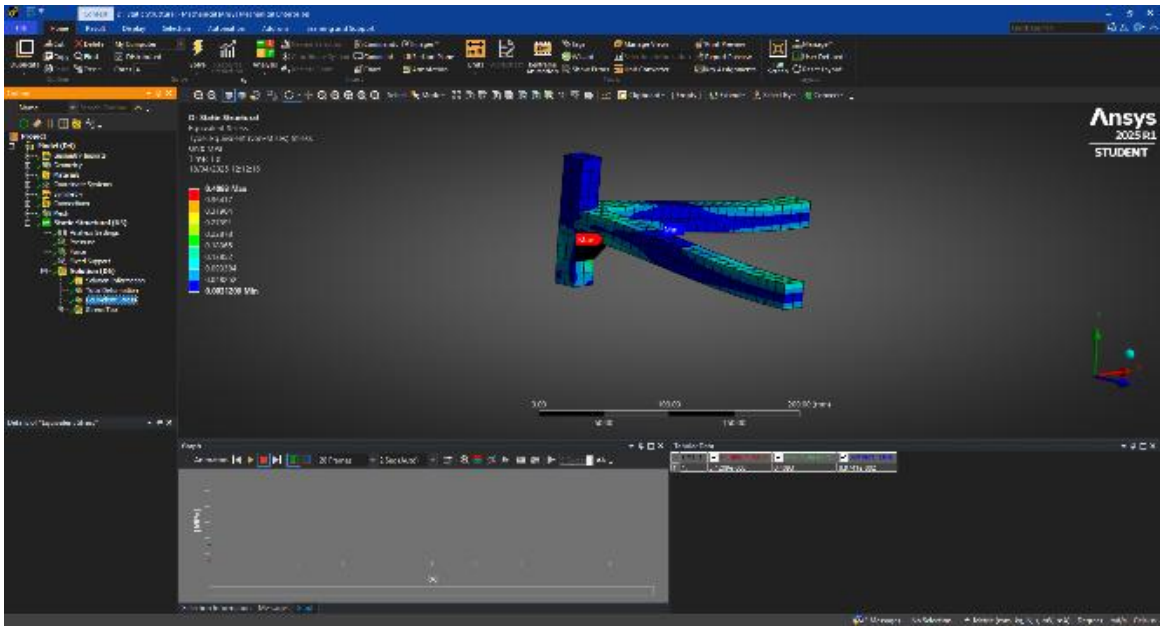

Figure 8.l: FEA 1: Equivalent Stress

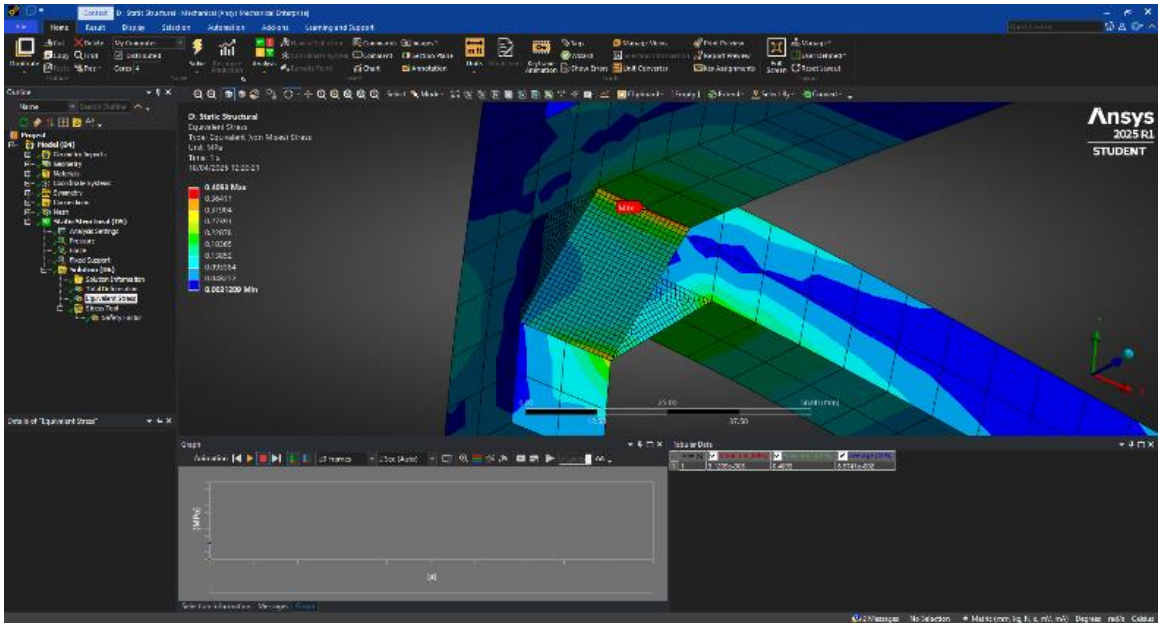

Figure 8.k: FEA 1: Close up on stress concentrations.

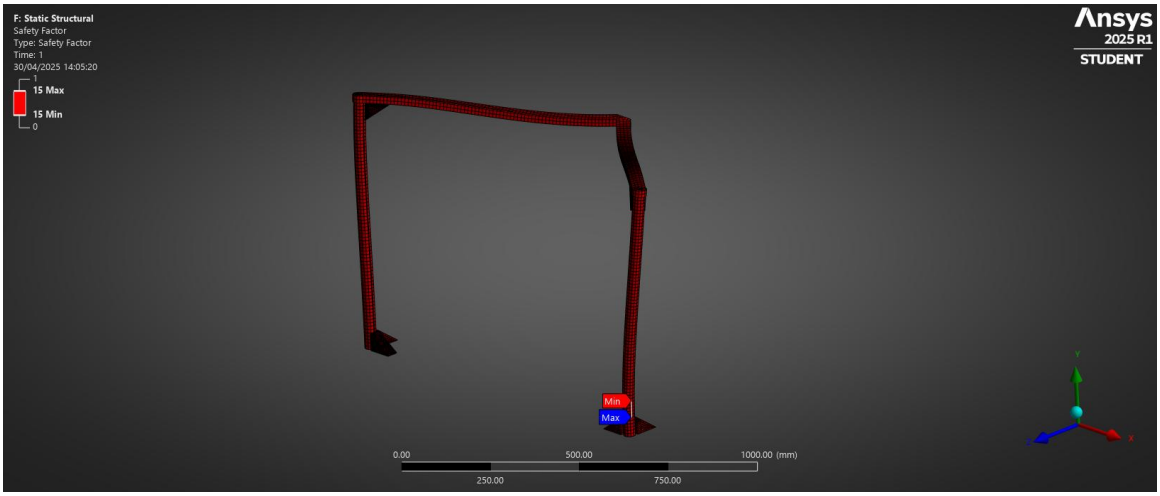

Figure 8.j: Proof of unusable Factor of Safety Tool

Simulation Setup

To reduce computational complexity, only half of the full deployable structure was modelled using symmetry boundary conditions. This approach allowed the simulation to remain representative of the full assembly while significantly lowering processing time. The geometry included two telescopic legs, their corresponding scissor struts, and simplified representations of the modular joints, which were intentionally modelled with less geometric detail to keep meshing and solving manageable.

Two primary load cases were considered:

- **Vertical weight load:** A uniformly distributed pressure simulating a 10 kg mass resting on the upper surfaces of the scissor struts. This load represents the dual axis solar tracking platform that would be mounted on the top of the deployable unit's structure. This equated to a pressure of:

$$Pressure = \frac{Force}{Area} = \frac{10 \times 9.81}{115248\, mm^2} = 0.000828\, MPa$$

- **Wind load:** A lateral pressure was applied to the side face of the structure to simulate wind conditions typical for Manchester, UK. Based on peak wind speeds (~25 m/s), the resulting dynamic wind pressure was calculated as:

$$P = 0.5 \times \rho \times v^2 = 0.5 \times 1.225 \times (25)^2 = 382.81 \frac{N}{m^2} = 0.000383\, MPa$$

All structural components were assigned aluminium 6061-T6 as the material, maintaining consistency with the prototype to ensure that comparative results would be meaningful. For boundary conditions, the bottom faces of the legs were fully fixed to represent ground contact and simulate realistic structural constraints during loading.

Meshing was carried out with emphasis on balancing computational efficiency and solution accuracy. The scissor struts and legs were assigned a global element size of 10 mm, while a finer mesh of 5 mm was used around joint regions, where stress concentrations were expected. This allowed for improved result resolution in these critical areas without overwhelming the solver with unnecessary detail in less sensitive regions.

Component	Failure Mode	S	O	D	RPN
Scissor Strut	Plastic deformation under excessive load	8	3	4	96
	Brittle fracture in extreme conditions	9	2	5	90
	Pin failure at pivot joint due to shear stress	6	3	5	90
	Loosening of pivot pin over time	4	5	4	80
	Fatigue failure at stress concentration points	7	3	6	126
	Corrosion of metal surfaces over time	5	3	6	90
	Incorrect installation of struts	7	2	5	70
	Misalignment due to uneven loading	6	2	4	48
Telescopic Legs	Buckling under compressive loads	9	2	4	72
	Failure of detent pin due to shearing/bending	7	3	5	105
	Detent pin misalignment	3	6	4	72
	Telescopic mechanism jamming	5	4	5	100
	Excessive deformation between telescopic segments	6	4	4	96
	Fatigue failure at detent pin hole	8	2	6	96
	Base joint failure due to stress at ground contact	9	2	5	90
	Improper engagement of height adjustment holes	6	3	5	90
Hinges	Spring failure leading to improper hinge function	5	4	4	80
	Pin shearing under excessive rotational force	6	3	5	90
	Loosening of hinge screws over time	5	4	4	80
	Corrosion of hinge components	4	4	6	96
	Rivet failure due to cyclic loading	7	3	5	105
	Hinge lock mechanism failure	7	2	5	70
	Over-rotation leading to mechanical interference	5	3	5	75
	Misalignment due to manufacturing tolerances	5	2	5	50

Figure 8.m - FMEA RPN scores 2

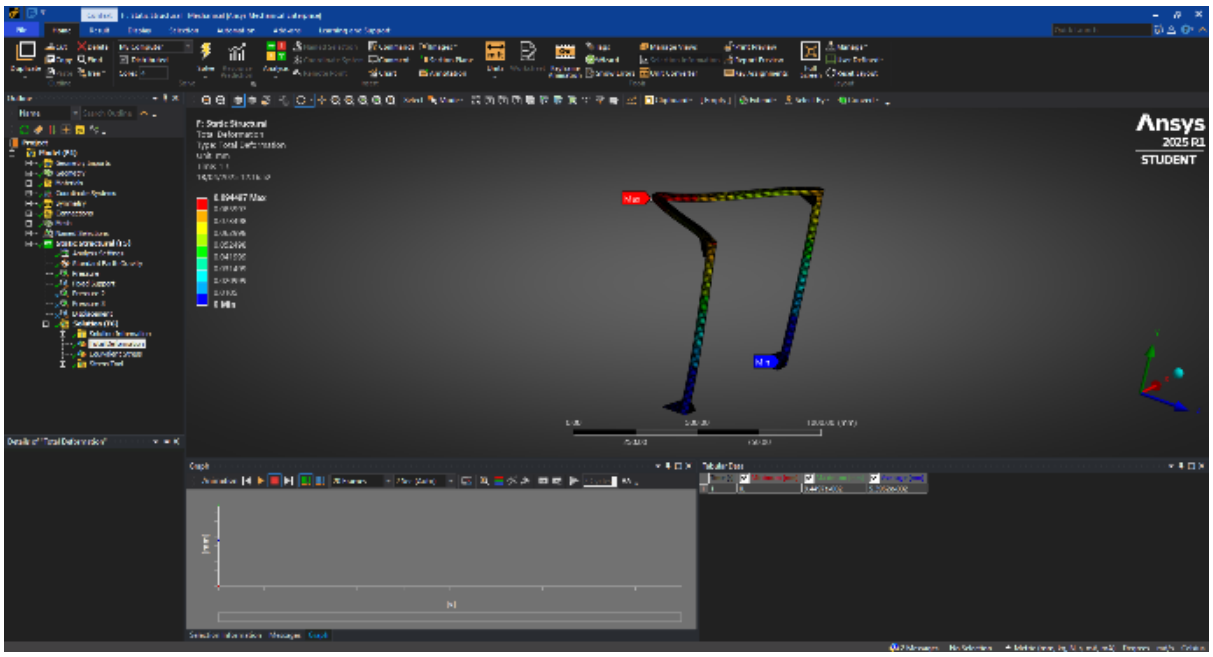

Figure 8.o – FEA 2: Total Deflection

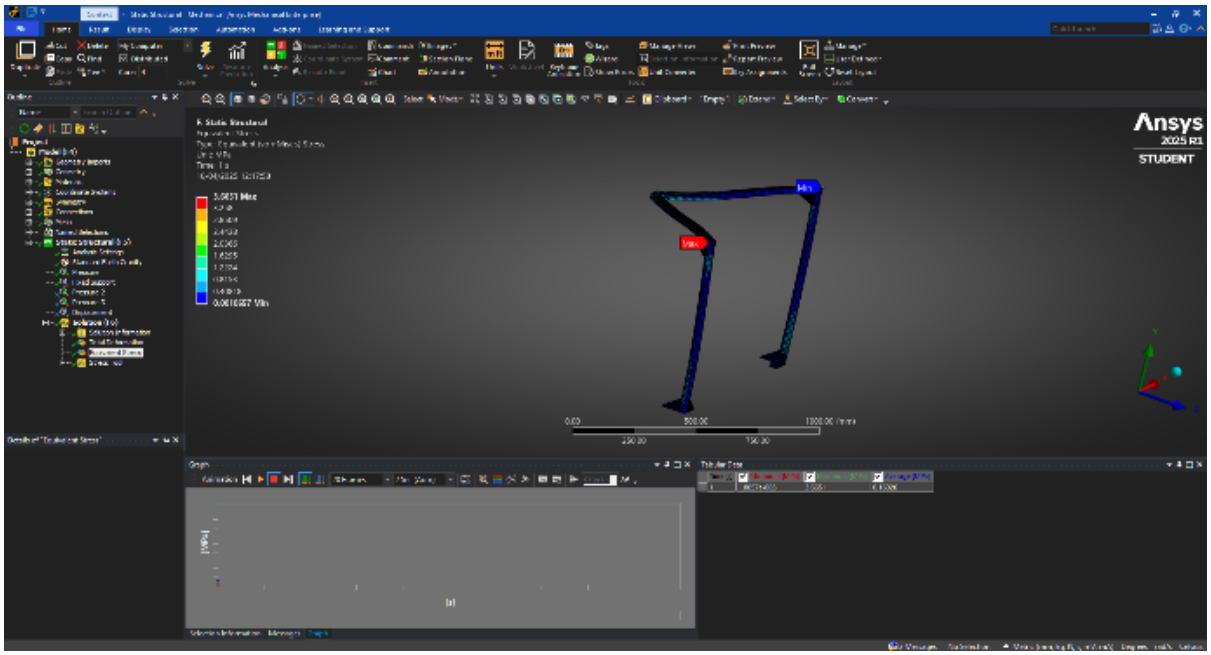

Figure 8.n: FEA 2 Equivalent Stress

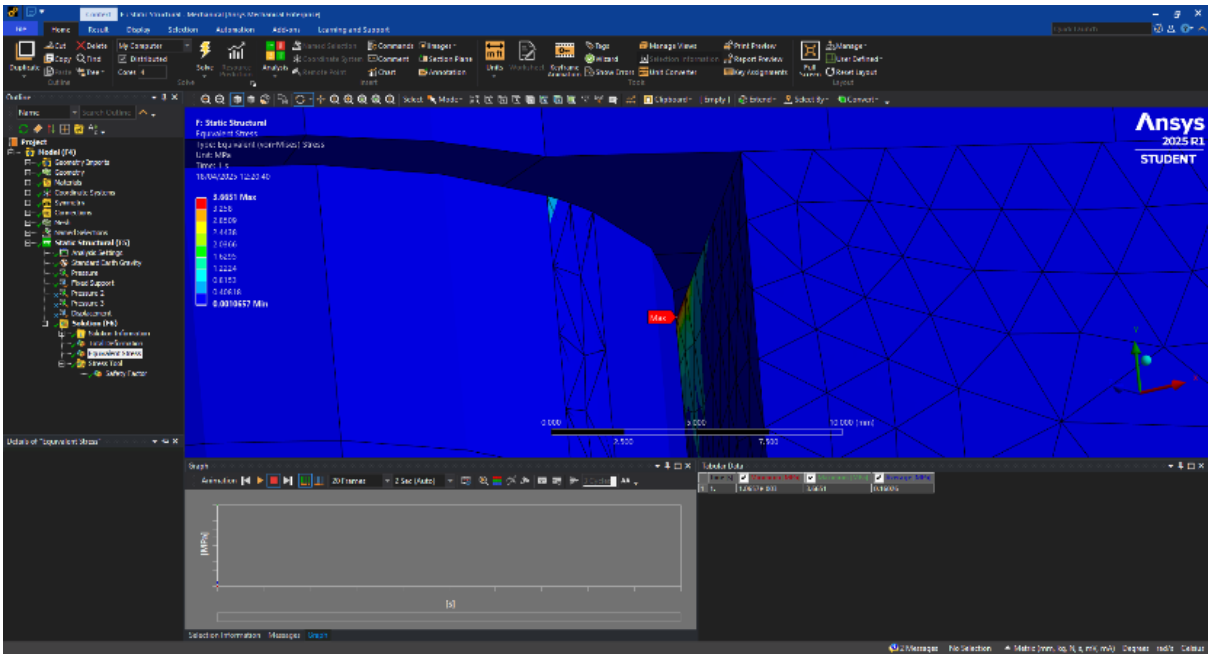

Figure 8.q - FEA 2: Close up on stress concentration

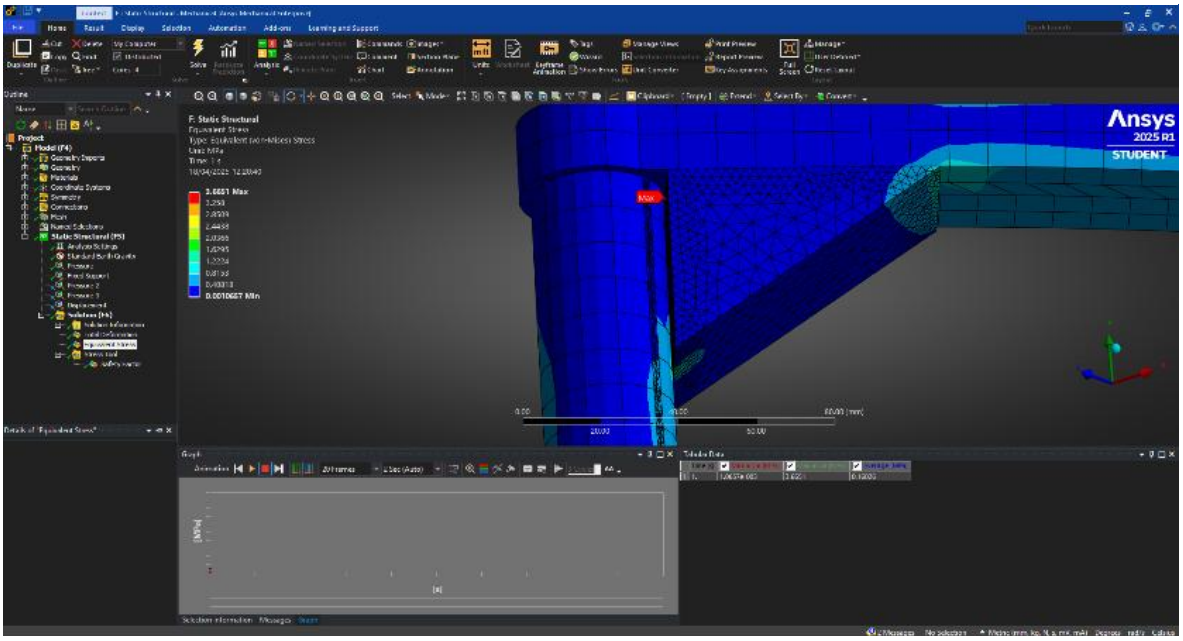

Figure 8.p - FEA 2: Close up on stress concentration

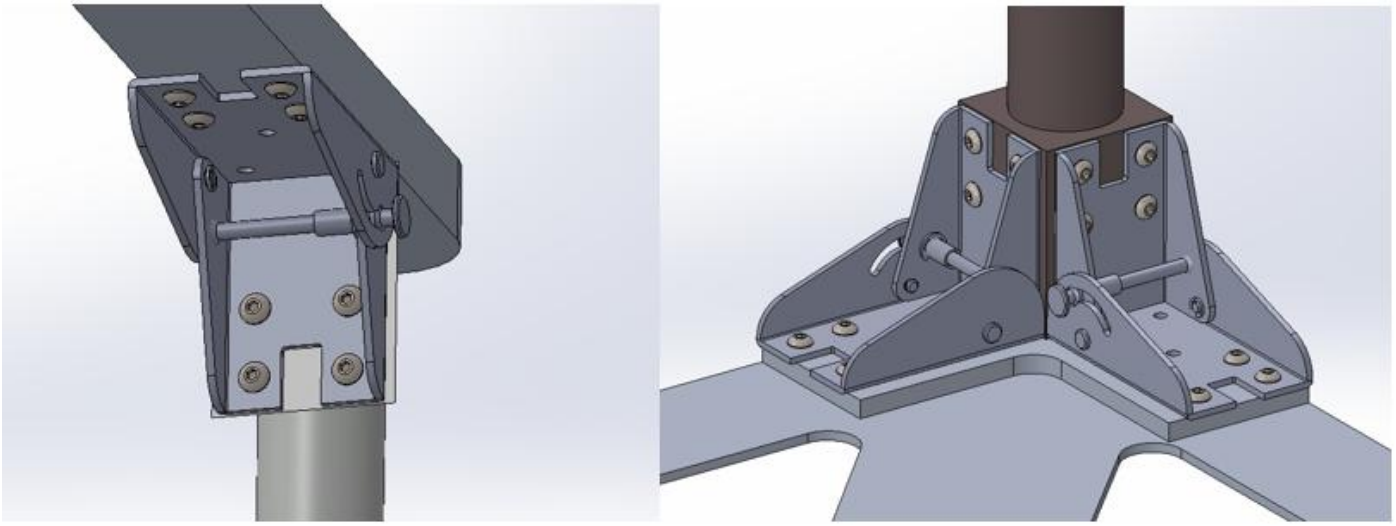

Figure 8.r: Connection layout of the cage subassembly showing scissor struts, pivot pins, and foldable hinges.

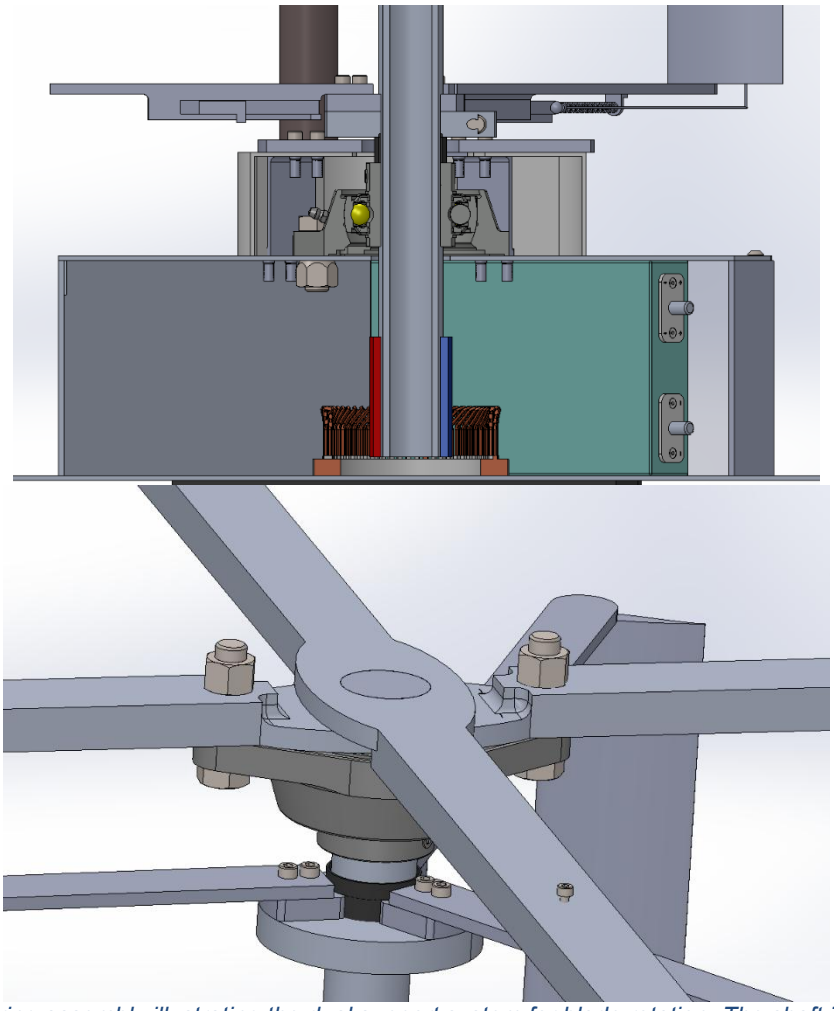

Figure 8.s: Shaft and bearing assembly illustrating the dual support system for blade rotation. The shaft is held by another bearing on top and the bearing is bolted onto the scissor struts (Top Image).

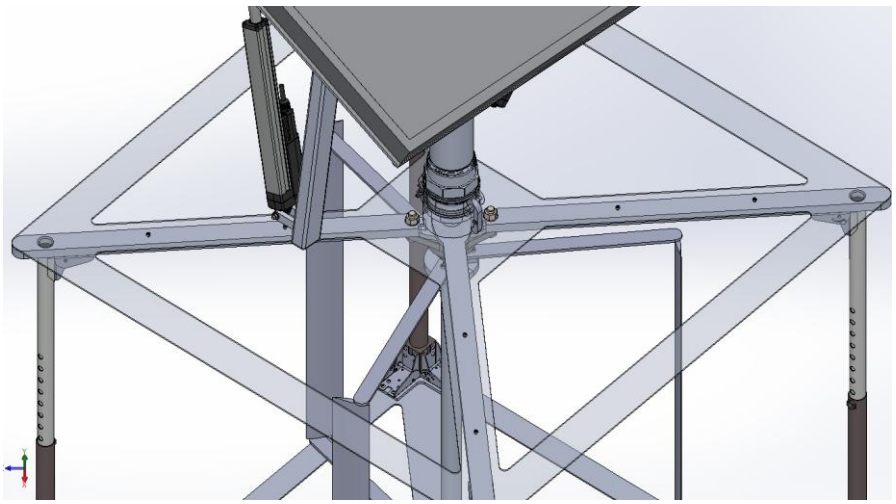

Figure 8.t: Solar panel mounting setup with adjustable brackets fixed atop the cage.

The *solar* assembly base is bolted onto the *scissor struts.* The solar pillar is connected to the overall assembly by cam lock mechanism.

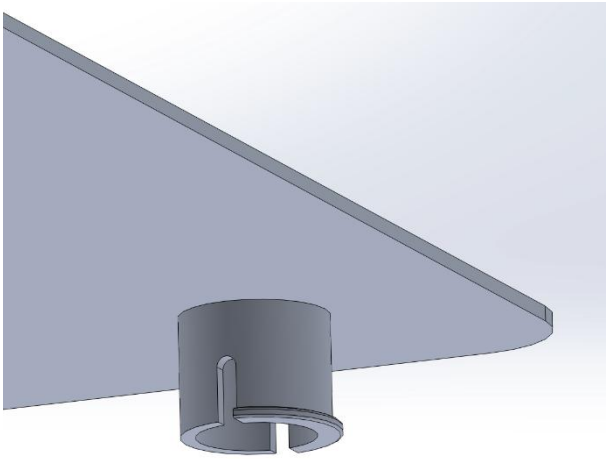

Figure 8.u: Solar panel mounting setup with technic pins connected the cage. The technic pins are connected to the edge of the scissor struts. Supported by screws to keep it in place.

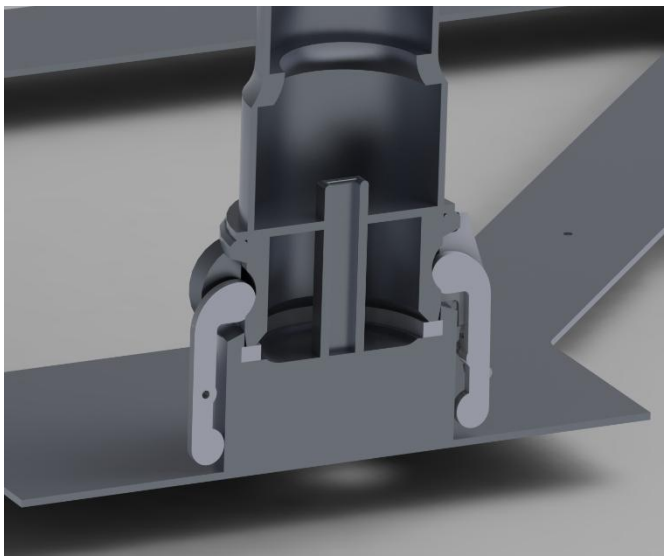

Figure 8.v: Shaft mounting setup with camlock system.

The solar pillar is connected to the overall assembly by cam lock mechanism. Rotation is not considered due to the square shaft in the middle of the camlock preventing rotation.

Figure 8.w: Solar panel mounting setup with hinges.

The solar panel is hinged onto the solar pillar to provide rotation and tilt, through a shaft and coupler in the middle.

Appendix A.3

Property	ASA Plastic	Fiberglass (FRP)	Carbon Fibre (CFRP)
Density (kg/m³)	~1,070	~1,800–2,000	~1,550–1,600
Tensile Strength (MPa)	~35-50.5	~480-1,600	~1,720-3,690
Elastic Modulus (GPa)	~2.2	~20-51	~120-580
UV/Weather Resistance	Moderate	Good	Excellent
Manufacturing Cost	Low	Medium	High

Figure 8.x: Material Properties

Material	Advantages	Disadvantages

ASA Plastic	- Easy and cheap to 3D print - Moderate UV resistance - Lightweight	- Low mechanical strength - Poor fatigue resistance - Not suitable for high wind loads - Deforms easily under stress
Fiberglass (FRP)	- High strength-to-weight ratio - Good fatigue resistance - Good corrosion and UV resistance - Moderate cost	- Heavier than carbon fibre - More brittle than metals under extreme impact - Manufacturing requires careful handling (resin cure process)
Carbon Fibre (CFRP)	- Extremely high tensile strength and stiffness - Lightweight - Excellent fatigue and corrosion resistance - Good performance in harsh environments	- Very expensive material and manufacturing - More brittle compared to fiberglass - Requires specialist fabrication techniques

Figure 8.y: Advantages and Disadvantages of Each Material.

Stress Analysis

Stress calculation formula:

$$\sigma = F/A$$

Where:

F = Applied wind forces

A = Blade cross-section area

Wind forces applied incrementally from **50 N to 500** N and the value of the cross-sectional of the blade is **435.686393 mm^2 (final blade design property).**

Deflection Analysis

Cantilever beam bending equation:

$$\delta = (FL^3)/3EI$$

Where:

F = Applied wind forces E = Elastic Modulus

L = Blade length I = Moment of Inertia

The value of blade length used is **400 mm**. The value of E used is based on different materials and the value of I used is **1.8614 x 10^-5 m^4 (final blade design property)**.

Components	References
Foldable Hinges	https://www.amazon.co.uk/Stainless-Furniture-Telescopic-Adjustable-Protective/dp/B0831KJ2TD/ref=asc_df_B0831KJ2TD?mcid=5ed17baab86637fda67f0f57eb0cbb70&tag=googshopuk-21&linkCode=df0&hvadid=697265147963&hvpos=&hvnetw=g&hvrand=303531774024103634&hvpone=&hvptwo=&hvqmt=&hvdev=c&hvdvcmdl=&hvlocint=&hvlocphy=9046639&hvtargid=pla-1687718573944&gad_source=1&th=1
Rubber Padding Feet	https://liftgiant.co.uk/rubber-lifting-pads-20mm-x-4/?utm_term=&utm_source=google&utm_medium=cpc&gad_source=1&gbraid=0AAAAABaE8vzc-LbpD81XsbVRR12r76FX_&gclid=Cj0KCQjww-HABhCGARIsALLO6XwbkHhhGx05Oa8GcCOsgUB9BWT99xiqhnHhI0gzD4Ao-XNMeySrUb0aAhK1EALw_wcB
Spring	https://uk.misumi-ec.com/vona2/detail/110300268470/?list=PageCategory
Monocrystalline Solar Panel	
Shaft Bearings NSK6800DD	https://uk.rs-online.com/web/p/ball-bearings/4921850
Linear Actuator (200mm & 300mm)	https://www.timotion.com/en/products/linear-actuators/ma4-series
Linear Bearing SC10UU	https://uk.misumi-ec.com/vona2/detail/221000091814/?HissuCode=SC10UU
Anti-Slip Motor Coupling 10mm	https://www.optimusdigital.ro/en/coupling-hubs/11420-easymech-anti-slip-motor-coupling-10-mm-internal-diameter.html

Figure 8.z: External components that are not manufactured

8.2 Appendix B

Figure 12.14.1 – Shared Google Calendar (example from March 2024)

ID	Task Mode	Task Name	Duration	Start	Finish
1		**Prototype Building & Testing**	**60 days**	**Mon 27/1/25**	**Fri 18/4/25**
2		Monitor parts arrived	1 wk	Mon 27/1/25	Fri 31/1/25
3		Correspond with technicians on item delivery and manufacturing progress	4 wks	Mon 27/1/25	Fri 21/2/25
4		Prototype assembly for solar	4 wks	Mon 3/2/25	Fri 28/2/25
5		Prototype assembly for wind turbine	5 wks	Mon 3/2/25	Fri 7/3/25
6		Electrical assembly	3 wks	Mon 3/2/25	Fri 21/2/25
7		Coding for Single-axis solar panel movement	2 wks	Mon 10/2/25	Fri 21/2/25
8		Prototype major assembly	3 wks	Mon 10/3/25	Fri 28/3/25
9		Prototype design changes	1 wk	Mon 31/3/25	Fri 4/4/25
10		Prototype testing	1 wk	Mon 7/4/25	Fri 11/4/25
11		FMEA analysis for prototype	1 wk	Mon 14/4/25	Fri 18/4/25
12		Protoype result analysis solar and wind	2 wks	Mon 7/4/25	Fri 18/4/25
13		**Deployable Unit**	**60 days**	**Mon 27/1/25**	**Fri 18/4/25**
14		Modify specification from prototype for deployable unit	2 wks	Mon 27/1/25	Fri 7/2/25
15		Sketch design ideas for deployable unit	1 wk	Mon 10/2/25	Fri 14/2/25
16		Research mass manufacture methods fo the deplyable unit (10,000 units)	2 wks	Mon 10/2/25	Fri 21/2/25
17		Research on structural analysis and material properties for optimisation	2 wks	Mon 10/2/25	Fri 21/2/25
18		Research on solar panel accuracy optimisation	2 wks	Mon 10/2/25	Fri 21/2/25
19		Research on wind turbine blade optimisation	2 wks	Mon 10/2/25	Fri 21/2/25
20		**Iterative optimisation**	**40 days**	**Mon 24/2/25**	**Fri 18/4/25**
21		Solar tracking accuracy optimisation	2 wks	Mon 24/2/25	Fri 7/3/25
22		CFD Ansys simulation for wind and noise for turbine blade	3 wks	Mon 24/2/25	Fri 14/3/25
23		VAWT turbine optimisation using Qblade and Ansys	3 wks	Mon 24/2/25	Fri 14/3/25
24		CAD design model for deployable un	3 wks	Mon 17/3/25	Fri 4/4/25
25		FEA analysis on overall structure	2 wks	Mon 7/4/25	Fri 18/4/25
26		Fatigue analysis	2 wks	Mon 7/4/25	Fri 18/4/25
27		Deployable Solidwork animation vid	2 wks	Mon 7/4/25	Fri 18/4/25
28		CAD Drawings	2 wks	Mon 21/4/25	Fri 2/5/25
29		**Demostration and Presentation**	**23 days**	**Mon 7/4/25**	**Tue 6/5/25**
30		Powerpoint Presentation	4 wks	Mon 7/4/25	Fri 2/5/25
31		Deployable animation video	4 wks	Mon 7/4/25	Fri 2/5/25
32		Edit video for demonstration	2 wks	Mon 21/4/25	Fri 2/5/25
33		Final Presentation	1 day	Tue 6/5/25	Tue 6/5/25
34		**Report Writing**	**74 days**	**Mon 27/1/25**	**Wed 7/5/25**
35		Write Report B skeletal structure	2 wks	Mon 27/1/25	Fri 7/2/25
36		Write introduction	2 wks	Mon 10/2/25	Fri 21/2/25
37		Create new specification list	2 wks	Mon 14/4/25	Fri 25/4/25
38		Write assembly and testing section	3 wks	Mon 14/4/25	Fri 2/5/25
39		Write professional practice statement and supporting evidence	2 wks	Mon 21/4/25	Fri 2/5/25
40		Write conclusion	1 wk	Mon 28/4/25	Fri 2/5/25
41		Finalise Report B	4 days	Sat 3/5/25	Wed 7/5/25
42		Report B submission	1 day	Wed 7/5/25	Wed 7/5/25

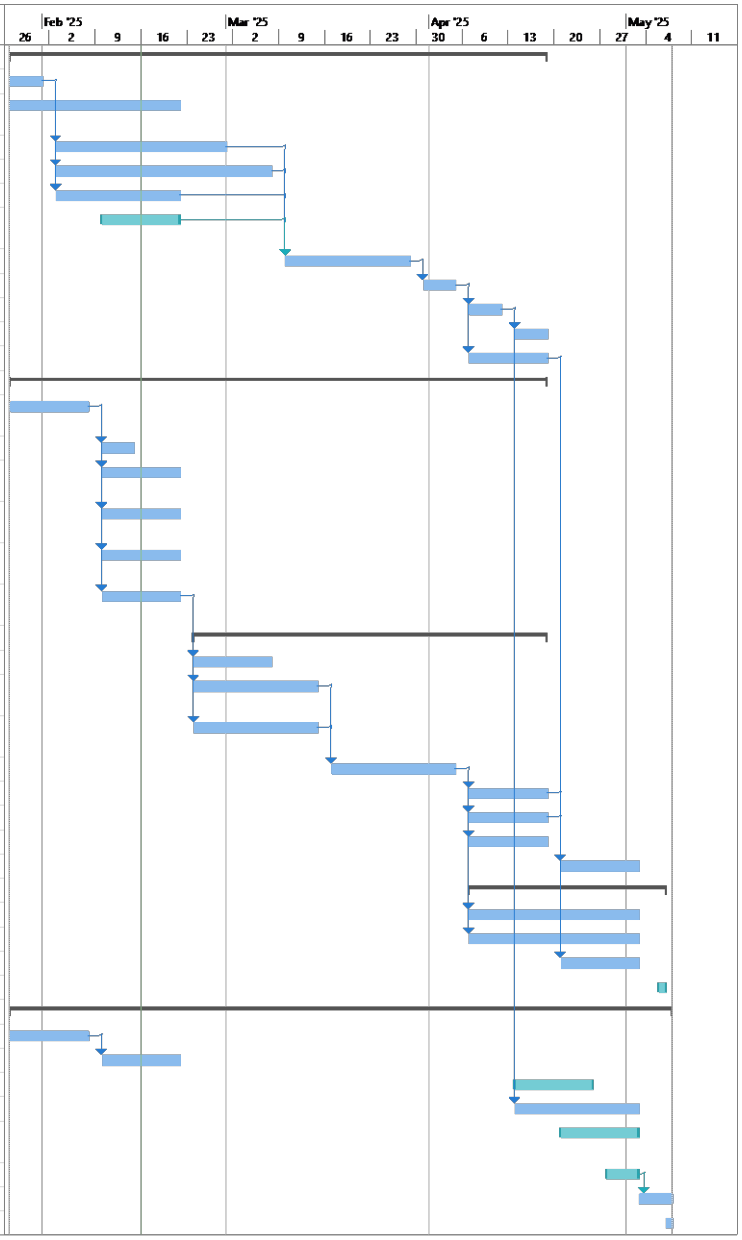

Figure 8.aa Semester 2 initial Gantt Chart

Final Feedback notes

Use Hole Wizard for shaft holes

Use PCD, perimeter circle diameter, for Top base to show distance between holes. DONT NEED TO DO SINCE WE ARE REMOVING PLATES

Tap holes THRU ALL for arm airfoil connection. Done

Put standard airfoil name in drawing 'made from this standard airfoil'. Done

Cut extrude out of airfoil, and back fill on chord line. Will be done.

Separate drawings for welded parts. Done

Threaded inserts for Brilliant's housing, speak to techs to find out what size holes to make.

30 mm main shaft, new bearing housing, smaller sleeve diameter (found a shaft that's 30mm by 5mm wall thickness, and a housing bearing that's got a 30mm inner diameter, but will need checking because the bearing is not included, so need to find right bearing)

General tolerancing on sheet, specific tolerancing on holes. Done

Get rid of aluminium plating, just use a profile cage. i.e. struts across the cage to mount the housing bearings on.

New shaft link

https://www.metals4u.co.uk/materials/aluminium/aluminium-tube/30mm-x-5mm-aluminium-tube-p

New bearing housing link

https://uk.rubix.com/en/oval-flanged-housing/p-G1321144839

Figure 8.bb Design Review Meeting Notes

Engineering Professional Reflection-on-Practice competences - Team						
			Rate 1 - 4 (1 = low, 4 = high)			
			Review Point 1	Review Point 2	Review Point 3	Review Point 4
Personal and social skills	*Emotional awareness*	P1. We manage my emotions			3	
	Awareness of needs	P2. We show awareness of needs and concerns of others			3	
	Diversity & equality	P3. We demonstrate awareness of diversity and equality issues				4
	Flexibility	P4. We show flexibility when dealing with interpersonal situations				4
	Relationships	P5. We create and maintain productive working relationships, resolving conflict where necessary				4
Lead and develop teams	*Project co-ordination*	T1. We co-ordinate project activities by identifying, and agreeing collective goals			3	
	Team work and planning	T2. We contribute to establishing individual and team objectives and work plans			3	
	Giving feedback	T3. We give feedback to others in relation to individual and team objectives and goals			3	
	Responding to feedback	T4. We gather, evaluate and learn from feedback				4
	Recommending improvements	T5. We recommend improvements			3	
	Professional standards	T6. We reinforce team commitment to professional standards				4
Communication	*Meetings*	C1. We chair and keep records of meetings and discussions			3	
	Presenting & reporting	C2. We contribute to the preparation of communications, documents and reports (technical or complex matters)				4
	Providing advice	C3. We am proactive in exchanging information and providing advice			3	
	Working ethically	C4. We understand and apply ethical principles to my work, and encourage it within my team				4
		C5. We uphold or challenge ethical principles where necessary				4

Figure 8.cc: Professional Reflection on Practice Competences

Table 1: The UoM Engineering Professional Competencies

Personal and social skills		
P1.	EMOTIONAL AWARENESS	to manage my emotions
P2.	AWARENESS OF NEEDS	to show awareness of needs and concerns of others
P3.	DIVERSITY & EQUITY	to demonstrate awareness of diversity and equality issues
P4.	FLEXIBILITY	to show flexibility when dealing with interpersonal situations
P5.	RELATIONSHIPS & CONFLICT	to create and maintain productive working relationships, resolving conflict where necessary
Leading and developing teams		
T1.	PROJECT COORDINATION	to coordinate project activities by identifying, and agreeing collective goals
T2.	TEAM WORK PLANNING	to contribute to establishing individual and team objectives and work plans
T3.	GIVING FEEDBACK	to give feedback to others in relation to individual and team objectives and goals
T4.	RESPONDING TO FEEDBACK	to gather, evaluate and learn from feedback
T5.	RECOMMENDING IMPROVEMENTS	to recommend improvements
T6.	PROFESSIONAL STANDARDS	to reinforce team commitment to professional standards
Communication		
C1.	MEETING RECORDING	to be or support the chair and keep records of meetings and discussions
C2.	PRESENTING & REPORTING	to contribute to the preparation of communications, documents and reports (technical or complex matters)
C3.	PROVIDING ADVICE	to be proactive in exchanging information and providing advice
C4.	WORKING ETHICALLY	to understand and apply ethical principles to work, and encourage it within the team

Figure 8.hh UoM Engineering Professional Practice Competencies

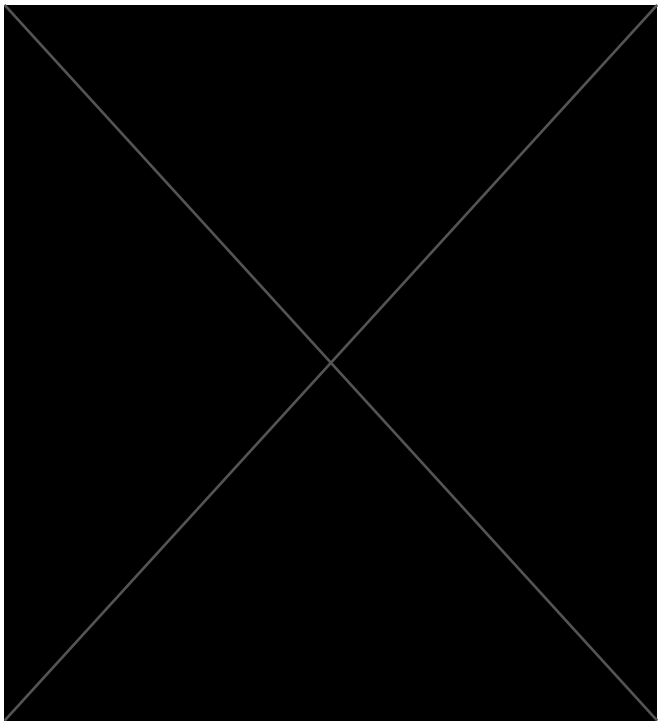

Figure 8.ii WhatsApp communications

Brilliant Purnawan > Mechanical Design Project Group 10 > **Semester 1**

Name	Modified	Modified By	File size	Sharing
Design Concepts, Drawings & Figures	6 days ago	Brilliant Purnawan	3 items	Shared
Gantt Chart & Planning	6 days ago	Brilliant Purnawan	1 item	Shared
Guidelines	6 days ago	Brilliant Purnawan	8 items	Shared
Presentation	6 days ago	Brilliant Purnawan	2 items	Shared
Purchasing & Manufacturing Requests	6 days ago	Brilliant Purnawan	0 items	Shared
Appeal	6 days ago	Brilliant Purnawan	2 items	Shared
Report	6 days ago	Brilliant Purnawan	5 items	Shared
Design CAD & Electronic Schematics	6 days ago	Brilliant Purnawan	11 items	Shared
Product Requirement & Specifications.xlsx	January 29	Muhammad Yusman	78.8 KB	Shared
Analysis.docx	December 12, 2024	Hanif Mohd Fadhillah	248 KB	Shared
Selection of Airfoil Blade for a Compact Ver...	December 10, 2024	Margarita Simpson	17.1 KB	Shared
Final Feedback notes.docx	December 8, 2024	Hanif Mohd Fadhillah	14.2 KB	Shared

Figure 8.jj Shared One Drive for semester one and two

Meeting Logs – Project: Deployable Dual Source Renewable Energy Device
Timeframe: January 27th, 2025 – May 5th, 2025
Frequency: Weekly meetings every Tuesday (12:30–3:00 PM) and either Wednesday or Thursday sessions (10:00 AM–1:00 PM) being used for Assembly or Testing

Week of Jan 27th, 2025

- *Revisited project scope and prototype outcomes.*
- *Discussed key learnings from the prototype to inform full system design.*
- *Drafted initial design specs, aligned with expected operational environments.*

Week of Feb 3rd, 2025

- *Explored potential applications: disaster relief, remote construction, off-grid use.*
- *Identified and ranked core specs: ease of assembly, portability, power reliability.*
- *Set early criteria for assessing future design trade-offs.*

Week of Feb 10th, 2025

- *Reviewed various optimisation methods.*
- *Agreed on FMEA, FTA, DFA, and DFR as primary approaches.*
- *Assigned methods based on individual interest and technical strengths.*

Week of Feb 17th, 2025

- *Independent research on assigned methods.*
- *Shared brief updates on tool selection (e.g., FMEA sheets, QBlade) and application areas.*
- *Began mapping methods to key subsystems.*

Week of Feb 24th, 2025

- *Applied methods to identify weak points: e.g., FTA flagged blade geometry, DFA raised structural concerns.*
- *Confirmed coverage across mechanical, structural, and electrical domains.*
- *Started documenting early optimisation leads.*

Week of Mar 3rd, 2025

- *Progressed to numerical validation.*
- *DFA/FMEA users quantified assembly improvements; others used simulations (aero, structural).*
- *Peer reviews during meetings provided technical critique and refinement suggestions.*

Week of Mar 10th, 2025

- *Took stock of collective progress.*
- *Resolved overlapping efforts and filled in any gaps.*
- *Set direction for integrating results into the final deliverables.*

Week of Mar 17th, 2025

- *Finalised most optimisation tasks.*
- *Began drafting report sections and building visuals (figures, diagrams).*
- *Framed findings in context of project goals and performance metrics.*

Week of Mar 24th, 2025

- *Formal task split for report writing and presentation.*
- *Defined responsibilities and deadlines for drafts.*
- *Mapped each member's optimisation work to a meaningful contribution in the final output.*

Week of Mar 31st, 2025

- *Collated individual sections into full draft.*
- *Unified formatting, tone, and technical language.*
- *Peer-edited for cohesion, ensuring alignment with rubric.*

Easter Break – No Meetings (April 5–27th)

Week of Arp 28th, 2025

- *Collated optimisation write ups for conclusions.*
- *Reviewed and finalised technical documents.*
- *Reviewed and practised the Presentation.*

Week of May 5th, 2025

- *Focused on rehearsals and slide refinement.*
- *Made final report tweaks: formatting, citations, layout.*
- *Wrapped up with team debrief on key takeaways and professional growth.*